Report on WRF model sensitivity studies and specifications for the mesoscale wind atlas production runs

Deliverable D4.3

Witha, Björn; Hahmann, Andrea N.; Sile, Tija; Dörenkämper, Martin; Ezber, Yasemin; Bustamante, Elena Garcia ; Gonzalez-Rouco, J. Fidel; Leroy, Grégoire; Navarro, Jorge

Link to article, DOI:
10.5281/zenodo.2682604

Publication date:
2019

Report on WRF model sensitivity studies and specifications for the mesoscale wind atlas production runs

Deliverable D4.3

Edited by: Björn Witha
Delivery date: 9 May 2019
Dissemination level: Public

With financial support from NEWA ERA-NET Plus, topic FP7-ENERGY.2013.10.1.2.

Author Information

Name	Organisation	E-mail
Björn Witha	ForWind, Germany	bjoern.witha@uol.de
Andrea N. Hahmann	DTU, Denmark	ahah@dtu.dk
Tija Sīle	University of Latvia	
Martin Dörenkämper	Fraunhofer IWES, Germany	
Yasemin Ezber	Istanbul Technical University	
Elena García-Bustamante	CIEMAT, Spain	
J. Fidel González-Rouco	Univ. Complutense Madrid	
Grégoire Leroy	3E, Belgium	
Jorge Navarro	CIEMAT, Spain	

Contents

Executive Summary

This report describes the sensitivity studies performed with the mesoscale model WRF in preparation of the mesoscale wind atlas production runs. The objective of this work was to find a model setup that is not just a best practice setup but well-founded and based on scientific evaluation.

We started with performing some initial sensitivity experiments changing the PBL scheme and the initialisation of the model. The work was distributed among several partners, each conducting the same set of experiments but on a different domain. The objective of this first phase was to ensure that everybody speaks the same language in terms of applying WRF in the context of NEWA. The results were analysed and compared in terms of the mean wind climate. To draw conclusions regarding the quality of the experiments, the results of one domain were compared to tall mast observations. Overall the model showed a good performance with slightly better results for one of the two tested PBL schemes (MYNN) and weekly initialisation of simulations (compared to daily).

In the next phase, further sensitivity tests were conducted for one of the previously defined domains, varying a multitude of parameters as e.g. model version, vertical resolution, forcing data and land surface parameterisation. These studies showed that virtually each parameter change is affecting the results in some way, while significant effects on the wind climate are mostly obtained by changes in physical parameterisation e.g. PBL scheme, representation of the land surface and surface roughness. However, also non-physical parameters as the simulation length and the domain size affects the results considerably. The results suggest to use rather small domains and not too long simulations (in the order of 1–2 weeks).

One of the objectives of NEWA is to create a probabilistic wind atlas, i.e. to provide uncertainty information to the mesoscale wind atlas (see Deliverables D3.1 and D4.4). This will be achieved by generating an ensemble of WRF simulations with different model configurations. While the final ensemble to be run over the complete NEWA domain will only include a few members, a much larger ensemble was run for a smaller sub-domain to find the ensemble members that generate the largest spread and will be used in the final NEWA ensemble. A second objective of this initial large ensemble was to find an optimal setup for the mesoscale production run. Based on the experience gained in the previous sensitivity experiments, a 47-member ensemble was assembled and run. The individual members were compared against each other, as well as against tall mast observations. Different metrics were explored to assess the performance of the members, i.e. not only the usual statistical measures as RMSE, BIAS and correlation but also metrics that compare the wind speed distributions.

In the final part of this report we present the ultimate WRF setup for the NEWA production run that was run between August 2018 and March 2019 on the MareNostrum supercomputer in Barcelona.

1 Introduction

A wind resource atlas is associated to the planning phase of wind energy development, which can last several years from strategic spatial planning, to site prospecting, to wind farm design and financing. Detailed, accurate and robust information about the wind resource across an area is crucial for the commercial evaluation of a wind farm. Today a number of well-established models and methodologies exist for estimating resources and design parameters. These can work well if sufficiently long and high quality local measurement data are available, but the wind energy community is still hampered by large negative discrepancies between calculated and actual resources and design conditions.

1.1 Wind atlas scope

The New European Wind Atlas (NEWA) will provide a unified high-resolution and publicly available dataset of wind resource and siting parameters in Europe. Wind statistics will cover onshore Europe and 100 km offshore plus the Baltic and the North Seas (Figure 1), with a horizontal grid spacing of 50 meters at 3 wind-turbine relevant heights. The dataset will be based on 30 years of mesoscale simulations with the Weather, Research and Forecasting (WRF) model at 3 km $\times$ 3 km $\times$ 30 min resolution that are downscaled with a linearised microscale model using a statistical downscaling approach to the final 50 m grid.

In addition to the wind resource information, the new wind atlas will provide information about site suitability conditions (turbulence intensity, wind shear, extreme wind speed), wind variability as well as wind power predictability from day-ahead to decadal time scales. The predictability assessment methodology using climate models is introduced in a separate Deliverable (D3.2).

Besides variables of immediate use by resource planners, the wind atlas will provide means to

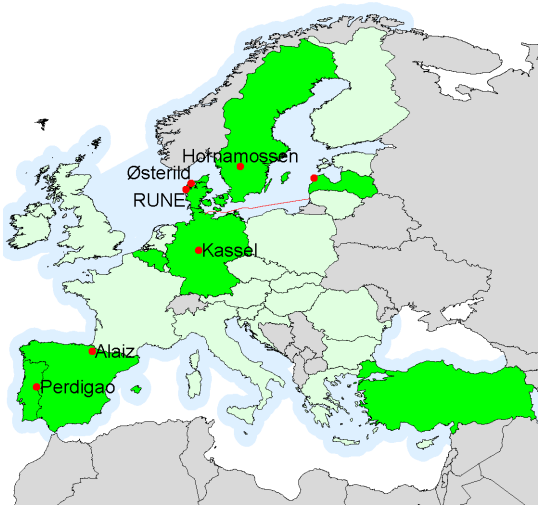

Figure 1. Initial extension of the European domain for the New European Wind Atlas and location of high fidelity experimental campaign sites. The strong green states are members of the NEWA project, light green are the 28 members of the European Union.

feed boundary conditions to microscale models. This will allow not only to improve the wind atlas predictions at local level when better site data becomes available but also to allow a coherent integration with wind farm design tools. Hence, a generalised wind atlas, i.e. free of site effects, will also be part of the NEWA database. Downscaling methodologies with microscale models are introduced in the Deliverable D3.3.

Integral to the wind atlas methodology is the assessment of the associated uncertainties. The ultimate goal of the wind atlas is to reduce the uncertainties on the assessment of wind resource and the wind conditions that affect the design of wind turbines. To this end, the mesoscale-microscale model chain will be thoroughly validated across Europe with dedicated experiments and historical wind resource assessment campaigns from industry. This model evaluation strategy is described in Deliverables D3.4 and D4.4. The uncertainty quantification in NEWA will mainly be based on an ensemble of different WRF model configurations. While the NEWA Ensemble will primarily be described in Deliverable D4.4 it will also briefly be touched in this Deliverable as it also served to determine the setup of the NEWA mesoscale production run.

1.2 Mesoscale modelling for wind energy applications

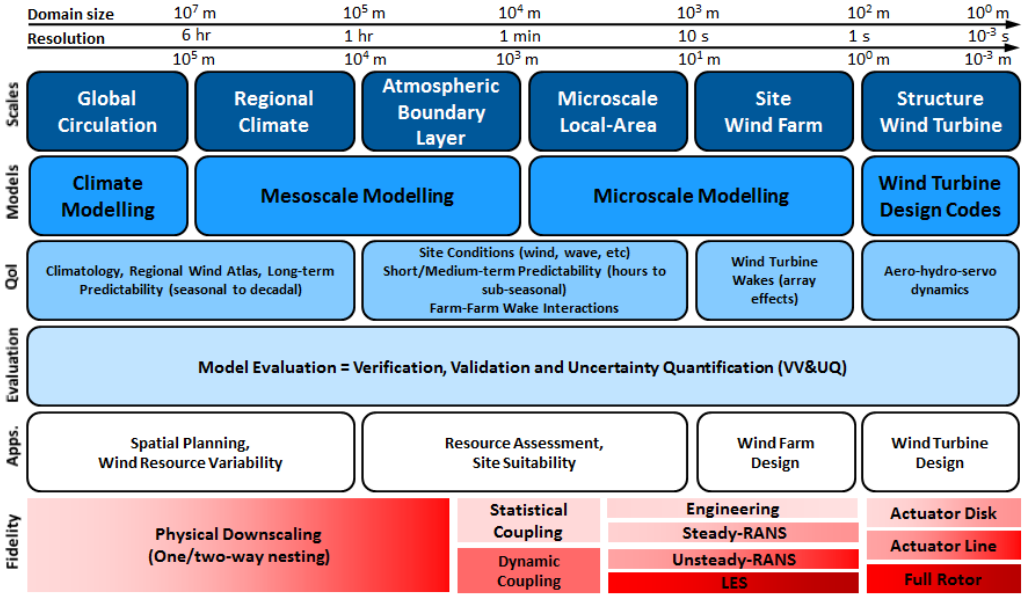

Figure 2. Wind assessment modelling framework indicating typical model scale ranges, relevant outputs for different applications and high-level fidelity levels (the shading indicates the computational cost). Source: (Sanz Rodrigo et al., 2017)

Figure 2 schematically shows the wind assessment model-chain framework with a typical range of scales for each sub-model level and associated applications and flow modelling approaches of various physical fidelity levels (Sanz Rodrigo et al., 2017). Mesoscale models, also called limited-area models, cover a limited portion of the planet so they require lateral boundary conditions from a global circulation model (GCM). GCM models use data assimilation to produce the best possible representation of the state of the atmosphere every 6 hours at horizontal resolutions of several tens of kilometres. These large-scale fields are called analysis in forecasting mode or reanalysis in hindcast mode, when a frozen version of the GCM model is used. For example, the European Centre for Medium-Range Weather Forecasts (ECMWF) continuously updates the ERA-Interim global reanalysis (Dee et al., 2011) using a fixed numerical model, released in 2006, that assimilates data since 1979 at approximately 80 km horizontal resolution. The analysis, in

contrast, uses the most updated forecasting model to provide the best possible forecast; hence backwards consistency of the data is not satisfied. From a wind atlas perspective we should use reanalysis products as the best guarantee to maintain historical wind climate homogeneity.

Physical downscaling is often done with telescopic nested uniform grids that progressively increase the horizontal resolution down to a few kilometres. This is the case for the Advanced Research WRF (WRF-ARW, where WRF stands for the Weather Research and Forecasting) model, the most widely used open-source mesoscale model (Skamarock et al., 2008). Sub-grid parameterisations are introduced to account for unresolved physics, of which the most relevant for wind is that of the planetary boundary layer (Draxl et al., 2014; Kleczek et al., 2014).

Mesoscale models are, in general, not specifically developed for wind energy applications. On the other hand, there is a majority of wind energy meteorologists working with the WRF community model in operational as well as research conditions. The initial objective of the mesoscale group in NEWA is to gather best practices on using WRF for wind resource assessment to come up with a unified modelling methodology. A reference model facilitates the process of "speaking the same language", a fundamental objective for the interpretation of simulation objectives and results.

1.3 Sensitivity experiments / Structure of the report

The setting up of an optimal WRF configuration for wind assessment is not a straightforward task considering the large number of degrees of freedom in the configuration of the model as well as in the input data. The WRF model offers a multitude of configuration options that can be chosen by the user. These include physical parameterisations (e.g. planetary boundary layer, surface layer, land surface, microphysics, radiation) as well as numerical/technical options (e.g. domain layout, resolution, time step) and initialisation of atmosphere, sea surface and land surface. It is not feasible to test each and every possible combination of parameters, these would mean thousands of experiments at the least. The approach within NEWA is to use the experience of the mesoscale modellers in the project, to start with a best practice setup and then test the sensitivity of the results against certain parameter options leaving everything else fixed based on the experts consensus. These include parameters which are already known to have a large impact on the wind resource but also cover a wide range of parameters types (both physical and numerical). The overall objective is to find a model setup for the mesoscale wind atlas production run that is not just best practice but well-founded and based on scientific evaluation.

The initial phase of sensitivity experiments described in Chapter 2.1 aimed at verifying that the modellers from the various institutes spoke the same language when it comes to conducting simulations with WRF. While the focus initially was to investigate the relative differences among different model configurations compared to a baseline result, also a (limited) comparison with tall mast observations was done. The study concentrated on the planetary boundary layer (PBL) scheme and the initialisation strategy (simulation length and nudging).

Another crucial configuration factor is the model domain layout that will be discussed in Chapter 2.2. The size of the domain can affect the results, the computational resources and is also relevant regarding the management and handling of the output from the simulations.

The second phase of sensitivity experiments was a more systematic approach with the final goal of finding a robust setup for the mesoscale wind atlas production runs that generates results that are close to the observations. While in the first phase only the PBL scheme and the initialisation strategy have been varied, in this second phase much more WRF parameters that could have an effect on the results have been examined (parameterisations, initial and boundary conditions, vertical resolution, etc.). These experiments are discussed in Chapter 2.3.

While the NEWA mesoscale ensemble runs are mainly dealt with in Deliverable D4.4, a summary of the first stage of the Ensemble runs is given also in this report (Chapter 2.4) as these runs are a continuation of the sensitivity experiments and also have the objective to find the optimal setup for the mesoscale production runs which is presented in the final chapter of this report (Chapter 3).

2 Sensitivity Studies

2.1 Initial sensitivity experiments in five different domains

The scope of these initial sensitivity experiments was to ensure that all project partners involved in the mesoscale modelling in NEWA are speaking the same language when it comes to conducting simulations with the WRF model. A more systematic approach exploring many different configuration settings and their combinations was not intended in this early stage. This was done later on as described in Chapters 2.3 and 2.4. Instead, we used the experience of the mesoscale modellers in NEWA to determine a few fundamental settings and strategies that are known to have the largest impact on the wind resource, namely the PBL scheme and initialisation strategy (simulation length and nudging). Everything else was left fixed based on the experts consensus.

2.1.1 WRF domain configuration

Early in the project it was decided that 3 km horizontal grid spacing will be used for the innermost domains during sensitivity testing and eventually for the final product, because this resolution seems to be de-facto standard (Hahmann et al., 2014; Olsen et al., 2017). Similarly, all project partners agreed, as a standard practice, to use 1:3 resolution ratio between inner and outer domains for grid nesting, leading to 3 different resolutions being used: 27 km for outer domain, and 9 km and 3 km for inner, nested domains. The model top was set to be at 50 hPa, following the best practices of recommended by the WRF NCAR group (Wang et al., 2019).

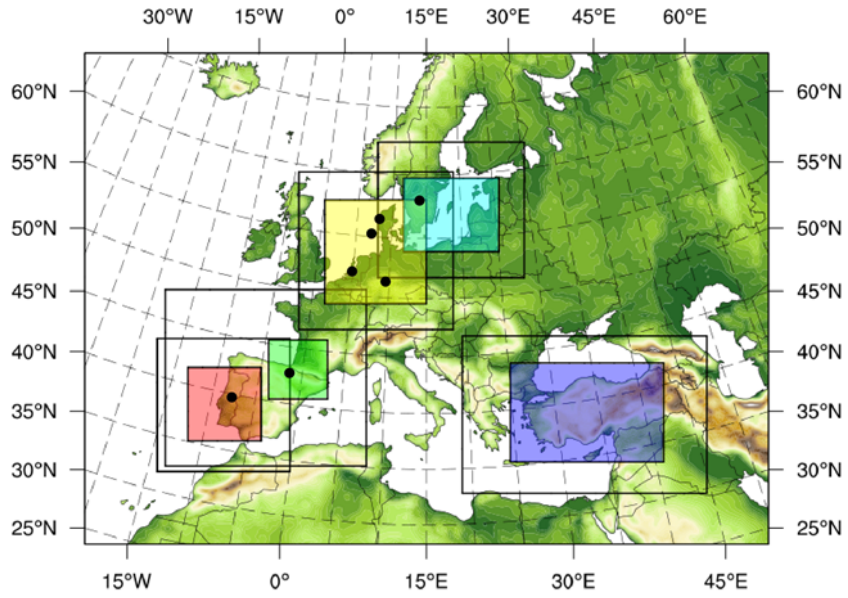

Figure 3. The five WRF model domains used in the initial model sensitivity experiments: NE (turquoise), NW (yellow), PD (red), SW (green) and SE (purple). The dots represent the positions of the NEWA field experiment sites.

In the initial steps the NEWA mesoscale group conducted a series of sensitivity experiments for five European sub-domains as shown in Figure 3. The five 3 km sensitivity domains share an identical outer domain at 27 km, covering the area displayed in Figure 3, but were run independently by each modelling group. The locations and grid sizes for each 3 km sub-domain are shown in Table 1.

Domain	Inner grid size	Centre (lat/lon)
NE	316×244	56.85°N, 18.64°E
NW	337×343	53.77°N, 7.92°E
PD	244×244	38.98°N, 8.41°W
SW	196×196	43.11°N, 0.56°W
SE	508×328	38.94°N, 33.51°E

Table 1. Grid sizes and central latitude and longitude for the five inner WRF domains of the sensitivity experiments in Figure 3.

The location of domains was chosen to cover several regions within Europe with different geographical characteristics that included also the locations of high quality measurements or experiments carried out during NEWA project (see Mann et al. (2017) for an overview of the NEWA experiments). The NW domain contains the location of Kassel forested hill experiments, RUNE and Østerild experiments and the FINO masts. The NE domain contains the location of the Hornamossen and Ryningsnäs forest experiments and high masts in Latvia. The SW and PD domains are centred on the experimental sites of Alaiz and Perdigão, respectively. The SE domain covers all of Turkey and contains many tall masts used in validation further in this report (see Chapter 2.3.4). The terrain height in each of the domains is shown in Figure 4. The NE domain is mostly flat and contains large offshore areas, the NW domain has significant elevation changes only in its southern areas while the rest is either flat or offshore. The SE, SW and PD domains contain significant mountain ranges. Figure 4 also shows for each domain the surface roughness length in meters, a parameter that is well known to have a significant influence on the simulated wind field. Larger z_0 values are associated with forests and typically lead to slower wind speeds at the same height than over a smoother surface.

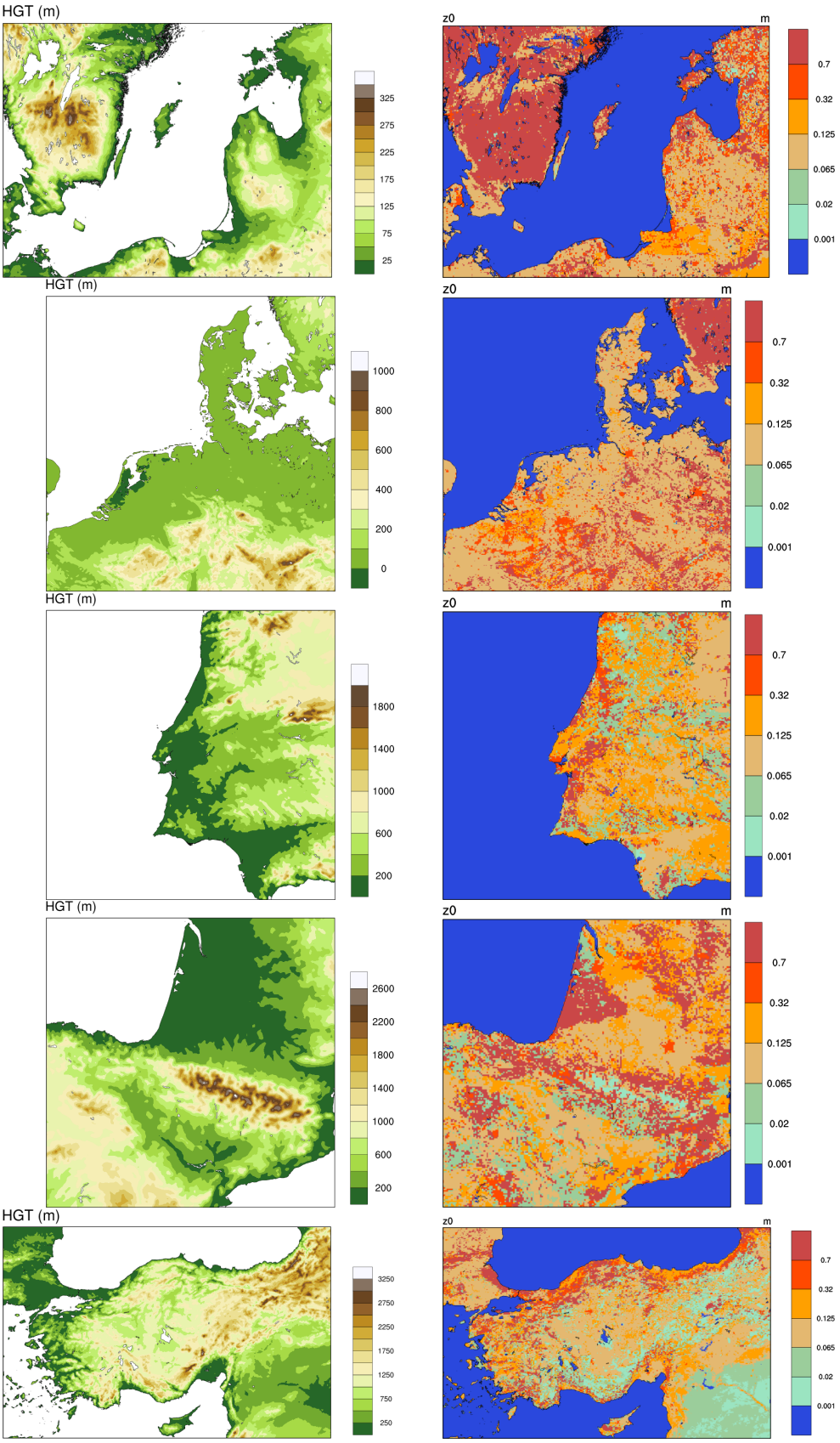

Figure 4. Terrain height (m, left) and surface roughness length (m, right) of the five (from top to bottom: NE, NW, PD, SW, and SE) 3 km × 3 km domains of the NEWA sensitivity experiments. Note that the colour range in the terrain height plots varies between the different domains.

2.1.2 Setup

Six year-long WRF model experiments were conducted for each of the five domains. The simulations were conducted with a common setup outlined in Table 2.

WRF version	3.6.1
Grid	3 nests: 27 km, 9 km, 3 km, 61; vertical levels
Land use data	CORINE 100m, Copernicus Land Monitoring Service (2019)
Dynamical forcing	ERA-Interim, Dee et al. (2011)
SST	OISST, Reynolds et al. (2002)
Land surface model	NOAH-LSM, Chen (2007)
Longwave Radiation	RRTMG scheme (4), Iacono et al. (2008)
Microphysics	WRF Single-Moment 5-class scheme (4), Hong et al. (2004)
Shortwave Radiation	RRTMG shortwave (4), Iacono et al. (2008)
Cumulus Parameterisation	Kain-Fritsch scheme (1), Kain (2004) on D1 and D2
Diffusion	Simple diffusion (option 1) 2D deformation (option 4) 6th order positive definite numerical diffusion (option 2) rates of 0.06, 0.08, and 0.1 for D1, D2, and D3 vertical damping.
Advection	Positive definite advection of moisture and scalars.
Grid relaxation zone	5 points
Nudging	Spectral nudging (2), Miguez-Macho et al. (2004) nudging coefficients: 0.0003 s^{-1} nudging above the PBL (u and v) and above level 20 wave numbers: 15 (x) and 11 (y) in D1, variable in D2 and D3.

Table 2. WRF configuration common to all initial sensitivity experiments.

The alternate options to be part of the initial sensitivity analysis are described in Table 3. The experiments were run using two PBL parameterisations, the YSU (Hu et al., 2013) and MYNN (Nakanishi and Niino, 2006) schemes, and three integration methods: daily initialisation (S1), weekly initialisation with spectral nudging only in the external domain (W1), and weekly initialisation with spectral nudging in all domains (W3). The details of the nudging parameters are also given in Table 2. In the S1 runs, initialised at 00:00 GMT, the first 12 hours of the simulations were discarded, while in the W1 and W3 simulations, initialised at 12:00 GMT, the first day was discarded. Besides the PBL scheme and the use of spectral nudging, all other options described in the WRF model namelist are identical among all simulations and correspond to the "baseline" column in Table 7.

The resulting 6 experiments were repeated for all 5 domains (Figure 3) covering the whole year 2015.

2.1.3 Results

The most important parameters (wind speed and direction, stability, temperature and others) were extracted and interpolated from the WRF hybrid pressure coordinates to geometric heights. The

Experiment	PBL scheme	simulation length	spin-up length	nudging
MYNL61S1	MYNN	36 hours	12 hours	none
MYNL61W1	MYNN	8 days	24 hours	spectral nudging D1
MYNL61W3	MYNN	8 days	24 hours	spectral nudging D1–D3
YSUL61S1	YSU	36 hours	12 hours	none
YSUL61W1	YSU	8 days	24 hours	spectral nudging D1
YSUL61W3	YSU	8 days	24 hours	spectral nudging D1–D3

Table 3. Summary of the initial sensitivity tests.

annual average wind speed at 100 m of the simulated year 2015 using the YSU parameterisation scheme and daily initialisation is shown in Figure 5 for the five simulated domains. The yearly average wind speed is highly variable in each of the domains and ranges between 2 and 12 $\mathrm{m\,s^{-1}}$. There are differences between the northern and southern domains. In the northern domains (NW, NE) the largest differences in wind speed are related to differences between land and sea, however orography (recall Figure 4) plays an important role in the southern domains (SW, SE).

PBL scheme In the next step, the differences between the different PBL schemes were evaluated. The differences between the simulations using YSU and MYNN scheme (daily initialisation) at 100 m height are shown in Figure 6. Over the land, the simulation with the YSU scheme yields higher wind speeds than that using the MYNN scheme. The differences are largest in regions such as Southern Sweden, Aquitaine (France) and border between Lithuania and Belarus. These are forested regions where the surface roughness length has the highest value (cf. Figure 4), therefore allowing to conclude that the pattern and magnitude of these differences are mostly related to the underlying surface roughness length. In the northern domains, over the North and Baltic Seas, the simulation using the YSU scheme yields lower wind speeds than that using the MYNN scheme. Over the sea in southern domains the situation is not so clear-cut. Over the Atlantic near the Portuguese coast the simulation with the YSU scheme exhibits higher wind speeds than the simulation using the MYNN scheme, however over the Bay of Biscay and the seas surrounding Turkey the opposite is true.

At lower levels (25 m) the simulation using the MYNN scheme mostly shows higher wind speeds for most of the NW domain (Figure 7). The same is true for the NE domain (not shown). In the southern domains, the situation is more complicated and it seems that the reverse is true in low-wind areas in the Mediterranean Seas (French Riviera and Turkey, not shown) and in higher elevated regions where MYNN scheme shows lower wind speeds. At 25 m height the differences can reach 0.5 $\mathrm{m\,s^{-1}}$ over the Baltic Sea and 0.9 $\mathrm{m\,s^{-1}}$ in southern Portugal.

The conclusions are the same for the longer duration simulations (MYNNL61W1 and YSUL61W1) although some of the differences are enhanced with longer spin-up time. The nudging in D1 does not "homogenise" the simulations with different PBL schemes.

PBL scheme and stability The simulations show that atmospheric stability is an important parameter to explain the model sensitivity. Here, the atmospheric stability is characterised using the Obukhov length, L, which is a model output field. The boundaries of the stability classes are taken from Gryning et al. (2007). For the MYNL61S1 simulation, stable conditions (i.e., $1/L > 0.005\,\mathrm{m^{-1}}$, shown in Figure 8) are common over land, especially in the three southern domains and can reach over 50% of the time in mountainous areas in Turkey and the Pyrenees. Unstable conditions (i.e., $1/L <$ -0.005 $\mathrm{m^{-1}}$, shown in Figure 9) are found over the oceans, especially in the Atlantic and Mediterranean off the coast of France and Turkey. In some regions, unstable atmospheric conditions can exist during 70% of the simulation time. Neutral conditions (i.e., $|1/L| < 0.005\,\mathrm{m^{-1}}$, shown in Figure 10) occur frequently especially in the northern domains (up

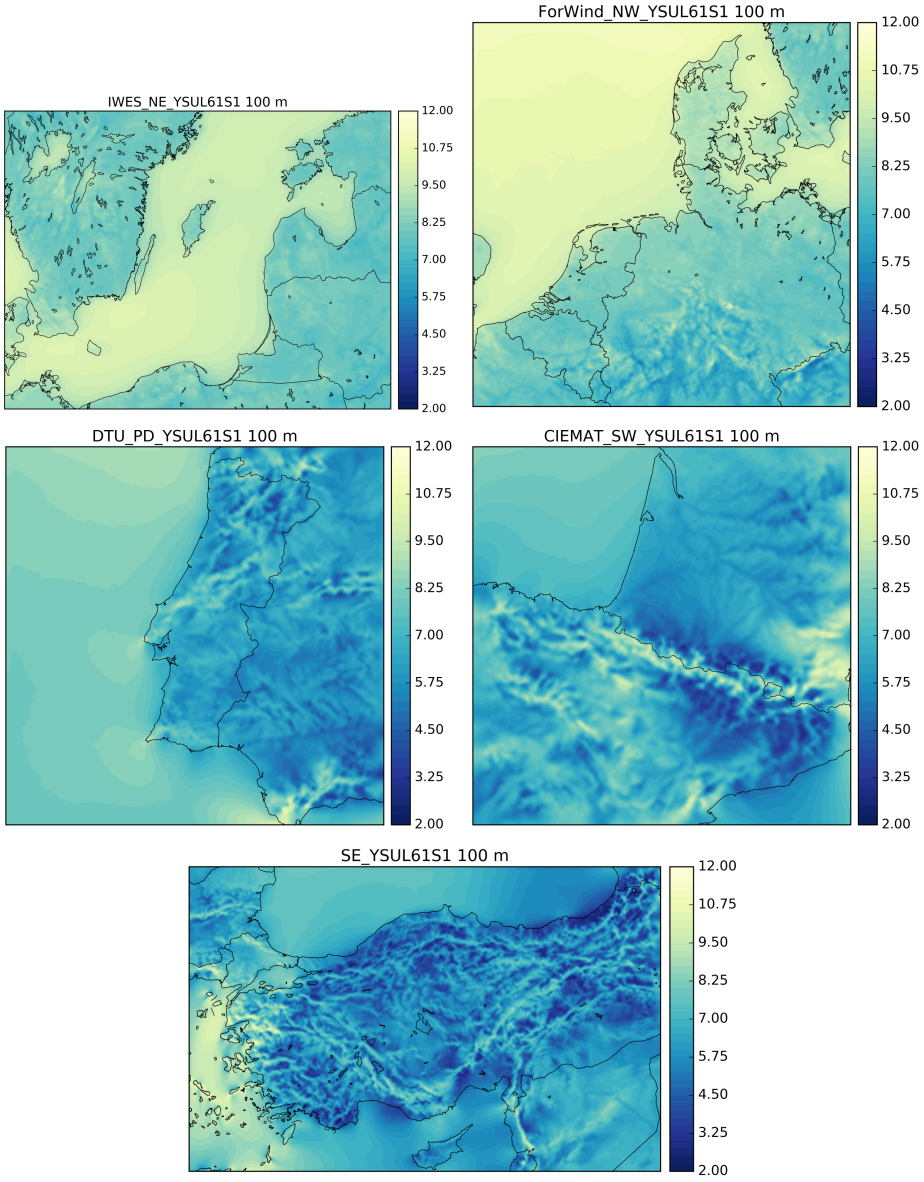

Figure 5. Annual average wind speed ($m\,s^{-1}$) during 2015 at 100 m for the five simulated domains using the YSUL61S1 setup.

to 70% of the time over some cities and forested areas).

If the YSU parameterisation scheme is used instead of MYNN scheme, the frequencies of different stability conditions are significantly changed (Figure 11 – Figure 13), and there are differences in response to PBL scheme change between land and sea regions.

Over the land areas MYNN yields a lower percentage of stable cases compared to YSU (Figure 11), but MYNN also has a lower percentage of unstable cases (Figure 13). As a result, MYNN has a larger number of cases when the atmospheric stability is neutral (Figure 12). These conclusions are valid for the entire land areas over Europe — in northern and southern domains and in flat and mountainous areas.

For some of the regions over the sea the conclusions are similar to those carried out for land, but over some regions, e.g. Atlantic Ocean near the southern coasts of Spain and Portugal, or Eastern Mediterranean near Turkey, MYNN has stable conditions more often than YSU, and YSU has neutral conditions more often than MYNN.

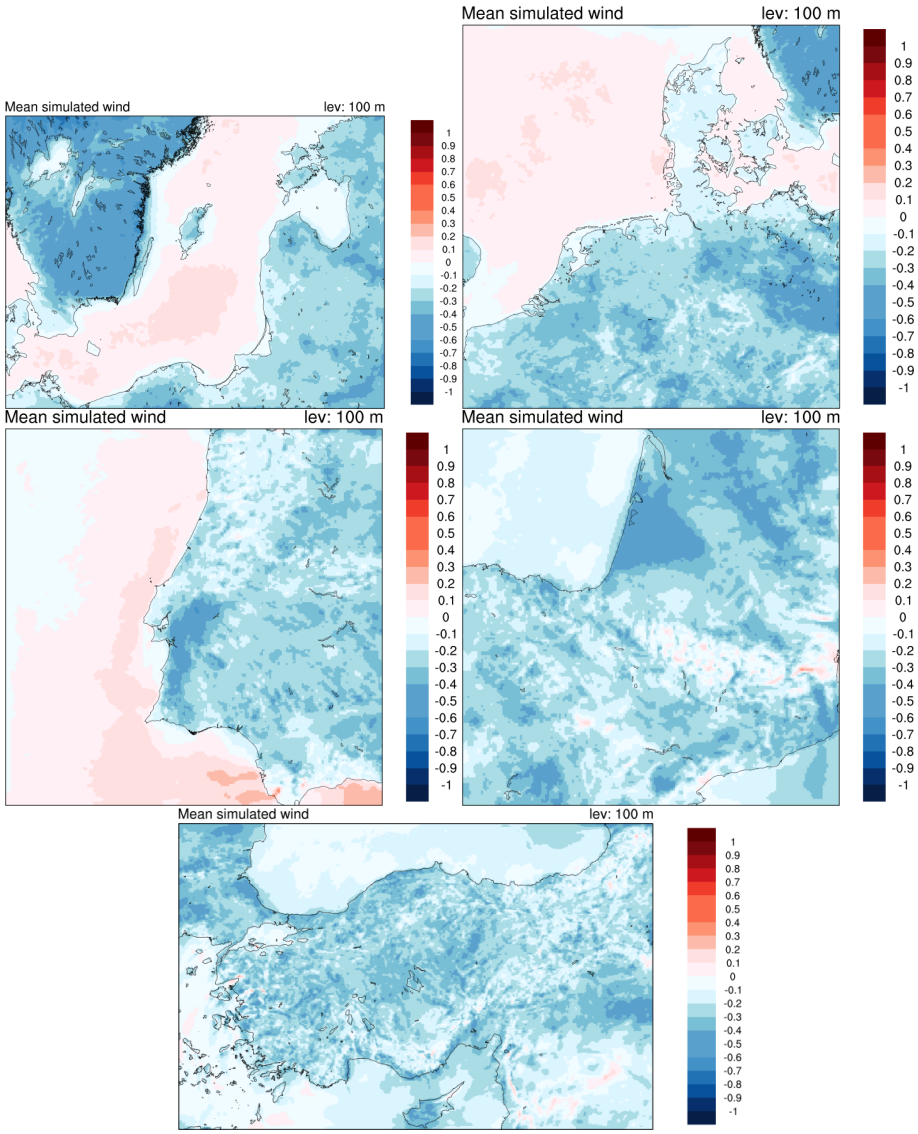

Figure 6. Differences in annual mean wind speed ($m\,s^{-1}$) for 2015 at 100 m between the MYNL61S1 and YSUL61S1 simulations for the five simulated domains.

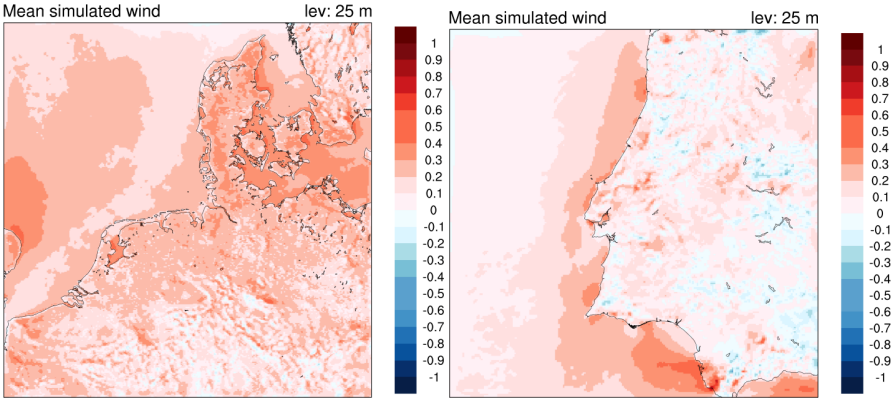

Figure 7. Differences in annual mean wind speed ($m\,s^{-1}$) for 2015 at 25 m between the MYNL61S1 and YSUL61S1 simulations for NW and PD domains.

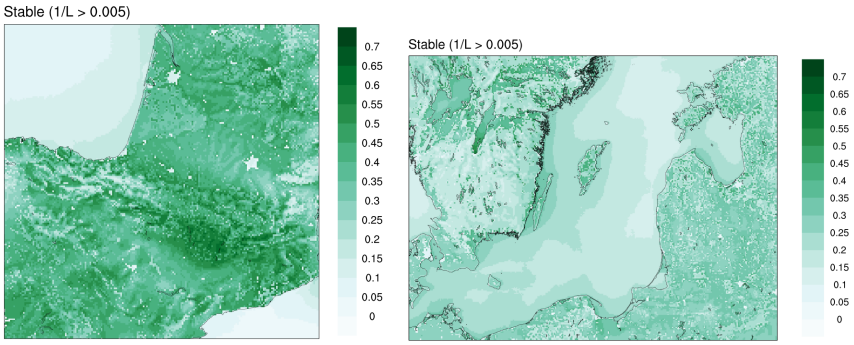

Figure 8. Fraction of the year 2015 when the atmospheric conditions are stable, SW and NE domains in the MYNL61S1 simulation.

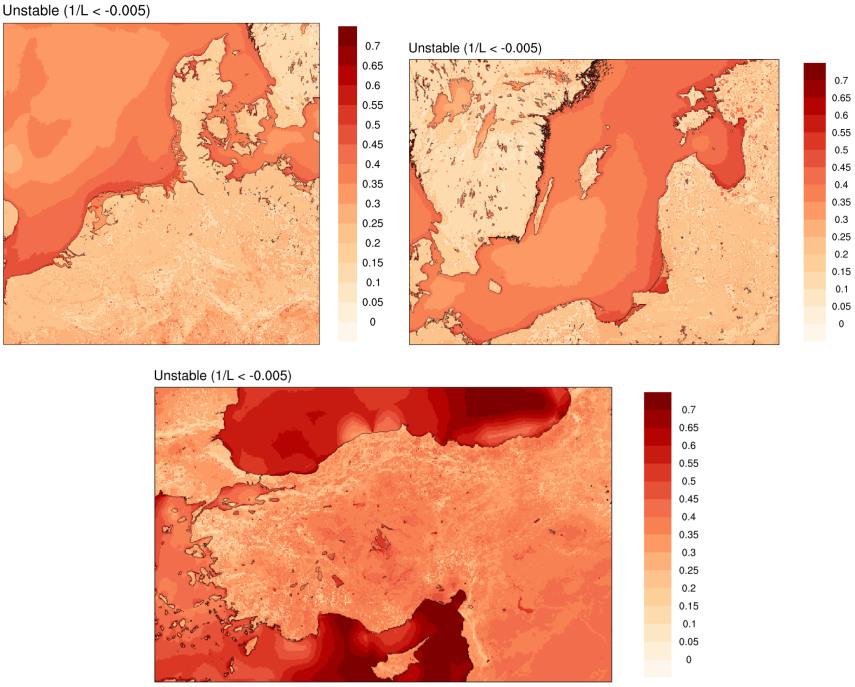

Figure 9. Fraction of the year 2015 when the atmospheric conditions are unstable, NW, NE and SW domains in the MYNL61S1 simulation.

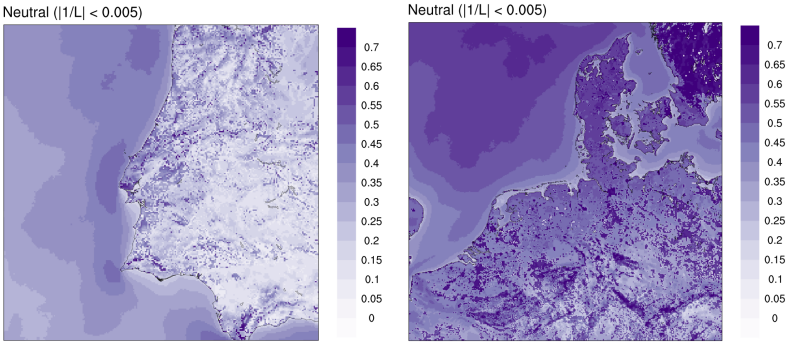

Figure 10. Fraction of the year 2015 when the atmospheric conditions are neutral, PD and NW domains in the MYNL61S1 simulation.

Another way how to depict these changes is to look at the distribution of the $1/L$ parameter in a single grid point. A representative land grid point, 50 km from the coastline, corresponding to one of the measurement locations in Latvia was chosen in NE domain, although regrettably no stability data are easily available in that grid point. In Figure 14 the histogram of $1/L$ values for that grid point is shown (full year 2015). The first and the last bin of the histogram contain all the data points in the interval to and from infinity. The histogram shows how the parameterisation scheme influences the atmospheric stability. There are more cases where the $1/L$ is close to 0 (neutral conditions) when using the MYNN scheme compared to the YSU scheme, consistently with what was shown above.

Therefore, although systematic biases between the different simulations are difficult to detect so far, it can be concluded at this stage that the choice of PBL scheme has a significant effect on the simulated wind and other parameters relevant for the wind resource assessment.

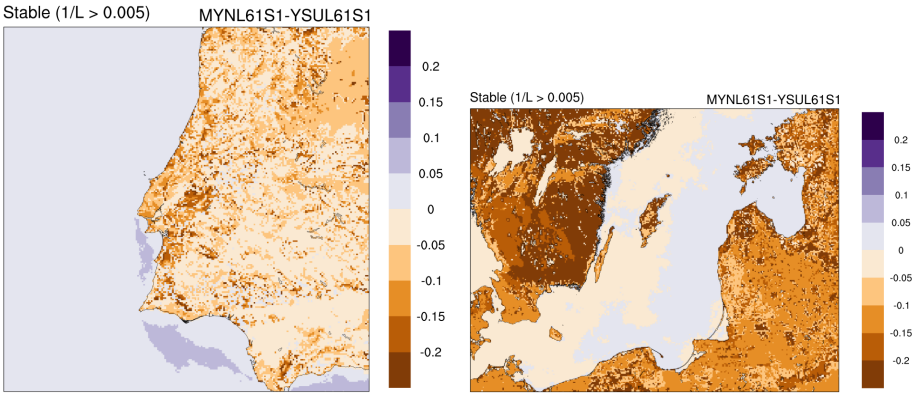

Figure 11. Difference in the fraction of time during 2015 when atmospheric conditions are stable between simulations MYNL61S1 and YSUL61S1 in the PD and NE domains. Brown indicates regions where MYNN has stable conditions less often than YSU, purple indicates that MYNN has stable conditions more often than YSU.

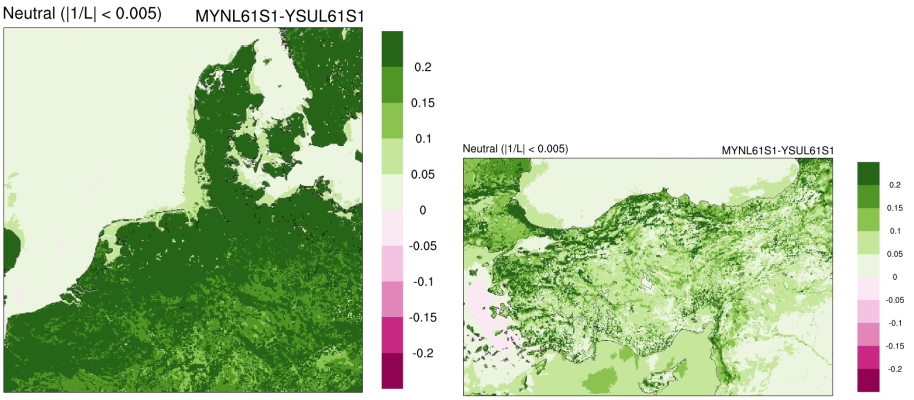

Figure 12. As in Figure 11 but for neutral conditions for the NW and SE domains.

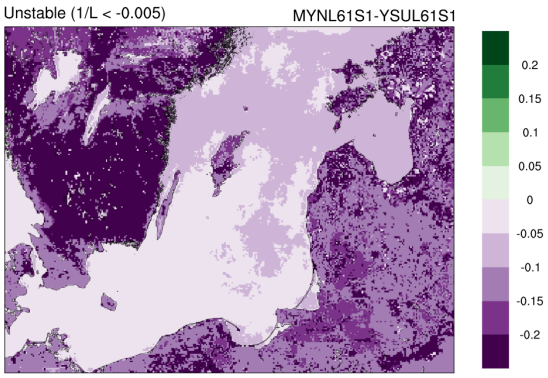

Figure 13. As in Figure 11 but for unstable conditions for the NE domain.

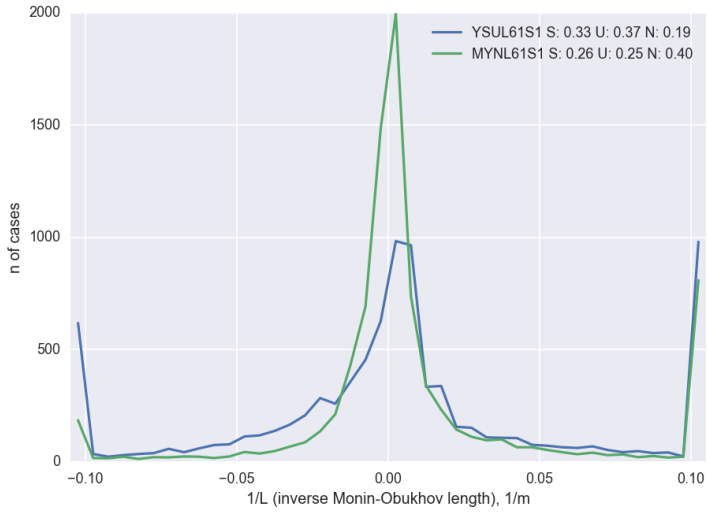

Figure 14. Histograms of inverse Obukhov length $1/L\,m^{-1}$ for the YSUL61S1 (blue) and MYNL61S1 (green) simulations during 2015. The first and the last bin contains all data points from and to infinity. Data are shown for a land grid point in the NE domain located at (57.710°N, 25.162°E).

Initialisation strategy As in any NWP model, errors in the simulation are expected to grow with the simulation length. There are two ways how to counter that. The first is to periodically re-initialise the calculations (e.g. daily), and the second is to force the simulations to follow the boundary conditions applying a nudging technique. In our sensitivity tests we have compared two nudging strategies: nudging in the outer domain (D1) only or in all domains (D1–D3, see Table 3). In the longer (weekly) simulations it is expected that the atmospheric flow will be better adjusted to the details of the terrain elevation and roughness absent in the forcing reanalysis. When comparing the wind speed simulated in the daily runs with that of the weekly runs using D1 nudging, the spatial pattern of differences is similar for both parameterisation schemes and seems to be determined primarily by orography. Figure 15 shows the difference between weekly and daily initialisation for both MYNN and YSU scheme for the PD domain. The differences have a magnitude of up to 0.5 m s^{-1}, thus only slightly less than the effect of the PBL scheme. Similar conclusions can be made for other regions. The differences between daily and weekly runs are smallest in the NE domain (not shown) that is the least mountainous.

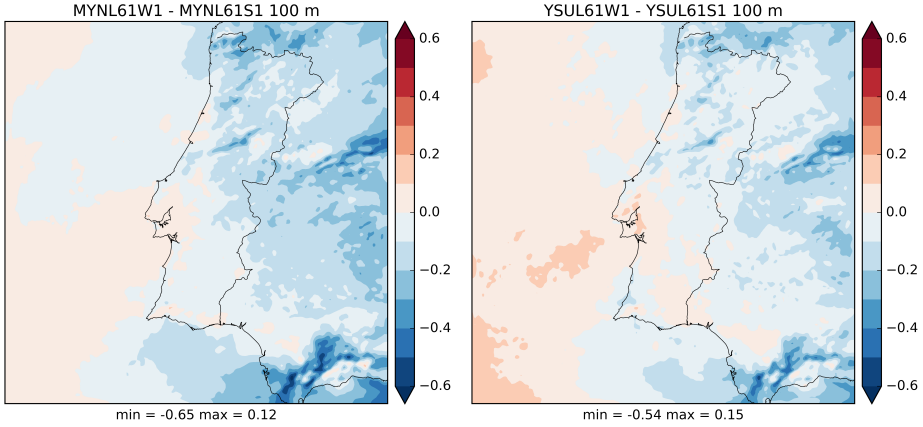

Figure 15. Differences in annual mean wind speed (m s^{-1}) for 2015 at 100 m in the PD domain between the MYNL61W1 and MYNL61S1 simulations (left), and the YSUL61W1 and YSUL61S1 simulations (right).

For the NW domain, the change from daily to weekly initialisation leads to a decreased wind speed in the whole domain (Figure 16 top). Applying nudging in all domains (right) amplifies this trend. For the SW domain the situation is more complicated (Figure 16 bottom). The change from daily to weekly initialisation with D1 nudging leads to both lower annual mean wind speeds in most of the domain but also to increased wind speeds in small regions. There seems to be some correlation with orography, i.e. lower wind speeds over elevated terrain in W3 compared to W1 simulations. Using the nudging in all domains leads again to an amplification of the differences in both directions. Some of these effects, including effects to the variance of the wind speed, have been explored by Vincent and Hahmann (2015).

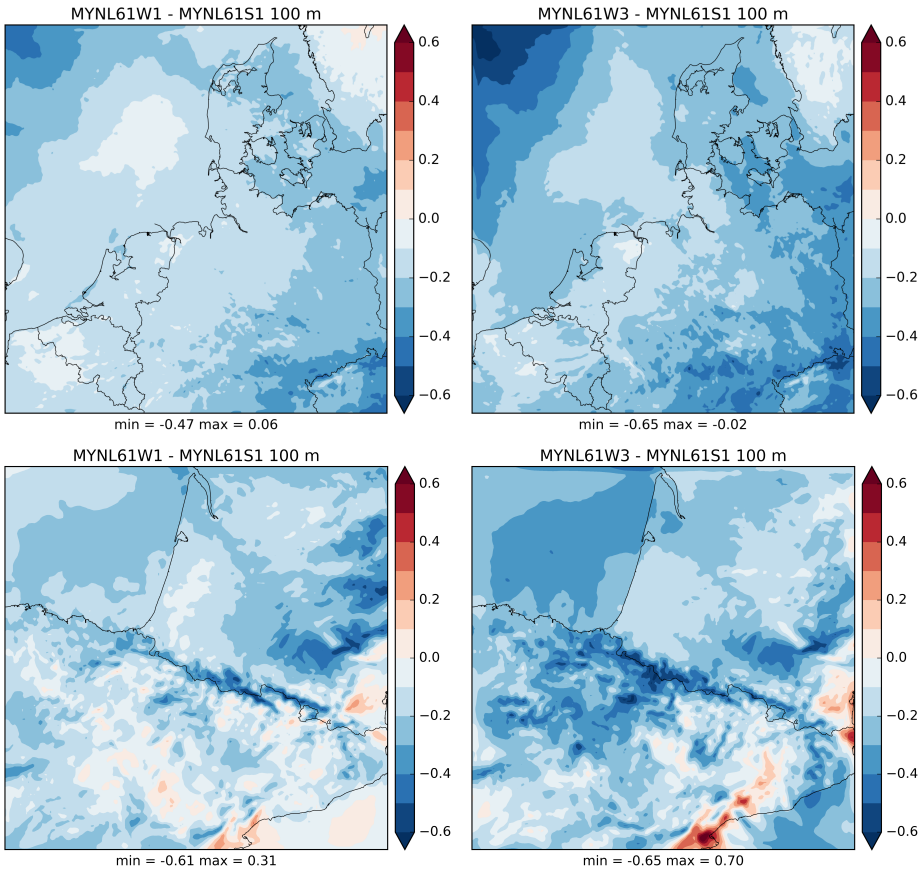

Figure 16. Differences in annual mean wind speed ($m\,s^{-1}$) for 2015 at 100 m between the MYNL61W1 and MYNL61S1 simulations (left), and the MYNL61W3 and MYNL61S1 simulations (right) for the NW (top) and SW (bottom) domains.

Analysis of variance The spatial distribution of the standard deviation of the hourly wind speed at 100 m height is similar to the distribution of wind speed (Figure 17) because it is a positive definite variable and therefore its values range from zero to the maximum wind speed. The standard deviation has high values ($> 4.5\,\mathrm{m\,s^{-1}}$) over the sea. Over the land, the highest values of standard deviation occur over complex terrain.

The change in the PBL scheme has a similar impact on the hourly wind speed variance than on the wind speed (Figure 18). The MYNN scheme results in lower variance over land, especially over the forested regions such as Southern Sweden where the variance in the MYNN results can reach less than 75% of the value for YSU scheme.

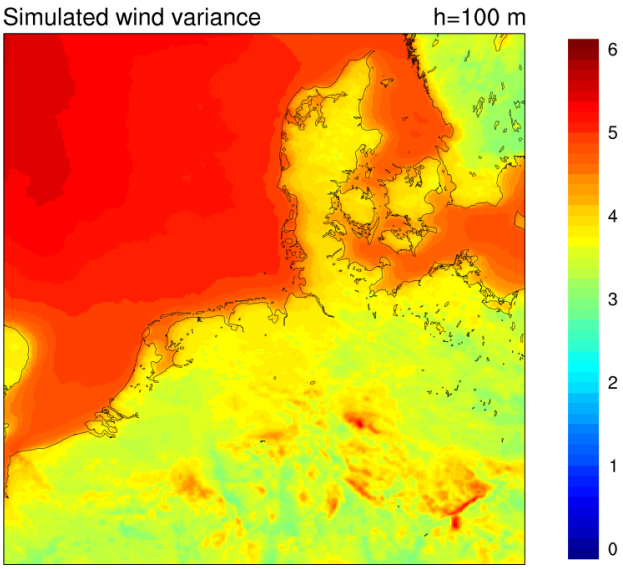

Figure 17. Standard deviation of hourly wind speed ($m\,s^{-1}$) at 100 m during 2015 in the MYNL61S1 simulation in the NW domain.

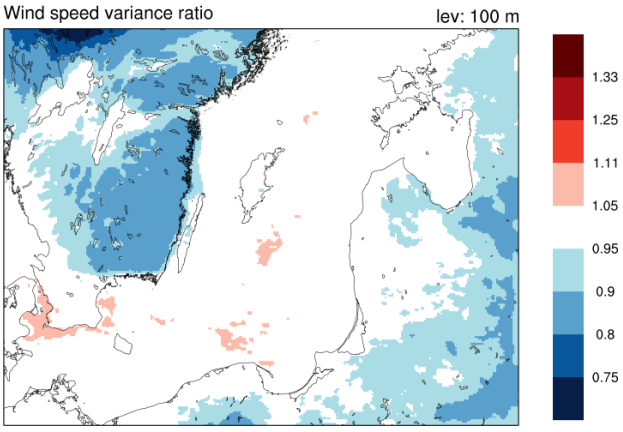

Figure 18. Ratio of the variance of the hourly wind speed at 100 m during 2015 between MYNL61S1 and YSUL61S1 simulations over the NE domain.

If the weekly initialisation is used instead of the daily initialisation (Figure 19), the hourly wind speed variance is decreased in all studied regions and there is little difference between land and water bodies. On average, the runs with weekly initialisation have ∼90% of the variance of the daily runs, except in the mountainous regions in Southern Europe where for the weekly runs the variance decreases to ∼80% of weekly runs. Therefore, it seems that the choice of the PBL

scheme tends to imprint the wind variability in relation with processes such as land-sea interactions (recall Figure 18) while the initialisation strategy effect on the wind variability is more related to the topography of the terrain.

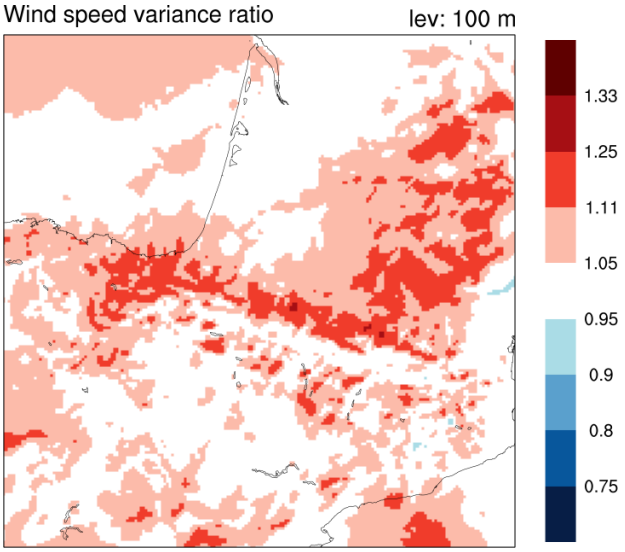

Figure 19. Ratio of the variance of the hourly wind speed during 2015 between the MYNL61S1 and MYNL61W1 simulations in the SW domain.

Analysis of overlapping domains As shown in Figure 3, the NW and NE domains overlap. This allows investigating the impact of computational domain placement on the results. The overlapping region is shown in Figure 20, it covers the southwestern corner of Sweden and parts of the Danish and German Baltic Sea coast. We selected six points (marked with crosses in Figure 20 for which we analysed the corresponding wind speed time series. For one of the points (the leftmost point offshore near the Swedish coast) the wind speed time series yielded by the two simulations (NW and NE) are compared for a period of one week in July 2015 in Figure 21 (left). While the general trend is similarly reproduced by the two simulations and the deviations are mostly within $1\,\mathrm{m\,s^{-1}}$, at certain time steps huge differences up to $8\,\mathrm{m\,s^{-1}}$ can occur. Figure 21 (right) displays the wind speed differences for all six points. For the other points the differences do not reach $8\,\mathrm{m\,s^{-1}}$ but are still significant. These differences can sometime occur due to phase errors, e.g. a wind speed ramp-up or ramp-down event is simulated with a small time-shift. Very often, maxima and minima have different amplitudes.

The spatial distribution of the differences between the NW and NE simulations is shown for one randomly selected point in time in Figure 22 (left). It shows large differences of the wind simulated in the two domains (up to $5\,\mathrm{m\,s^{-1}}$) confined in small areas. It is not an unexpected feature that the results of different simulations (with either different setup or different domain configuration) are not identical (Warner et al., 1997). At specific time steps, the simulated wind speed can deviate significantly from one simulation to the other. However, it is not necessarily relevant for the long-term statistics in which we are interested in terms of the wind atlas. Nonetheless, even on the annual average wind speed the domain placement has an effect (Figure 22 right). This is certainly much smaller than at hourly time scale but still on the order of $0.1\,\mathrm{m\,s^{-1}}$. Strong artefacts are visible near the northern and eastern boundaries of the overlap region (within 5–10 grid points) where the annual average wind speed can differ by up to $0.5\,\mathrm{m\,s^{-1}}$. These boundaries are corresponding to the domain boundaries of the NW domain. Thus, it is very important to consider a buffer zone near the domain boundaries that should be discarded when analysing the results.

The analysis of the standard deviation of wind speed reveals a spatial pattern that is correlated with orography, mainly with the distribution of land and sea (Figure 23). In general the standard

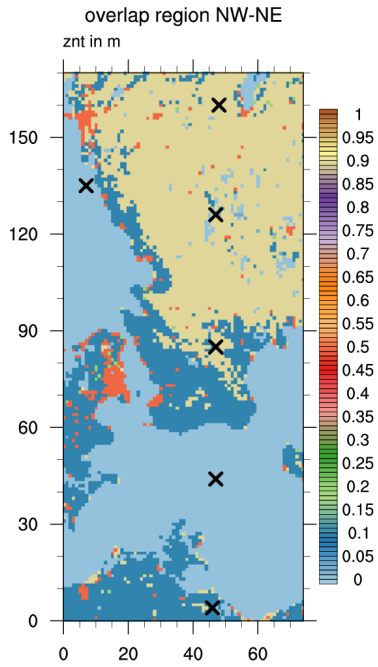

Figure 20. Surface roughness length (m) of the overlapping region between the NW and the NE domains. The crosses mark the evaluated points.

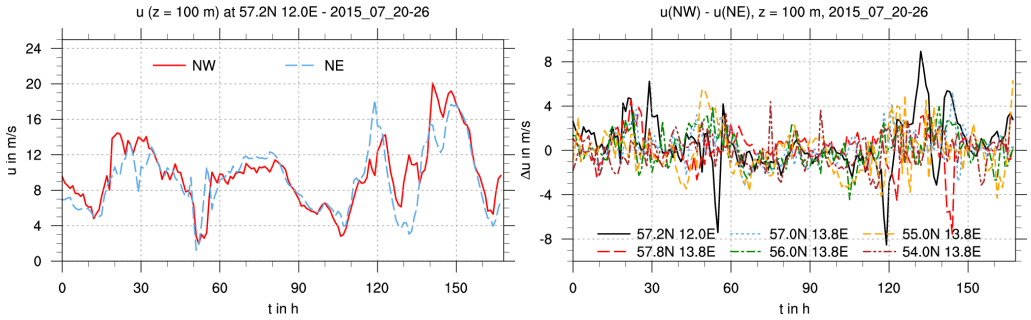

Figure 21. Left: One week long time series (20-26 July 2015) of wind speed at 100 m for one location simulated in NE and NW domains (westernmost point marked in Figure 20). Right: Difference between time series of wind speed at 100 m simulated in NE and NW domains for all the points marked in Figure 20 (same period as in left figure).

deviation is much higher over sea than over land which is not surprising given the higher offshore wind speeds. This pattern follows a clear annual cycle with highest standard deviations in spring and summer (when the water is usually much cooler than the air). Much lower standard deviations are found in autumn and winter when the land-sea pattern is not so pronounced.

Finally the wind speed distributions of the full year simulations are compared for two of the grid points (the previously mentioned point off the west coast of Sweden in the left plot and a point in the middle of the Swedish forest, second point from the top) presented in Fig. 24. While the distributions of the two points are quite different as expected, the distributions of the two simulations at each of the points are almost identical and show at least no systematic differences.

It can be concluded that the simulation results for particular locations or at certain time steps are largely depending on the domain configuration of the simulation. The differences depend on the location (land or sea) and season and can be significant when specific time steps or grid points

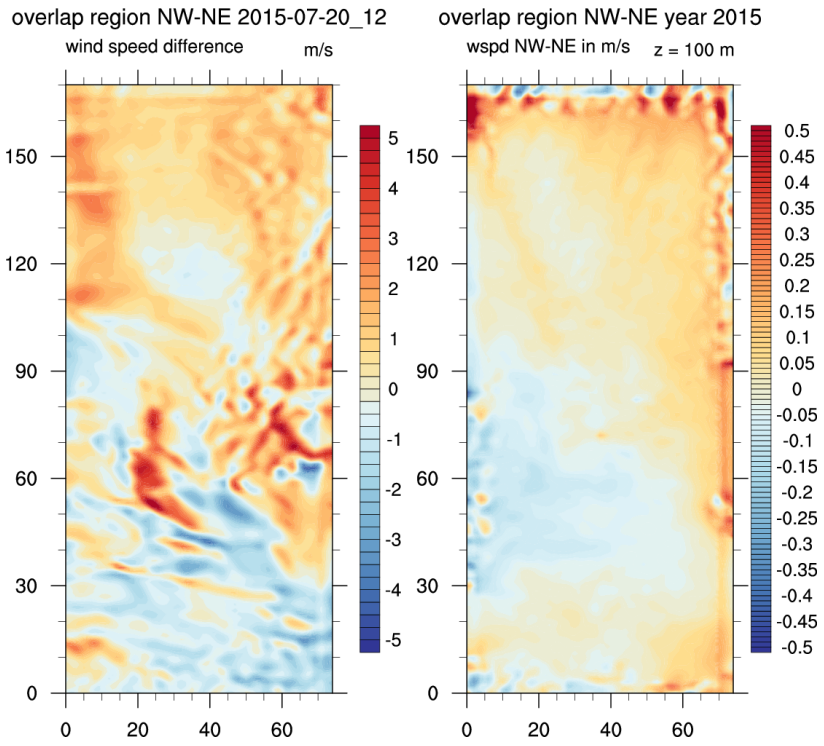

Figure 22. Differences in wind speed ($m\,s^{-1}$) at 100 m in the overlapping part of NW and NE domains. Left: Differences at one time step, right: differences in the annual average 2015. Note that the colour bars change. The axes are defined as grid point numbers of the overlapping part of the domain.

are analysed. They are however rather negligible regarding the long-term statistics. It is however important to discard data close to the boundaries of the simulation domain where the results show strange artefacts.

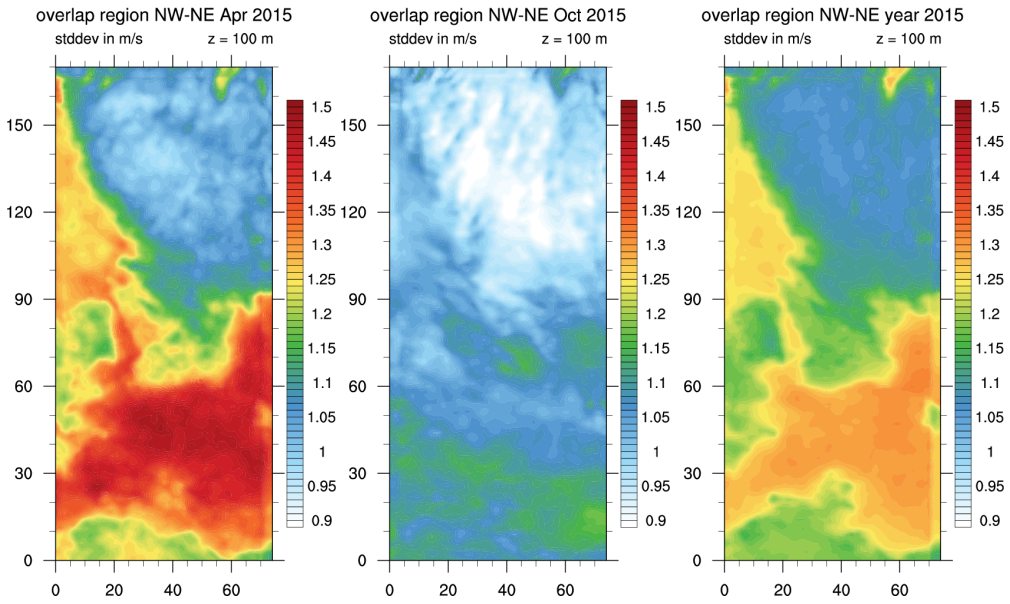

Figure 23. Standard deviation of the wind speed ($m\,s^{-1}$) at 100 m in the overlapping region of NW and NE domains for April (left), October (centre) and full year 2015 (right). The axes are defined as grid point numbers of the overlapping part of the domain.

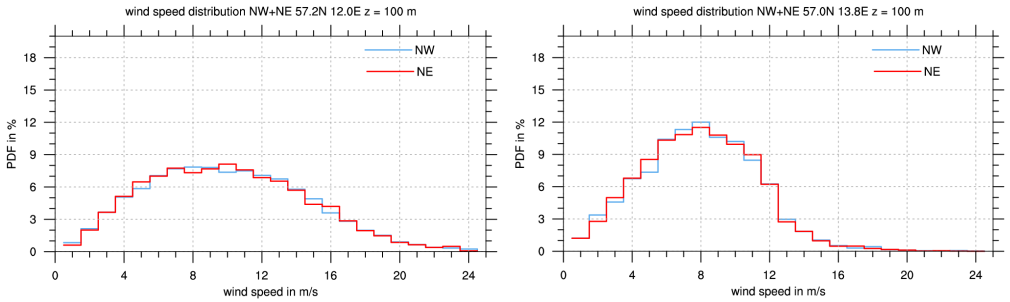

Figure 24. PDFs of the wind speed ($m\,s^{-1}$) for two grid points located off the west coast of Sweden (left) and in the Swedish forest (right) in the part of the overlapping domains.

2.1.4 Comparison with measurements

To complete the analysis of the initial sensitivity experiments, we compare the simulated wind in the NW domain results against wind observations from the tall masts described in Table 4, which are located as shown in Figure 25.

Of the eight sites used in the comparison, four are offshore, three are located over land, and one is coastal (i.e. within 2 km off the coast). The wind profiles were obtained by matching measurements and model values at each time and at all levels. The comparison in Figure 26 shows good agreement between measurements and WRF simulations for most sites, especially those offshore (FINO3 and IJmuiden) where the wind measurements are not affected by the mast flow distortion (e.g. FINO1 and FINO2). There are small differences among the various experiments, but most often the wind speed profile derived from the MYNNL61W1 simulation lies closer to the observations. The statistics in Figure 27 confirm this behaviour with MYNNL61W1 having lower biases in 5 out of 8 mast locations. For the correlations, the values range from 0.85 to

Site	Type	Heights AGL
FINO1	Offshore	100, 90, 80, 70, 60, 50, 40, 33 m
FINO2	Offshore	102, 92, 82, 72, 62, 52, 42 m
FINO3	Offshore	106, 100, 90, 80, 70, 60, 50, 40, 30 m
Høvsøre	Coastal	116.5, 100, 80, 60, 40, 10 m
Risø	Land	125, 118, 94, 77, 44 m
Østerild	Land	244, 210, 178, 140, 106, 70, 40, 10 m
Cabauw	Land	200, 140, 80, 40, 20, 10 m
IJmuiden	Offshore	315, 290, 265, 240, 215, 190, 165, 140, 115, 89, 58, 27 m

Table 4. Tall meteorological mast sites used in the wind speed comparison. The heights are those of the wind speed measurements. The measurements at IJmuiden are complemented by lidar above 100 m.

Figure 25. Location of the sites in Table 4 used in the comparison.

0.91, with almost identical values for the two weekly simulations. Overall, the weekly simulations (weakly) outperform the daily ones and the MYNN simulations (weakly) outperform the YSU simulations. However, the differences between the stations are in most cases larger than the differences between the simulations.

2.1.5 Implications for the NEWA Production run

The results from sensitivity experiments for all five domains showed that in most cases the conclusions about the sensitivity of results made for one of the domains can be reasonably applied to other domains. With this information in mind the next phase of sensitivity experiments described in Chapter 2.3 was performed only for one or two domains to efficiently use the available computational resources.

The results from the comparison against tall masts showed that on average the MYNN scheme run in weekly nudged mode (MYNL61W1 simulation) outperforms the other simulations. This simulation will thus be the reference configuration of the second phase of sensitivity simulations.

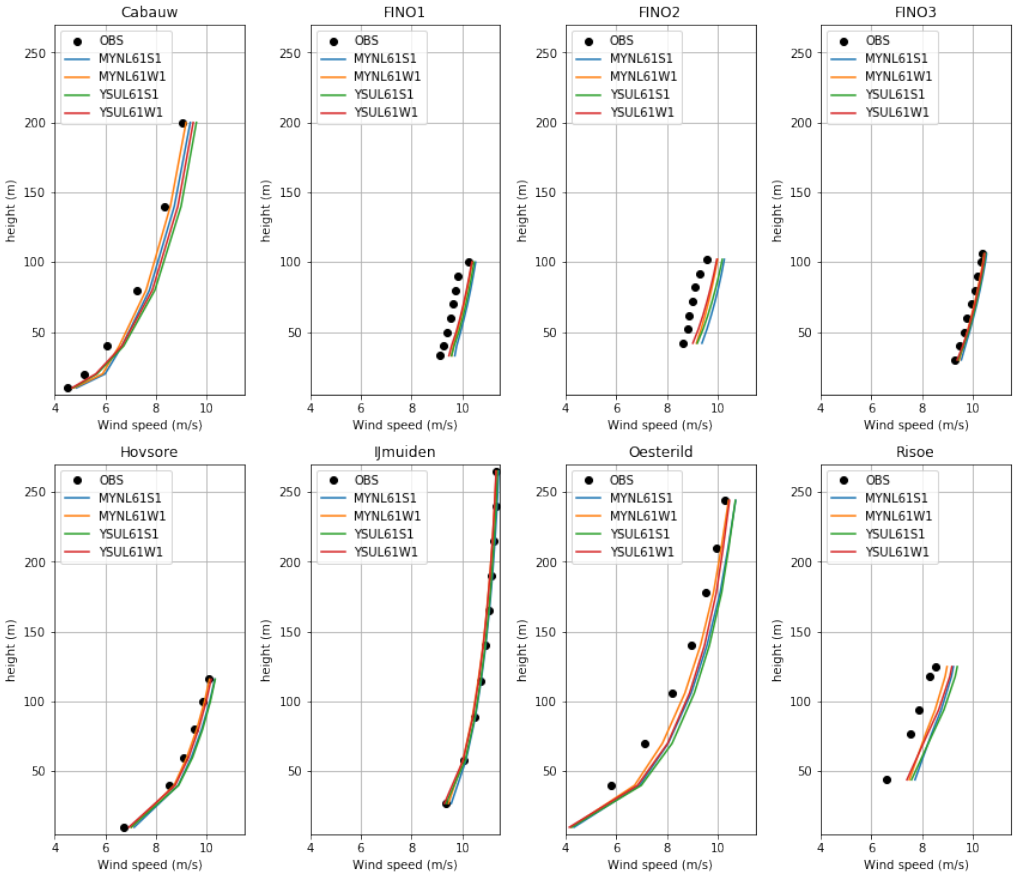

Figure 26. Annual mean wind speed ($m\,s^{-1}$) profile simulated by the various sensitivity experiments in Table 3, for the 8 sites in the NW domain. The black dots represent the measurements, the lines the WRF-derived winds.

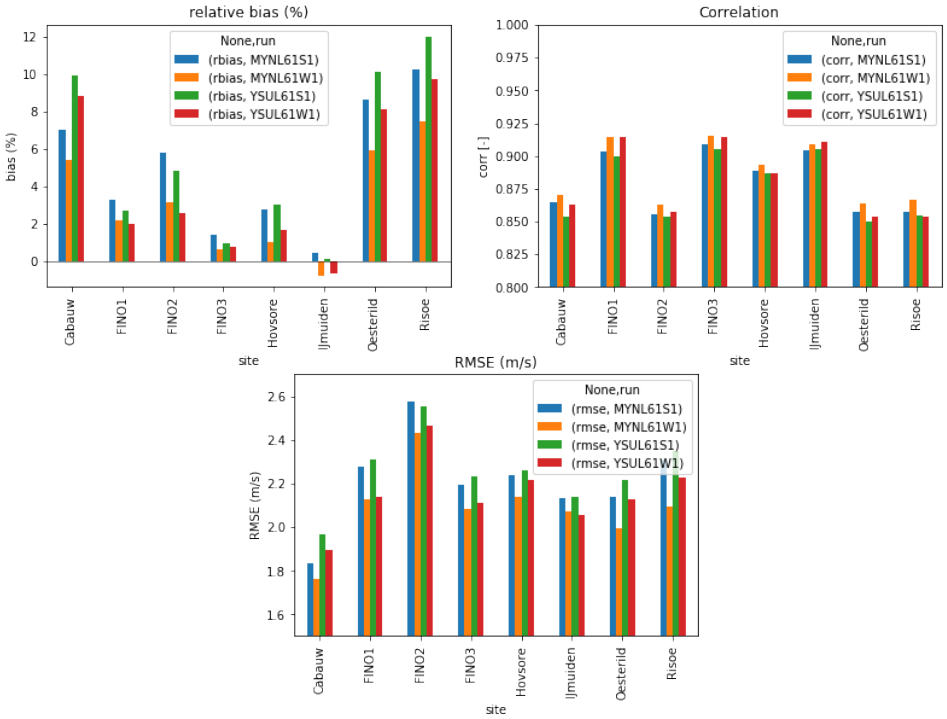

Figure 27. Comparison of the wind speed statistics (bias, top left, correlation, top right and RMSE bottom) from the various sites and simulations for 2015 and the various WRF simulations in Table 3.

2.2 Sensitivity to domain size

An additional decision to be made regarding the NEWA mesoscale simulations has to do with the domain configuration. The domain or several small domains need to cover all of Europe, but it is unclear what is the best approach. From a pure computational perspective, one single domain is more efficient, because the WRF model code scales better with larger domains and there is only data from one domain to post-process. However, the output files are very large and the simulation needs to be completed before post-processing can begin. Furthermore, large areas outside of the region of interest (the NEWA domain) would be simulated, e.g. parts of the Atlantic Ocean, the Norwegian Sea and non-EU countries in Eastern Europe, thus a substantial amount of computational resources would be wasted. Apart from these technical questions it was unknown how the domain size influences the quality of the simulated fields.

To study this we carried out simulations for three differently sized domains over the North Sea using the same resolution as in the previous experiments (27 km, 9 km, 3 km). The sizes are listed in Table 5 and the domains shown in Figure 28. The three domains are centred at the same coordinates and only differ by the number of grid points. Two sets of WRF simulations were done, one with daily runs (see MYNNL61S1 in Table 3, labelled "S1") and one with weekly runs (MYNNL61W1, labelled "W1"). The simulations cover the full year 2015.

name	num grid points	domain size
Small (SM)	121 x 121	360 x 360 km
Medium (MD)	241 x 241	720 x 720 km
Large (LG)	481 x 481	1440 x 1400 km

Table 5. Grid dimensions of the innermost domains used in the domain size experiments.

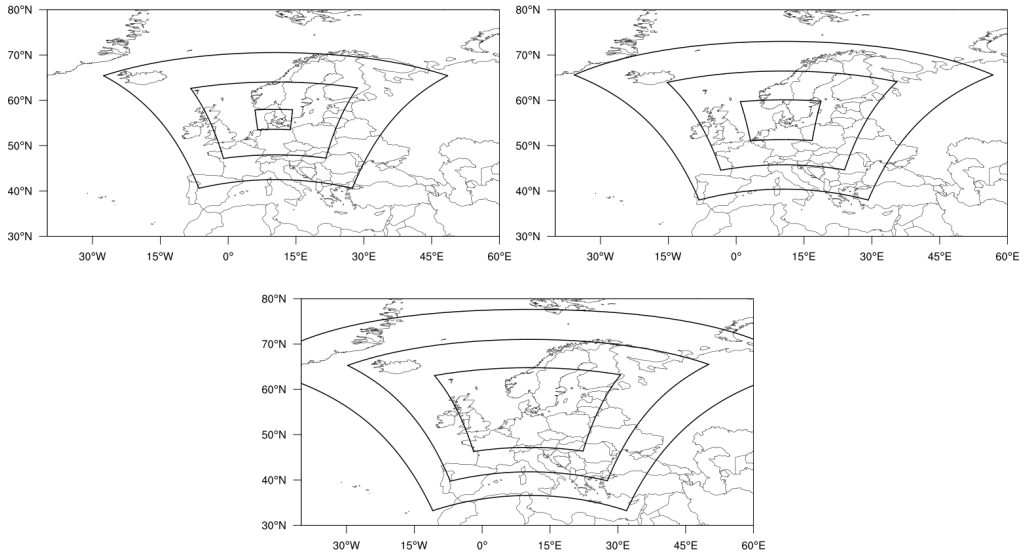

Figure 28. Size and location of the 3 domain configurations used in the simulations: SM (top-left), MD (top-right) and LG (bottom).

For evaluating the results of the simulations we use the same data as in Chapter 2.1.4, but only 6 of these masts are contained within the smallest (SM) domain. Figure 29 shows considerable

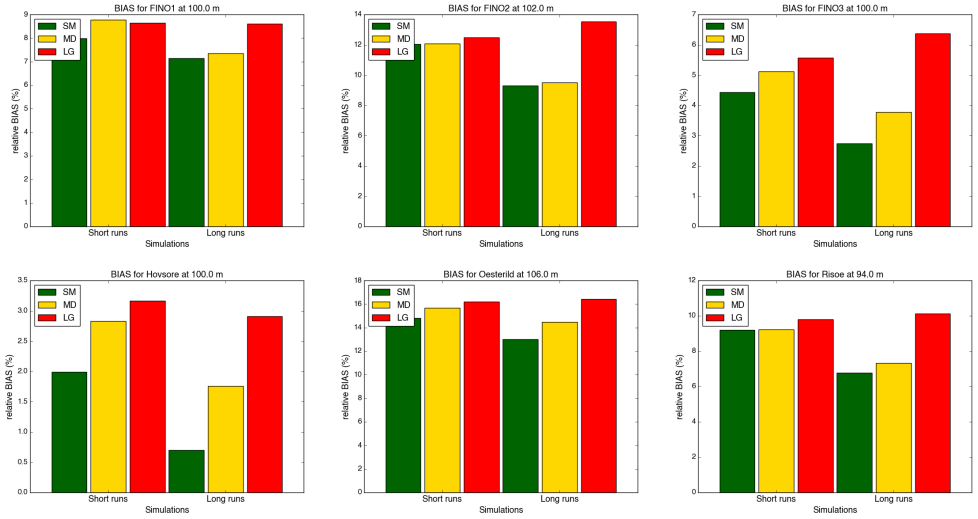

Figure 29. Relative bias (%) in annual mean wind speed for each domain size and simulation length for FINO1, FINO2, FINO3 (top) and Høvsøre, Østerild and Risø (bottom).

differences in the bias (with respect to the observations) among the results from the various domains. In general the biases are smaller in the SM domain and the weekly simulations (SM-W1).

site	height (m)	worst sim	bias (%)	best sim	bias (%)
FINO1	100	MD-S1	8.8	SM-W1	7.1
FINO2	102	LG-W1	13.5	SM-W1	9.3
FINO3	100	LG-W1	6.4	SM-W1	2.7
Høvsøre	100	LG-S1	3.2	SM-W1	0.7
Risø	94	LG-W1	10.1	SM-W1	6.8
Østerild	106	LG-W1	16.4	SM-W1	13.0

Table 6. Summary of the annual mean wind speed bias, $(\overline{U}_{WRF} - \overline{U}_{OBS})/\overline{U}_{OBS}$ among the simulations. The "worst" and "best" simulations with their value are specified.

The biases from all simulations are summarised in Table 6. For 5 out of 6 sites the LG-W1 simulation has the largest biases, and for all sites the SM-W1 simulation has the smallest biases. Similar results (not shown) emerge for the correlation and the RMSEs.

An interesting issue is to look at the spatial variations of the differences between the simulations. In Figure 30, we show the difference in annual mean wind speed between the MD and LG domains compared to the SM domain for the weekly (W1) simulations. The annual mean wind speeds in the MD and SM simulations are nearly identical, but the differences between the LG and SM are always positive and quite large. The results are almost identical in the short simulations. Further investigations (not shown) revealed that the results can be partly explained by the size of D2, but not entirely. An extra experiment was carried out changing the initialisation time from 00 to 12 GMT, this has negligible effect in mean wind speed.

In conclusion, biases in mean wind speed are influenced by the size (and possibly also location) of the domain, smaller domains have generally lower wind speeds and lower biases. This effect is most pronounced in the long and "nudged" simulations. Time correlations decrease (and RMSE increase) with increasing domain size and integration time.

The results from these experiments guided the design of the NEWA domains for the production

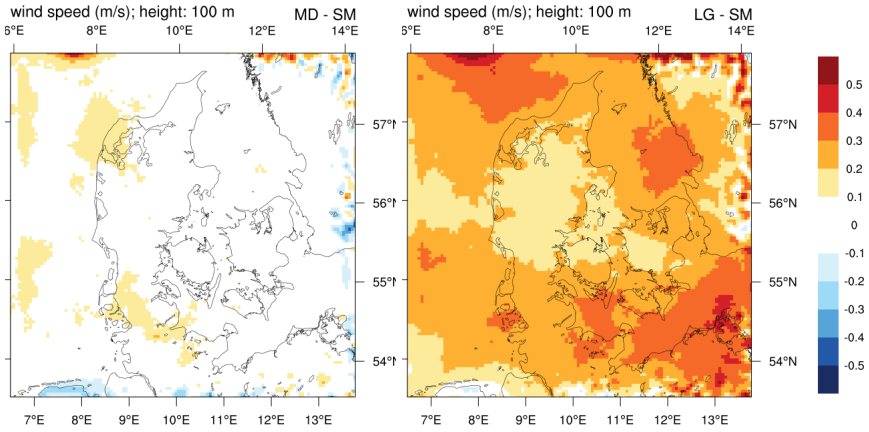

Figure 30. Differences in annual mean wind speed ($m\,s^{-1}$) from SM short simulations at 100 m AGL for: MD (left) and LG (right).

run. Instead of a single, or a few, very large domains, we chose to conduct the simulations in a rather large number of medium-sized domains. While generating different time series, overlap areas in simulations generally show similar wind climates (see Chapter 2.1.3). We decided, however, against very small domains as e.g. used in the Global Wind Atlas. In terms of accuracy they would probably perform better than our chosen configuration, but most countries would be covered by multiple domains and would face overlapping issues. We wanted each country to be covered by only one domain to avoid any overlapping issues (i.e. inconsistent time-series for neighbouring grid points, see also Chapter 2.1.3). The final domain configuration for the mesoscale wind atlas fulfils this requirement for all countries except Norway and Sweden which are so elongated that a correspondingly huge domain would be detrimental to the accuracy of the results.

The final domain configuration chosen for the production run of the NEWA mesoscale atlas will be presented in Chapter 3.

2.3 Further sensitivity experiments in the NW domain

After completion of the initial sensitivity experiments (Chapter 2.1) many other settings of the WRF model and the simulations required a final decision. Our approach was based on investigating each setting separately. This resulted in a large set of sensitivity tests that are documented in this chapter. This exercise contributes to evaluate the WRF simulated wind to various configuration alternatives as well as to other physical parameterisations potentially relevant for a realistic representation of the wind field. The sensitivity analysis was performed over a single European sub-domain to allow for a more intensive testing with multiple variants that would be computationally unaffordable if all domains are used in this part of the analysis.

2.3.1 Summary of the sensitivity tests

Early in the project only medium resolution reanalysis data such as ERA-Interim (∼80 km) or MERRA2 (∼50 km) were available, therefore the outer domain had significantly higher resolution (27 km) than the forcing data. With the more recent availability of ERA5 data with ∼30 km grid spacing, the outer domain has approximately the same grid spacing as the forcing data. As the final NEWA setup consists of a number of small domains (see Chapter 3) it was deemed necessary to keep a common outer domain to homogenise inputs to different inner domains.

The collaborative nature of the project led to the fact that a number of different HPC systems were used. Much work was devoted to ensure that technical setup details are harmonised between different groups, such as namelist parameters and input files. Some of the technical aspects and the main sensitivity experiments are summarised in the following paragraphs.

The WRF model allows to set the numerical time-step to a constant value or to allow it to change adaptively as a function of the time-varying CFL value, as a condition to deal with the stability of processes. Both of these options were tested. When a constant time step was used, the value of 90 seconds worked reasonably for flat domains and standard meteorological situations. However, it was necessary to reduce the time step to lower values (20–60 seconds) for some dates to avoid model crashing. Similarly, the adaptive time step sometimes leads to model crashes, probably because all the parameters needed were not correctly chosen. In particular, the `truelat1` and `truelat2` (set to 20°N and 40°N, respectively), which define the Lambert Conformal projection, made the map factors large (∼ 1.3) in the northern part of the outer domain because of the very large domain dimensions. Further investigation showed that the projection could be made more stable by modifying these parameters (to 30°N and 60°N) and thus moving the map factors closer to one.

The main sensitivity experiments were (see also Table 7):

- Each year a new **version of the WRF model** is released. Three different WRF versions were tested. Usually, significant changes to the physical parameterisations are implemented as new options. In version 3.8, however, the MYNN PBL scheme underwent significant changes that impacted the wind speed climate without a new name being assigned to it. Most of the verification statistics were altered for the worse. That necessitated tests whether changing a combination of namelist options can reverse impact on the wind speed climate.
- Tests were carried out to determine the effect of **vertical resolution**, both by increasing the number of levels to see whether that improves the results, and by decreasing the number of levels to see whether computational resources can be used more efficiently.
- Data from the ERA-Interim (Dee et al., 2011) reanalysis were used as baseline option for **forcing data**, and newly available reanalysis with higher resolution ERA5 (ECMWF, 2016)

was tested. In addition, the MERRA2 reanalysis (Gelaro et al., 2017) was investigated as a possible source of forcing data.

- Wind speed climate close to surface of the Earth is influenced by the properties of the surface and therefore **land surface parameterisation** schemes were investigated.
- By default in each grid cell only the **surface roughness** from the dominant category is used. As a way to improve results an approach that would take into account all the land use categories was tested.
- An effect of the **simulation length** on the results has already been found in the initial sensitivity experiments (Chapter 2.1) for weekly *vs.* daily simulations. Here, we made an additional test, comparing a continuous 8-week long simulation against the results of eight 1-week simulations.
- By default 1-way nesting has been used in all simulations, i.e. information is passed from the outer to the inner domains and not vice-versa. In one simulation a **2-way nesting** has been tested, i.e. information exchange from the inner domain back to the outer domains.
- Theoretically the results using the same model setup on two different **HPC systems** should provide identical results. In practice that is not the case and this question was investigated running the same model setups on a number of different HPC systems.

Option	**Baseline**	**Other tested options**
WRF version	3.6 with bug fixes	(1) WRF V3.8.1 (2) WRF V3.9.1 (3) Modified WRF V3.8.1
Model levels	61	(1) 91 (2) 41 (3) 41 with more levels in PBL
Nesting	1-way	2-way
Land Surface	Noah LSM	(1) Noah-MP (2) Noah-MP alternate SL drag coef. (3) RUC (4) CLM-4
Initial and Boundary conditions:		
	ERA Interim native resolution	(1) ERA Interim $0.75^\circ \times 0.75^\circ$ (2) ERA5 $1^\circ \times 1^\circ$ (3) ERA5 $0.25^\circ \times 0.25^\circ$ (4) MERRA2
Surface roughness	Dominant category	Aggregated roughness
HPC system	–	Eddy (ForWind [a]) MareNostrum4 (BSC, PRACE [b]) Marconi (CINECA, PRACE [c])

Table 7. Summary of the various options tested in the second phase of the sensitivity experiments.

[a] https://uol.de/fk5/wr/hochleistungsrechnen/hpc-facilities/eddy/
[b] https://www.bsc.es/marenostrum/marenostrum
[c] http://www.hpc.cineca.it/hardware/marconi

Other options were held constant for all model runs. We used the CORINE Land Cover (CLC, Copernicus Land Monitoring Service (2019)) at 100 m resolution. The surface roughness length for each land cell was assumed to be constant over time, i.e. the annual cycle variations were

disabled, except for the cases where the roughness coefficient is modified by the snow cover. The Sea Surface Temperature (SST) and sea ice concentration came from OISST (Reynolds et al., 2002). The simulations cover the period of 1 January to 30 December 2015, if not otherwise indicated. Physical parameterisation schemes other than the land surface model were not tested in this round of sensitivity experiments. The options used are described in Table 7. The numerical and nudging options also were held constant as summarised in Table 2.

2.3.2 WRF version

The change of the WRF version can lead to considerable changes in the simulated wind climate. This is often related to changes in parameterisations that inherently affect the results. However, if a WRF version upgrade contains a number of significant changes, then it can be quite difficult to trace back the exact cause of differences.

The initial sensitivity experiments (Chapter 2.1) were performed using WRF version 3.6.1, released 14 August 2014, which was the most recent stable WRF version at the time we drafted these experiments. When conducting this second phase of sensitivity experiments, a few more recent WRF versions were available, up to 3.9.1.1. Version 3.6.1 was therefore compared to V3.8.1 (released 12 August 2016) and V3.9.1.1 (released 28 August 2017). An overview of the comparisons and associated figures is given in Table 8. As Figure 31 (left) shows, the differences between WRF V3.8.1 and V3.6.1 are significant with considerably higher annual mean wind speeds over land (up to 1.25 m s^{-1}) and slightly lower wind speeds over sea (less than 0.5 m s^{-1}). In contrast, the differences between V3.9.1.1 and V3.8.1. are small (Figure 31 right) and do not exceed 0.15 m s^{-1}.

	V3.8.1	V3.8.1 mod v1	V3.8.1 mod v2	V3.9.1.1
V3.6.1	Figure 31	Figure 33	Figure 33	
V3.8.1		Figure 34	Figure 34	Figure 31
V3.8.1 mod v1			Figure 34	

Table 8. Overview of the figures showing differences between the various WRF versions. The differences are shown as the version in the column minus the version in the row.

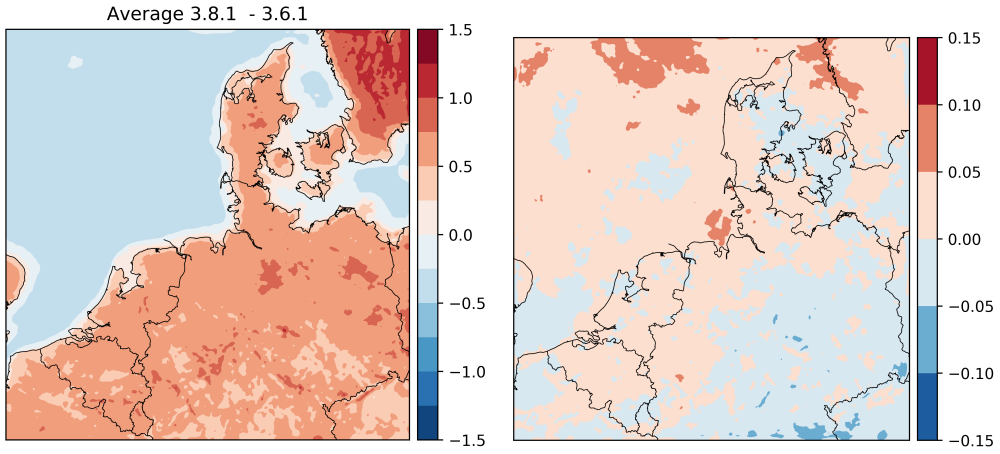

Figure 31. Differences in annual mean wind speed (m s^{-1}) at 100 m for 2015 between WRF versions: V3.8.1 minus V3.6.1 (left) and V3.9.1.1 minus V3.8.1 (right). Note the different scales.

To check if the simulated model wind climate have improved or deteriorated with WRF V3.8.1 (and V3.9.1.1) compared to V3.6.1, the results were compared against observations. The same sites as in Chapter 2.1.4 have been used. Figure 32 confirms the clear differences between V3.6.1 and V3.8.1, whereas V3.8.1 and V3.9.1.1 give almost identical results. For the majority of stations the results are in closer agreement to the observations with V3.6.1 than with the newer version, which shows a clear increase in bias.

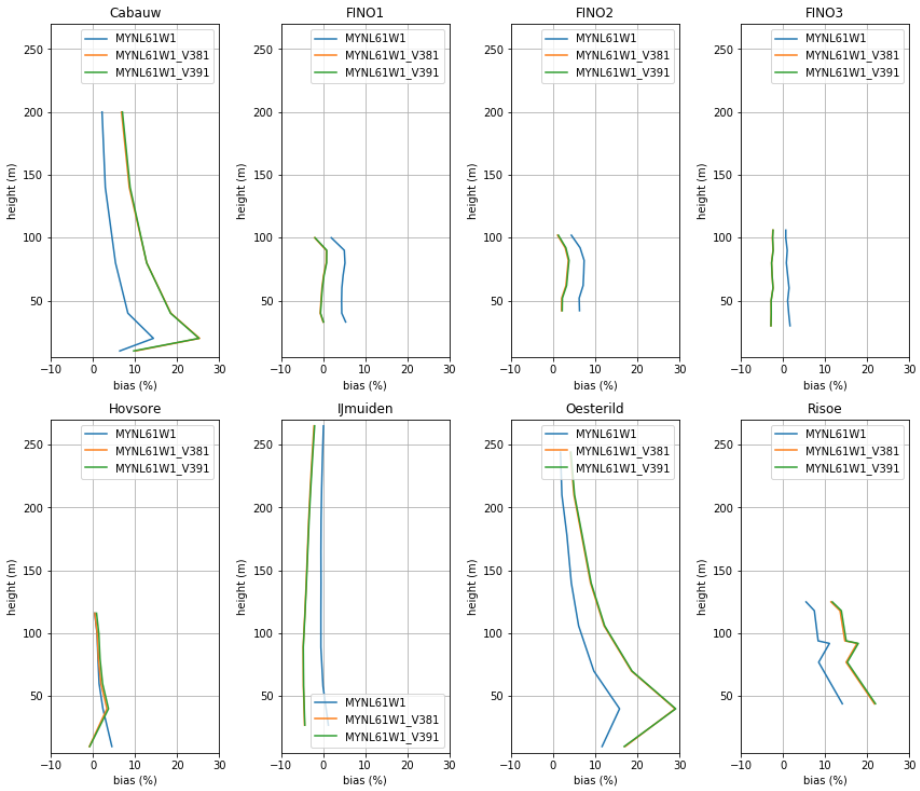

Figure 32. Vertical profiles of the bias (%) in the annual mean wind speed at 100 m height between WRF versions (V3.6.1, V3.8.1 and V3.9.1.1) and mast measurements. Note that the orange curves are superposed by the green curves.

The differences could be traced back to significant modifications of the MYNN PBL and surface layer schemes in WRF V3.8 (Olson et al., 2016). However, it was possible to revert two of the most important changes by external namelist parameters and a minor change in the code (see Olson et al., 2016). In the MYNN surface layer model, the drag coefficient parameterisation over water (COARE algorithm) was updated to version 3.5 (Edson et al., 2013). This change could be reverted by setting `COARE_OPT=3.0` in the MYNN surface layer model subroutine. In the MYNN PBL scheme, the mixing length formulation was revised and made controllable by a new namelist parameter. By switching `bl_mynn_mixlength` from the new default option 1 to option 0, the old version of the mixing length formulation can be restored. Two modified versions of WRF V3.8.1 were tested. The first version ("3.8.1 mod v1") used the option `bl_mynn_mixlength=0` , the second version ("3.8.1 mod v2") used both `bl_mynn_mixlength=0` and `COARE_OPT=3.0`.

To understand the impact of all these changes to the wind climatology, every two runs were compared (see Table 8 for explanation). The results show that it is not enough to just change the `bl_mynn_mixlength` option (Figure 33 left). WRF V3.8.1 mod v1 produces results that are similar to WRFV3.6.1 over land, but over the sea the wind speed is even lower than from the unmodified V3.8.1. Introducing both changes (Figure 33 right) leads to results that differ from the WRF V3.6.1 results by less than 0.5 m s^{-1}.

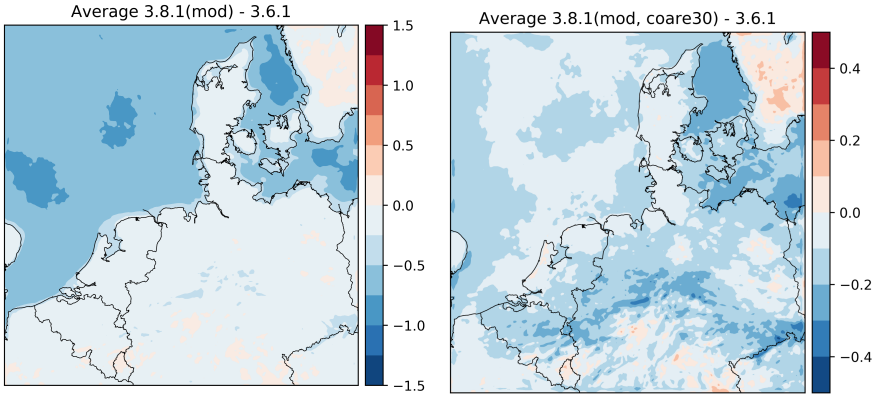

Figure 33. Differences in annual mean wind speed ($m\,s^{-1}$) at 100 m during 2015 in the NW domain between the modified versions of WRF: WRFV3.8.1 (mod v1) minus WRFV3.6.1 (left) and WRFV3.8.1 (mod v2) minus WRFV3.6.1 (right) .

The comparison of the modified and unmodified WRF V3.8.1 shows that changes in the first option (Figure 34 left) significantly lowers the wind speed over land, and minimally over water. Changes in both options (Figure 34 centre) lowers wind speed over the land and increases the wind speed over water. The effect of adding `COARE_OPT=3.0` can be seen in Figure 34 (right). The wind speed over land is unchanged, but it is increased over water.

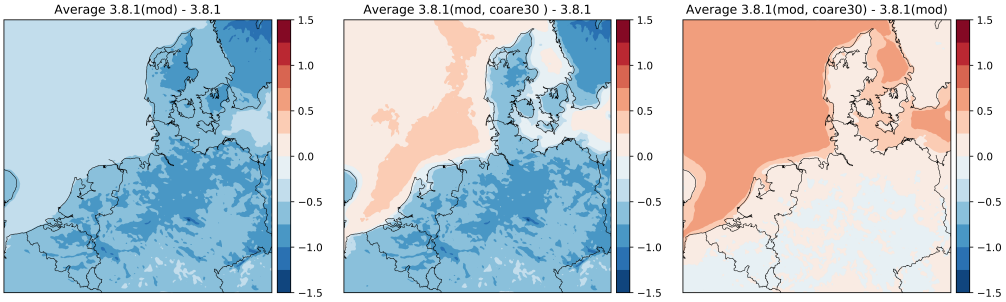

Figure 34. Differences in annual mean wind speed ($m\,s^{-1}$) at 100 m for 2015 and the NW domain between WRF versions: WRF V3.8.1 (mod v1) minus V3.8.1 (left), V3.8.1 (mod v2) minus V3.8.1 (centre), and V3.8.1 (mod v2) and V3.8.1 (mod v1) (right).

The comparison against measurements (Figure 35) confirms that for the majority of investigated locations using WRF V3.8.1 with reverted changes in MYNN improves the results and yields very similar results as V3.6.1.

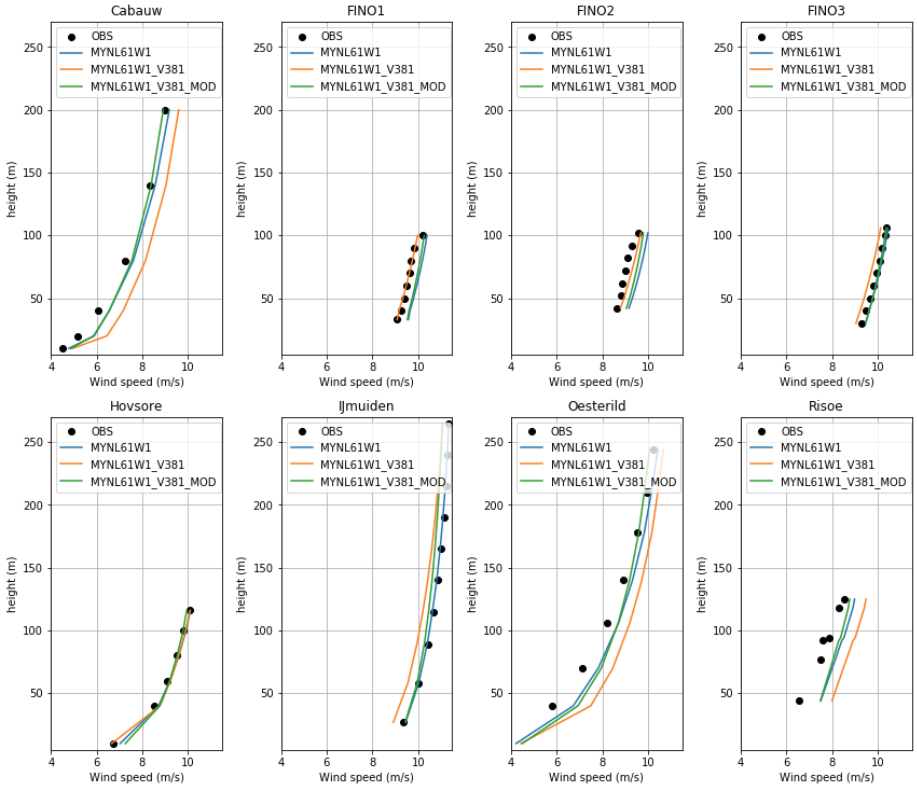

Figure 35. Comparison of annual mean wind speed ($m\,s^{-1}$) at 100 m of different WRF versions and measurements. Black dots are the observations, the blue lines correspond to WRF V3.6.1 simulated wind, orange lines to V3.8.1 and green lines to V3.8.1 (mod v2).

2.3.3 Number of vertical levels

The number of vertical levels used in the WRF simulations is a parameter that can be chosen freely, but should be chosen together with the horizontal grid spacing. Theoretically, an increase in the number of vertical levels should lead to more accurate results, however, that would also increase the computation time. The baseline number of levels of 61 was chosen from previous works (Hahmann et al., 2015; Zhang et al., 2016). The height of the lowest 10 levels (in m above the ground level (a.g.l.)), is approximately 6, 22, 40, 56, 73, 90, 113, 140, 179 and 205 m. Additional runs were carried out using 91 vertical levels. These runs did not significantly change the results and would require more computing power, and probably require to lower time steps to keep the simulations stable in mountainous regions.

To inquire whether it was possible to further reduce the computing time by decreasing the number of levels, additional simulations were carried out using 41 levels (for the NW domain and year 2015). All these simulations used the MYNL61W1 configuration and were initialised by ERA5 data. One of the runs had a large number of levels located in the PBL ("lev1") and the second was using the default WRF vertical distribution scheme ("lev2"). To better illustrate the differences, the vertical wind speed profile is plotted for a specific location, but the conclusions largely hold for the rest of the domain. The results shown here are for the location of the Cabauw mast (see also Figure 25).

The annual average wind speed profiles for 2015 at Cabauw using all three vertical level setups are shown in Figure 36 (left) while the bias towards the reference run in Figure 36 (right). The

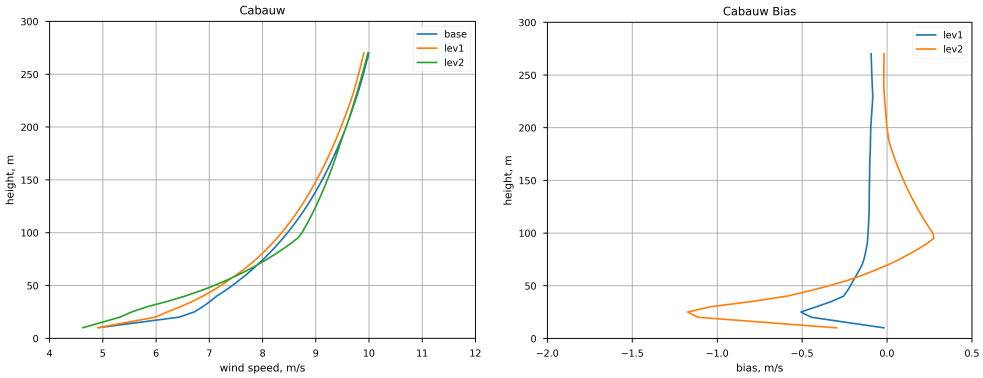

Figure 36. Left: Annual average wind speed ($m\,s^{-1}$) during 2015 at a grid point corresponding to the Cabauw mast. Reference run with 61 levels (blue), 41-level run with more levels in the PBL (orange) and 41-level run with standard distribution of levels (green). Right: Bias of the annual average wind speed ($m\,s^{-1}$) during 2015 of the two 41-level runs (blue: more levels in the PBL, orange: standard distribution of levels) towards the 61-level reference run at Cabauw.

41-level run with more levels in the PBL ("lev1") clearly shows results closer to the 61-level run compared to the run using default level spacing ("lev2"). Most of the differences between "lev1" and the reference run are concentrated in the lower 50 m. Above 50 m the difference is usually smaller than $0.25\,m\,s^{-1}$. For the default level spacing ("lev 2") the differences are much larger and can be more than $1.0\,m\,s^{-1}$ in the lower levels. While the bias is mostly negative, it turns to positive around 100 m height for the "lev2" case.

In conclusion, it was decided to keep the 61-level setup, as the 91-level setup is too computationally expensive and showed no significant improvement relative to the L61 setup. The 41-level setup gives worse results compared to observations, even with denser distribution of levels in the PBL.

2.3.4 Forcing: ERA-Interim, ERA5 and MERRA2

The ERA-Interim reanalysis (Dee et al., 2011) was a frequently used reanalysis that has showed good results when used as initial and boundary conditions in regional models simulations (Hahmann et al., 2015), but its production will be discontinued in favour of the new ERA5, which will become the new standard European Centre for Medium Range Weather Forecasting (ECMWF) reanalysis product (ECMWF, 2016). An alternative forcing data is the Modern-Era Retrospective Analysis for Research and Applications (MERRA2) reanalysis created by Global Modeling and Assimilation Office (GMAO) of NASA (Gelaro et al., 2017).

To assess the impact of the forcing data type and resolution on the simulation of the wind climate, we performed the following simulations, all covering the full year 2015 and using the MYNL61W1 reference setup described in Chapter 2.1:

- ERA-Interim, with native resolution
- ERA-Interim, at $0.75° \times 0.75°$
- ERA5, at $1° \times 1°$
- ERA5, at $0.25° \times 0.25°$
- MERRA2

The differences between ERA-Interim native and $0.75° \times 0.75°$ resolution are smaller than

$\pm 0.1\,\mathrm{m\,s^{-1}}$ for the annual average wind speed at 100 m. When comparing results from the WRF simulations using the ERA-Interim with newer ERA5 reanalysis, similarly the differences in yearly average wind speed were small and do not exceed $0.2\,\mathrm{m\,s^{-1}}$ both when $1.00^\circ \times 1.00^\circ$ resolution was used and even with significantly increased $0.25^\circ \times 0.25^\circ$ resolution (Figure 37, left). Surprisingly, the differences in wind speed when using MERRA2 reanalysis instead of ERA-Interim have the same order of magnitude ($\sim 0.2\,\mathrm{m\,s^{-1}}$, Figure 37, right).

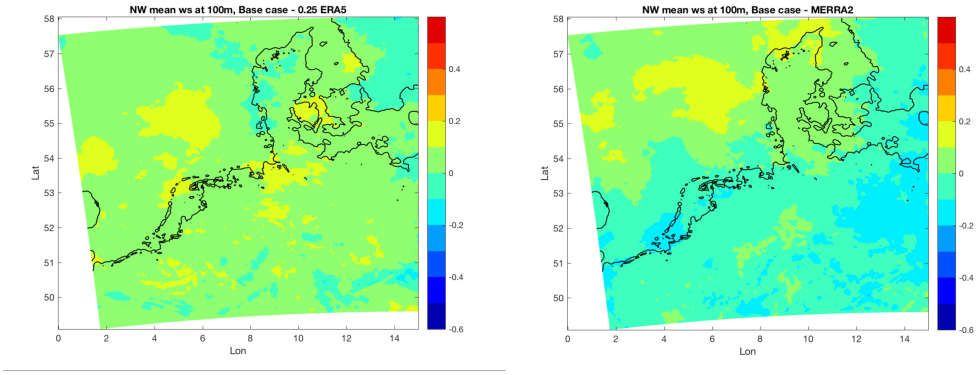

Figure 37. Differences in WRF-simulated annual mean wind speed ($m\,s^{-1}$) at 100 m for 2015 and the NW domain using different forcing data. Left: ERA-Interim (native resolution) minus ERA5 ($0.25^\circ \times 0.25^\circ$ resolution). Right ERA-Interim (native resolution) minus MERRA2.

A similar comparison has been performed for highly complex terrain over Turkey[1]. The mean wind speed of the NEWA production run setup, forced by ERA5 data, has been compared with the same setup but forced by ERA-Interim data. The results have been compared with observational data from 15 tall masts in Turkey.

Figure 38 (top) shows the difference in annual mean wind speed at 100 m height between the two simulations forced by ERA5 and ERA-Interim. Over Turkey the differences are not significant, mostly within $\pm 0.2\,\mathrm{m\,s^{-1}}$, while larger differences up to $0.6\,\mathrm{m\,s^{-1}}$ occur in the Levant. The differences vary with season as shown for example in winter (January–February) and summer (June–July–August) in Fig. 38, bottom. In most regions, the winter months have a slightly more positive bias than the summer months. In summer, the simulated wind shows a more pronounced negative bias over the Aegean Sea and Western Black Sea.

The tabulated results of the comparison with hourly averaged observations from 15 tall masts are shown in Figure 39. The measurements have been taken at 80 m height except the Mut mast, which measures at 60 m height. The WRF output (at 50, 75 and 100 m height) has been linearly interpolated to the corresponding measurement heights. Several statistic metrics have been evaluated: the correlation (r), the mean bias error (MBE), the mean absolute error (MAE), root-mean-square error (RMSE) and normalised RMSE for wind speed (NRMSE_s) and wind direction (NRMSE_d). The correlation is relatively compared between different regions in Turkey without applying any significance test. The statistics averaged over all stations give nearly identical values for both simulations, e.g. the average MAE and RMSE for the ERA5 run are $2.02\,\mathrm{m\,s^{-1}}$ and $2.68\,\mathrm{m\,s^{-1}}$, respectively, while the average MAE and RMSE for the ERA-Interim run are 2.03 and $2.69\,\mathrm{m\,s^{-1}}$, respectively. Looking at single stations, the differences are slightly larger but still very similar. The largest RMSE are found for stations in highly complex terrain (Amasya, Afyon) or at the Mediterranean coast (Mersin, Mut). The highest correlations are found in relatively flat terrain (Canakkale, Balikesir, Edirne) with values ≥ 0.8, the lowest correlations in the mountainous regions (Amasya, Afyon ≤ 0.7) and at the Mediterranean coast (Mut ≤ 0.6). The normalised RMSE for wind speed is for both simulations and all stations below 16% and on average 11%.

[1] For this study, the domain "TR" of the NEWA production (see Chapter 3) and ensemble runs was used which is larger than the "SE" domain.

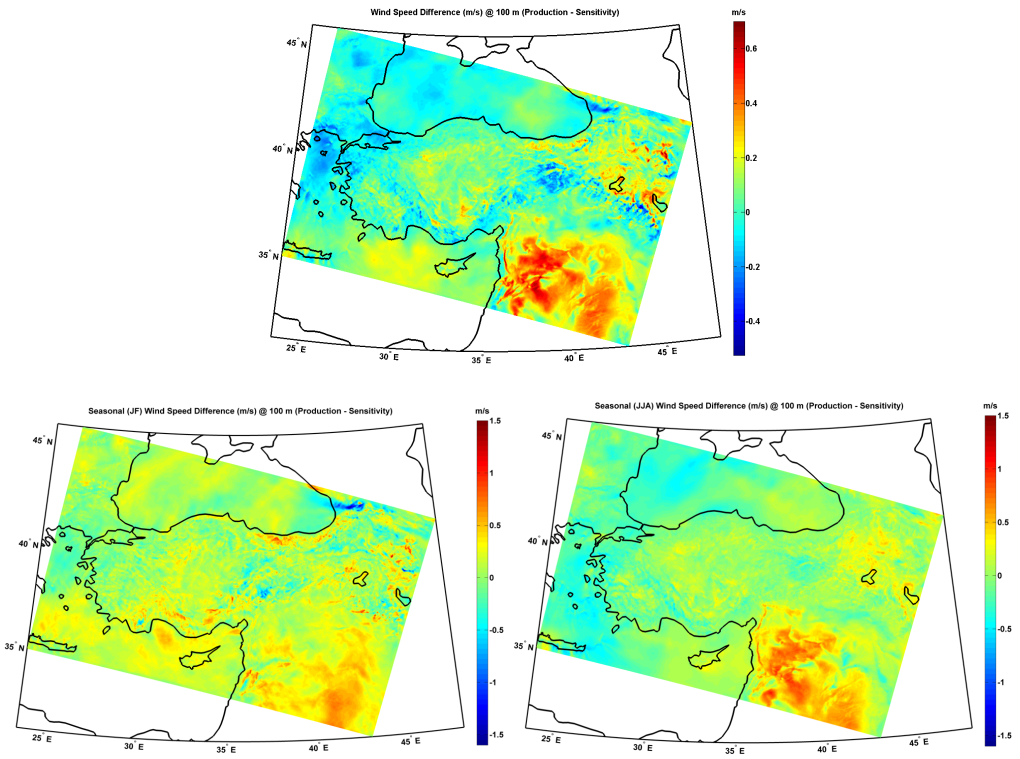

Figure 38. Seasonal differences in mean wind speed ($m\,s^{-1}$) at 100 m height between simulations forced by ERA5 and ERA-Interim for: all 2015 (top), January–February 2015 (left) and June–July–August 2015 (right).

For wind direction the normalised RMSE varies between 0.25 and 0.52 (average is 0.36). The large value for Ordu (0.52) is due to a west-east oriented mountain region diverting the flow so that westerly and easterly flow is dominating while the simulations prefer northerly and southerly flow.

The statistics have also been evaluated according to seasons as shown in Figure 40. In general higher correlations are obtained for winter and autumn and lower correlations in the summer. The MBE is rather positive in winter and rather negative in summer. Both MAE and RMSE are higher in winter than in the other seasons. The normalised RMSE for wind speed and wind direction show the opposite trend and are in agreement with the correlation: higher values in summer than in the other seasons.

Furthermore, the results have been filtered for northerly and southerly wind directions and compared to the results obtained for all wind directions (see Figure 41). The difference between the two simulations forced by ERA5 and ERA-Interim is not significant for any of the wind directions. Regarding the correlation to the observations, the results are generally better for southerly wind directions. Additionally, some sites show lower RMSE values for southerly winds while there are locations with best scores for northerly winds.

Finally, the two runs have been compared to hourly surface observations in Turkey, i.e. 40 meteorological stations that measure wind speed and direction at 10 m height. For that purpose, the 10 m wind speed output of WRF has been used. The stations are distributed through different parts of the country with focus on the northwestern coastal regions (Aegean and Marmara Seas), the Eastern Mediterranean coast and Central Anatolia. The correlation coefficients are shown in Figure 42. Similar to the comparison with tall masts, there are no significant differences between the two simulations (colours of points and stars in Figure 42 are the same). The correlation between simulations and measurements is satisfactory only in the Marmara region (0.65 - 0.81).

		r	mbe	mae	rmse	nrmse_s	nrmse_d
Afyon	production	0,66	0,07	2,33	3,15	11,41	0,32
	sensitivity	0,67	0,16	2,29	3,10	11,25	0,31
Aksaray	production	0,77	-0,41	1,92	2,60	8,67	0,33
	sensitivity	0,77	-0,52	1,91	2,61	8,72	0,34
Amasya	production	0,66	1,03	2,33	3,10	15,46	0,37
	sensitivity	0,66	1,01	2,36	3,14	15,64	0,37
Aydın	production	0,75	-0,48	2,17	2,90	10,65	0,30
	sensitivity	0,75	-0,44	2,16	2,88	10,60	0,29
Balıkesir	production	0,82	0,00	1,57	2,07	7,97	0,38
	sensitivity	0,81	0,12	1,62	2,13	8,17	0,38
Canakkale	production	0,81	0,09	1,53	1,96	10,69	0,24
	sensitivity	0,80	0,19	1,59	2,02	11,00	0,24
Edirne	production	0,81	-0,46	1,66	2,17	7,61	0,31
	sensitivity	0,80	-0,39	1,69	2,24	7,82	0,32
Hatay	production	0,68	-0,05	1,93	2,64	10,94	0,26
	sensitivity	0,68	-0,24	2,01	2,66	11,03	0,25
Karaman	production	0,78	-0,37	2,25	2,95	9,18	0,38
	sensitivity	0,78	-0,49	2,21	2,91	9,08	0,37
Kayseri	production	0,73	0,41	1,97	2,48	12,48	0,37
	sensitivity	0,72	0,42	1,98	2,52	12,73	0,36
Kırklareli	production	0,73	0,11	1,93	2,57	9,95	0,51
	sensitivity	0,73	0,26	1,95	2,62	10,15	0,51
Mersin	production	0,70	0,89	2,41	3,23	13,54	0,37
	sensitivity	0,71	0,98	2,50	3,31	13,88	0,36
Mut	production	0,59	0,36	2,44	3,40	13,17	0,37
	sensitivity	0,60	0,26	2,37	3,32	12,89	0,35
Ordu	production	0,72	-0,26	1,87	2,49	11,20	0,51
	sensitivity	0,72	-0,29	1,87	2,48	11,16	0,52
Yozgat	production	0,72	-0,42	1,93	2,46	11,16	0,30
	sensitivity	0,73	-0,48	1,92	2,43	11,02	0,31

Figure 39. Comparison of the WRF-simulated winds with observations for 15 masts over Turkey. "production" denotes the simulation with ERA5 forcing, "sensitivity" denotes the simulation with ERA-Interim forcing.

In the other regions is below 0.7, for some stations even below 0.5. Regarding MAE and RMSE (not shown) the performance is better in the Aegean and Central Anatolia regions. Poor results are obtained in the Mediterranean and Black Sea regions.

It can be concluded that the type and resolution of the forcing data has a rather small impact on the results if e.g. compared to the impact that the choice of PBL scheme has. It is not clear which forcing dataset is yielding better results, this might have a specific dependency on the particular region and therefore be more linked to the orography or other characteristics that govern the flow over the region. Finally, it was decided to use the ERA5 dataset for the NEWA production run. The arguments are that it is a European dataset and that it is the most recent dataset with the highest resolution.

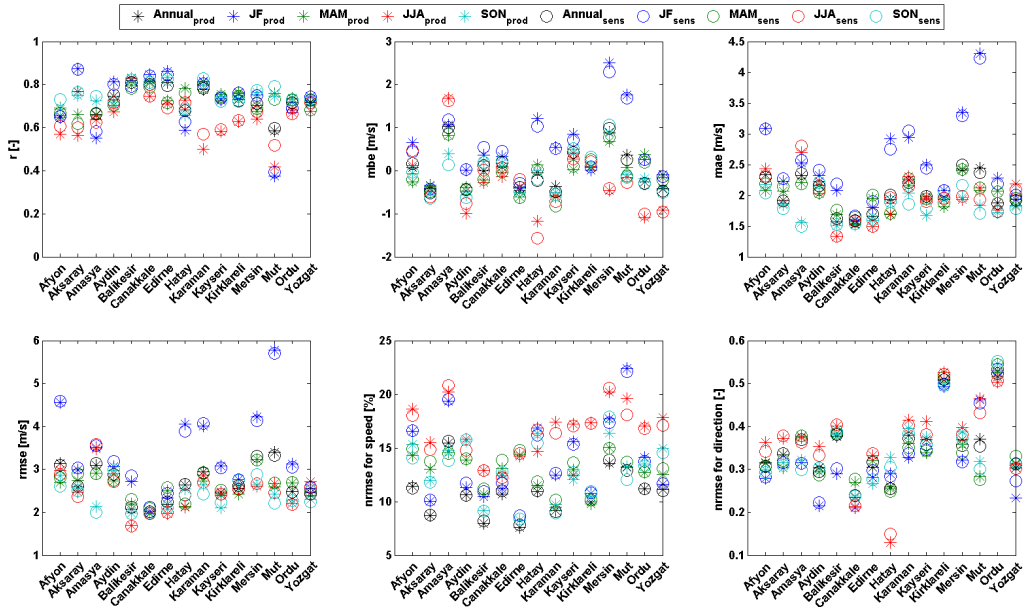

Figure 40. Comparison of the WRF-simulated winds forced by ERA5 and ERA-Interim with 15 masts over Turkey. Statistical metrics for different seasons.

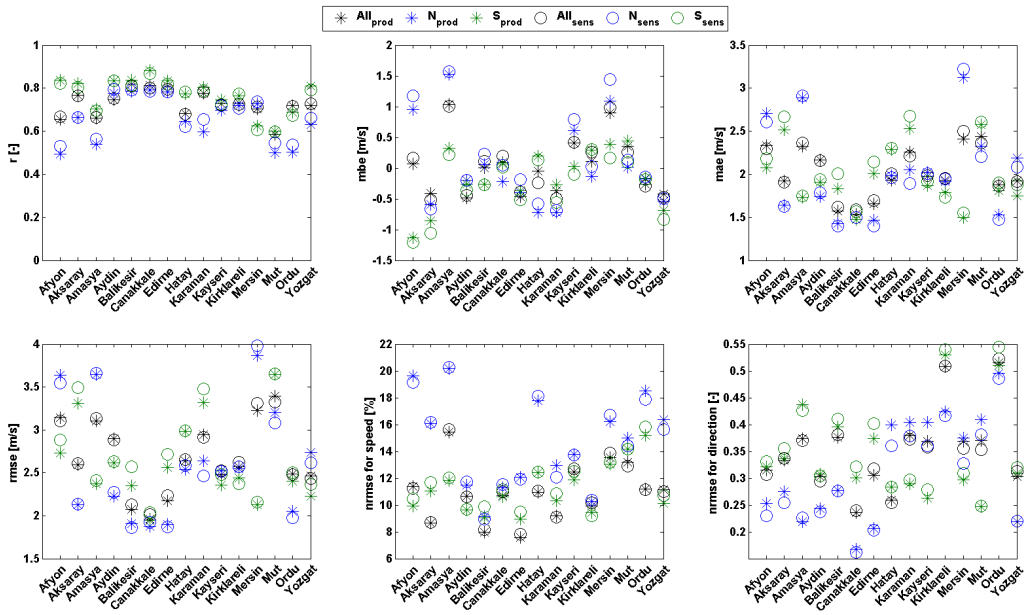

Figure 41. As in Figure 40 but for wind direction.

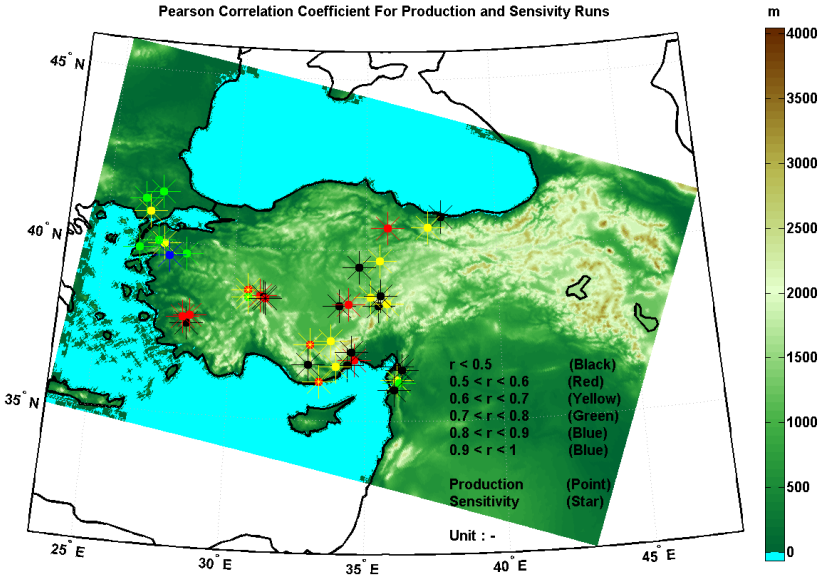

Figure 42. Correlation between the WRF-simulated wind forced by ERA5 and ERA-Interim and surface observations over Turkey.

2.3.5 Land surface parameterisation

Another aspect that deserves attention is the choice of the land surface parameterisation. The exchange of water and energy fluxes at the soil-atmosphere interface has proven a non-negligible impact on the regional climate variability in general (Seneviratne et al., 2010; Jerez et al., 2012), but also specifically on the wind field (Jiménez et al., 2011). In this section, we are therefore interested in evaluating to what extent the wind field simulated by the WRF model is affected by the use of a specific land-surface scheme.

To this end, five land-surface optional schemes have been tested by running a year-long (2015) simulation for the SW sub-domain (recall Figure 3). The schemes applied are listed in Table 7. The first case explored herein makes use of the Noah Land Surface Model (Chen, 2007, NH0 hereafter). This parameterisation is an unified NCEP/NCAR/AFWA scheme with soil temperature and moisture in four layers, fractional snow cover and frozen soil physics. This parameterisation is used as the reference case with which the rest of simulations will be compared. Another option that has been explored is the Noah-MP (multi-physics) Land Surface Model (Niu et al., 2011; Yang et al., 2011, MP0 hereafter) that uses multiple options for key land-atmosphere interaction processes and contains a separate vegetation canopy, multi-layer snow pack and four-layer soil column. The third land-surface option used is a variant of the previous. Applying that same scheme, the surface layer drag coefficient calculation is selected to be similarly calculated as in the Noah reference case (denoted as MP1 from here on). The following variant makes use of the RUC Land Surface Model (Smirnova et al., 2016), which is an operational scheme with soil temperature and moisture in six layers, multi-layer snow and frozen soil physics (RUCW1). Finally, the last option investigated is the CLM4 (Community Land Model Version 4, Lawrence et al., 2011). In this land surface model each grid cell is rated as one out of five primary sub-grid land cover types (glacier, lake, wetland, urban, and vegetated) and its vertical structure includes a single-layer vegetation canopy, a five-layer snow pack, and a ten-layer soil column. This option is referred to as CL0. The alternatives explored essentially differ in the number of sub-surface layers, the snow and vegetation description and the complexity of the multiple processes involved in the moisture and energy fluxes dynamics within the soil-atmosphere interactions.

The amount of observations to validate the behaviour of the simulated wind at heights above the surface (i.e. 10 m height) is limited. Nevertheless, it is necessary to evaluate the ability of the simulations to reproduce the observed wind in a network as dense as possible. This leads to the need of evaluating the model skill at the surface where observations are much more abundant. Although it is widely acknowledged that the reasons why a simulation would fail to reproduce the surface winds might not be necessarily the same reasons why the simulated wind departs from observed values at greater heights, it is still useful to have an estimation of how the regional model performs in those areas or sites where no mast observations are available. Thus, additional to the comparison of the effect of varying land-surface schemes in the WRF model, it is worth to evaluate to what extent the simulation is able to capture the realism of the wind variability at the surface and above in the SW domain. With this aim, the bias as well as the standard deviation ratio between the available observations over the region and the simulation has been represented in Figure 43, at the surface (10 m height, bottom) and also at 120 m height (top). The wind observations used with this purpose can be classified in station observations or gridded fields. Four wind mast series at heights that range between 40 and 118 m have been used in addition to 45 wind speed series measured at 10 m height that belong to the Wind Surface European Database (WiSED), which is being developed within the NEWA project. Regarding the gridded wind fields, the DecReg/MiKlip wind database[2] consisting in monthly and daily mean near-surface (10 m) wind speed (Brinckmann et al., 2015) has been used. Finally, to compare

[2] ftp : //ftp − cdc.dwd.de/

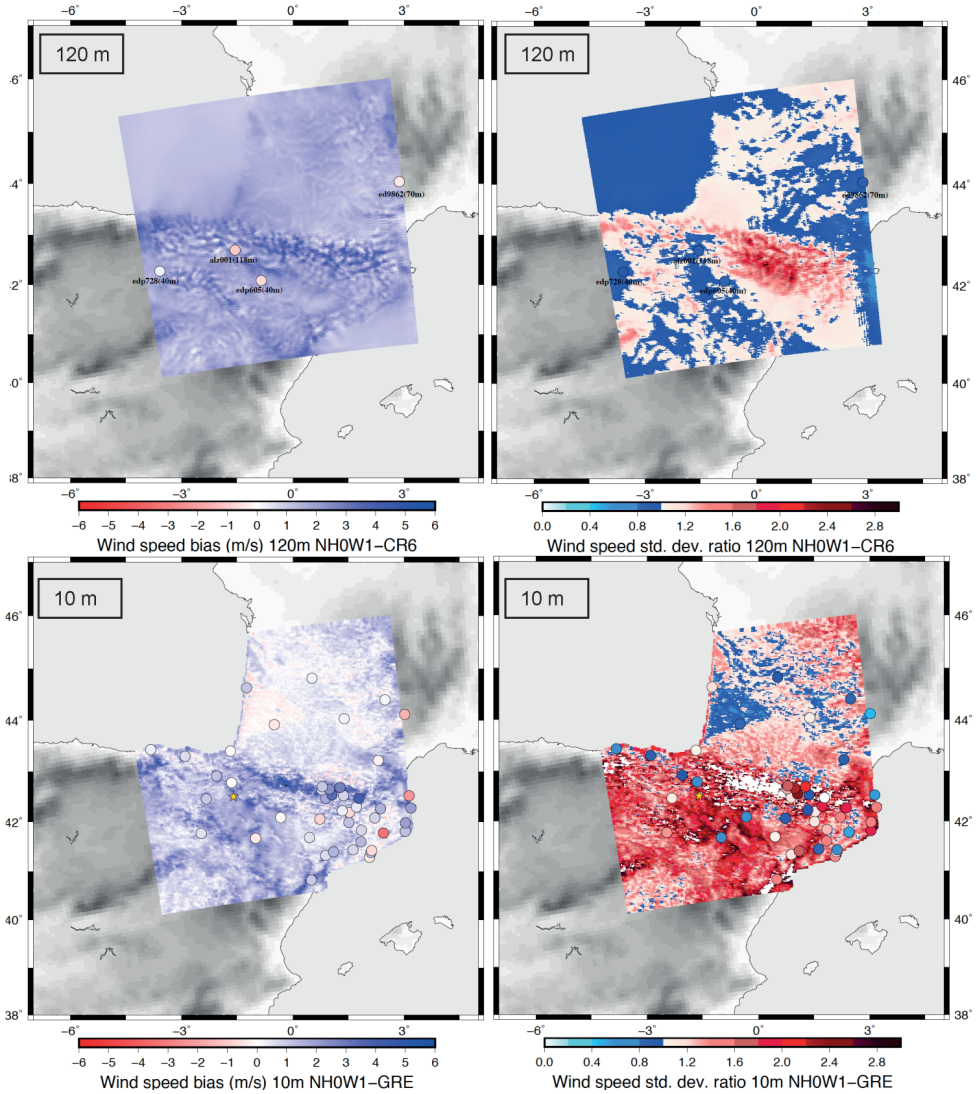

Figure 43. Bias (left) and standard deviation ratio (right) at 10 m height (bottom) and at 120 m height (top) between the one-year (2015) reference simulation (NH0, see text for details) and the available wind observations (circles represent bias at the observational sites and the shading corresponds to the comparison with the gridded fields) during the overlapping period.

simulations with observed evidence at 120 m it has also been used the information from the regional reanalysis COSMO-REA6 (Borsche et al., 2016; Kaiser-Weiss et al., 2015), defined as a high-resolution (6 km) reanalysis system based on the regional model COSMO for continental Europe that incorporates the assimilation of observational data.

Maps of the bias for the innermost WRF domain, calculated as the averaged differences between the daily wind from the reference simulation and gridded observations are shown in the left panels of Figure 43. Also, circles are located at the observational sites, were top and bottom correspond to wind above the surface (observed gridded *vs.* simulated wind at 120 m, masts are labelled with the corresponding height in the map) and to wind at the surface (gridded and site observations both at 10 m), respectively. The same applies for the maps in the right panels representing the standard deviation ratio of the simulated wind with respect to the observed one. The wind is underestimated on average by the simulation at mast sites, although the overall bias is smaller than 1 m s^{-1}. Conversely, the observed gridded wind seems to be overestimated by the regional model everywhere (top left). The latter could be related to the orography representation in the model as the topography is identifiable even in the bias map at 120 m height. At the surface

(bottom left) there are signs of both over- and under-estimation of the observed wind by the simulation at the observational sites. The bias at the measuring stations (circles) is nonetheless relatively small in most of the sites and it is also smaller compared to the bias at 120 m, if the simulation is evaluated against the observed gridded wind. Apparently, in both comparisons (site and gridded field) at the surface the bias seems to be somehow also related to orography and to some extent also to land cover issues like for instance the surface roughness definition (see for instance the Landes forest or the Pyrenees regions). With respect to the ratio of wind standard deviations (right panels in Figure 43), darker blue implies ratio values close to 1.0, both at the surface and above. Therefore, in most of the observational sites the simulation captures to a large degree the wind variability from observations. On the contrary, in the case of the gridded field the observed wind variability (standard deviation) is apparently overestimated (red) in most of the areas within the domain. It can be said that the model simulates reliably the wind field when it is compared to site observations and there are signs of overestimation of the observed wind from the gridded wind fields at the surface and above, which in turn produces overestimation by the simulation if compared with those fields.

In order to evaluate the impact of using different land surface schemes on the wind, bias maps (average daily wind differences) from each parameterisation with respect to the reference case have been calculated and are shown in Figure 44. Differences are more noticeable at the surface (bottom) than above as expected, since the influence of changes in the physics of the land-atmosphere interactions are expected to produce an imprint preferably near the surface. In general, all simulations tend to produce higher wind values over most of the domain compared to the reference case (notice that herein the middle domain is represented as well) which makes use of the Noah Land Surface Model. The bias of the daily wind speed is however close to zero or even negative, especially in the case of the RUCW1 parameterisation, where the Guadalquivir, Tajo or the Ebro Valleys are easily identified. Above, although smaller, the impact of changing the land physics is also visible. It is worth mentioning the reduction in the wind speed in both cases that make use of the Noah Multi-Physics (MP0 and MP1), where a deficit of wind (negative bias) with respect to the reference simulation is noticeable over the drier half of the Iberian Peninsula, therefore illustrating the effect of the soil moisture physics on the wind speed in these particular

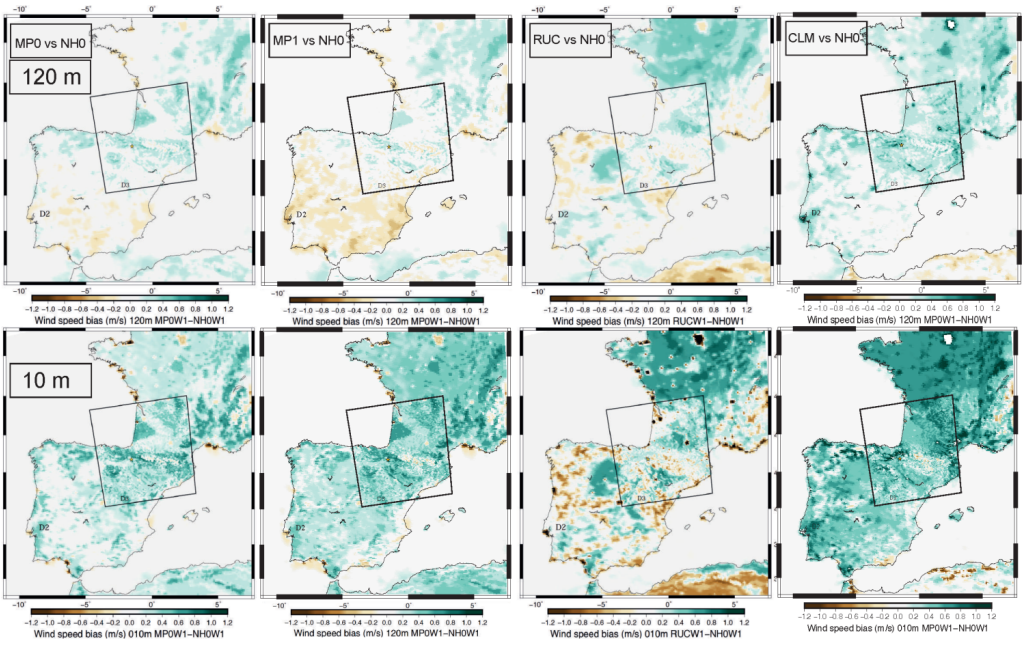

Figure 44. Maps of bias calculated for each of the simulations within the land-surface parameterisation sensitivity experiments with respect to the reference simulation (NH0, see text for details). Top (bottom) panels correspond to the average daily wind bias at 120 m height (10 m height).

simulations.

It can be assumed therefore that a simpler land scheme with less soil layers and/or poorer description of the interactions between the snow-pack/vegetation and the soil, might induce non-negligible differences in the magnitude of the wind speed that is simulated.

2.3.6 Simulation length

It was discovered already during the initial sensitivity experiments (Chapter 2.1) that the results are affected by the duration of the simulation. The difference between the 1-day long and 1-week long simulations was rather small and negligible compared to the difference between the PBL schemes. In view of configuring the final NEWA production run, the duration of the simulations is an important parameter. Longer simulations reduce the need of computational resources required for the model spin-up (e.g. 1 day per 1-week long simulation). Hence, the question is whether it is justified to perform even longer runs without loosing the veracity of the results.

Two sets of simulations for the NW domain were performed to test the effect of increasing the simulation length on the results:

1. Eight one-week long simulations
2. One continuous eight-week long simulation

Apart from the simulation length both simulations have the same setup (MYNN PBL scheme and nudging in D1). In particular, both simulations are nudged to the reanalysis data every six hours so that they will not drift away from the observed large-scale flow.

Comparing the average wind speed over the eight simulated weeks differences in the order of $\pm 0.5\,\mathrm{m\,s^{-1}}$ can be noticed (Figure 45). Taking into account that this is only an 8-week average and not an annual average, the difference is less than for other parameter changes, as e.g. the PBL scheme, but certainly not negligible. A comparison of weekly averages for each of the eight simulated weeks reveals interesting details (Figure 46). While in the first week the differences are in fact negligible ($\pm$ 0.1 $\mathrm{m\,s^{-1}}$), they increase with increasing simulation time. From the fourth week onward deviations in the order of $\pm$ 1 $\mathrm{m\,s^{-1}}$ can be observed. These are not randomly distributed but especially the strong deviations are organised in bands or patches. Some of the differences can be related to differences in surface roughness, e.g. due to differently placed snow covers but most differences are related to dynamical issues, e.g. weather systems moving on different paths or evolving differently. The patch with strong positive differences in the eighth week over Eastern Hungary (Figure 46 bottom right) is associated with a high pressure system with very low wind speeds in that region.

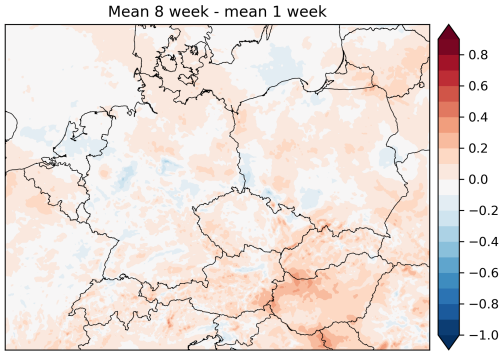

Figure 45. Difference in mean wind speed ($m\,s^{-1}$) at 100 m between the eight 1-week long runs and an 8-week long run averaged over 8 weeks.

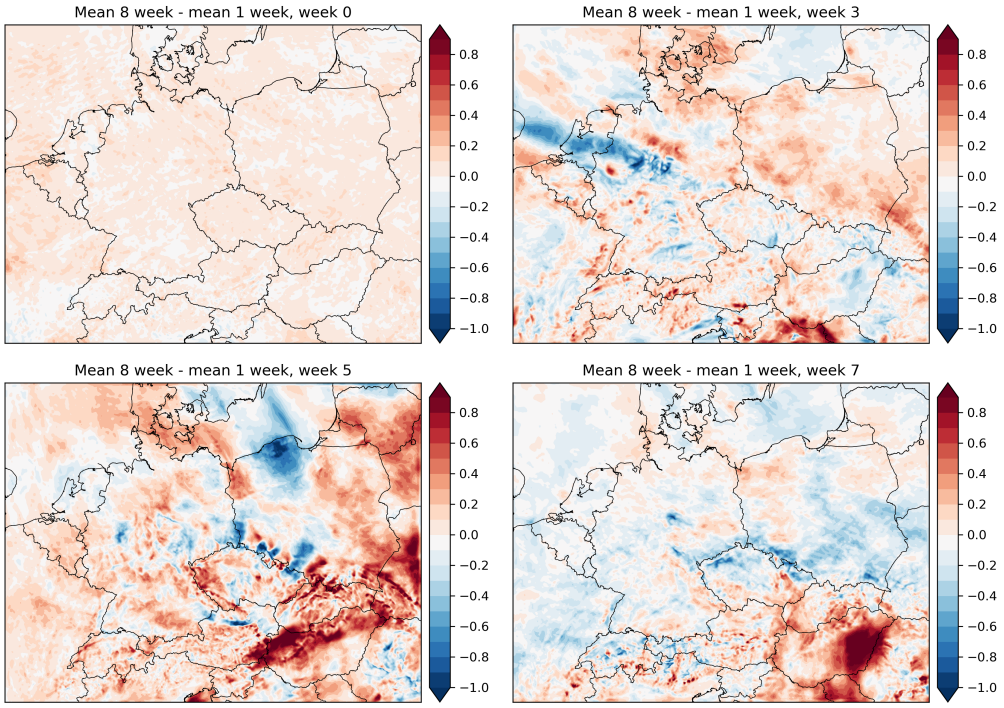

Figure 46. Difference in mean wind speed ($m\,s^{-1}$) at 100 m between 1-week long runs and an 8-week long run in terms of the 1-week average for the first week (top left), fourth week (top right), sixth week (bottom left) and eighth week (bottom right).

The results suggest to rather not use simulations longer than one week (at least with spectral nudging) even though these are continuously nudged to the reanalysis data. Although the results are a bit vague and further research is required to draw really sound conclusions and find explanations for this behaviour, we decided to stick to weekly simulations for the wind atlas production runs.

2.3.7 Dominant versus aggregated roughness

The default approach to define surface roughness for a mesoscale grid cell in WRF is to use the value of the dominant land use category found in the cell, whose areal fraction information comes directly from the high-resolution land cover dataset used in the initialisation.

Given the importance of surface roughness in the estimation of the wind resource, an alternative way of deriving surface roughness by means of aggregated weighting has been implemented in WRF and evaluated using an approach suggested by Mason (1988). The fraction of each land cover category within the mesoscale grid cell, found from the high-resolution land cover dataset, is used to weight the corresponding surface roughness associated with that category. The weighted roughness values for all land cover categories found in the mesoscale grid cell are then aggregated to derive the effective roughness length z_0^{eff}. This aggregated effective roughness is more representative of the actual variability in the cell than just the roughness of the dominant land use.

The implementation of the aggregated surface roughness scheme has been first validated by simply checking the roughness values obtained after a WRF simulation on the domains resulting from the dominant and aggregated schemes (Figure 47). It is clear from the figure that the aggre-

gated scheme yields a much higher spatial heterogeneity in terms of roughness values compared to the dominant scheme.

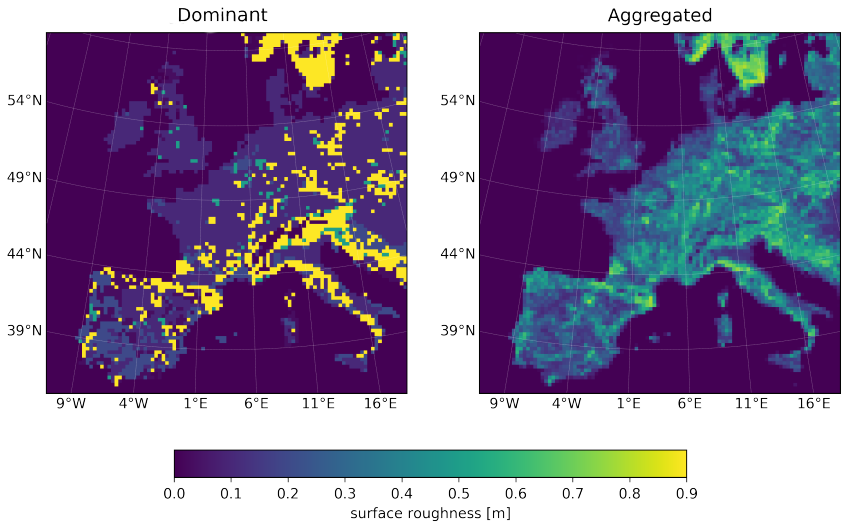

Figure 47. Surface roughness [m] from WRF simulation (27 km domain) using dominant (left) and aggregated (right) roughness schemes

In order to evaluate the impact of the aggregated roughness on the mesoscale wind climate, a set of simulations using a modified version of WRF V3.8.1 that includes the implementation of the weighted surface roughness scheme has been conducted. This model version slightly differs from the baseline. The model is configured with 3 nested domains (27:9:3 km) using a two-way nesting and 61 vertical levels. The high-resolution domain (3 km) uses a Lambert Conformal Conic projection and covers a region of about 300 km $\times$ 300 km in France. Only data from the inner domain is kept for the analysis. Initial and boundary conditions were taken every 6 hours from ERA-Interim reanalysis.

A set of four WRF experiments has been performed to test the impact of the aggregated roughness on the simulated wind resource using two different land cover datasets (Table 9).

experiment	**roughness scheme**	**land cover dataset**
dom_modis30s	dominant	IGBP-Modified MODIS[a] (900m)
wt_modis30s	aggregated	IGBP-Modified MODIS (900m)
dom_corine3s	dominant	CORINE Land Cover (100m)
wt_corine3s	aggregated	CORINE Land Cover (100m)

Table 9. WRF experiments and associated roughness schemes and land cover datasets

[a] https://modis.gsfc.nasa.gov/data/dataprod/mod12.php

The outputs of the four WRF experiments have been validated against tall meteorological masts (Table 10) data with at least one year of high quality wind speed and wind direction measurements. The location of the masts is confidential.

The results (Figure 48) suggest that the aggregated scheme allows to reduce the error on long-term mean wind speed compared to the default dominant scheme at the investigated sites. The reduc-

Mast	Height [m]	Site conditions
Site 1	83	Cropland / Forest mosaic Nearby urban patches
Site 2	60	Cropland / Urban mosaic Patchy forests nearby
Site 3	49.5	Cropland with nearby urban areas Nearby urban patches
Site 4	60	Cropland / Urban mosaic Patchy forests nearby

Table 10. Meteorological masts used for validation of the WRF experiments

tion of the error is even more pronounced when using the aggregated scheme together with higher resolution land cover dataset (here CORINE Land Cover instead of IGBP-modified MODIS).

Despite these promising results we have not used the aggregated roughness scheme for the mesoscale production run, as there was no time to perform a full analysis, i.e. to compare with the downscaled results.

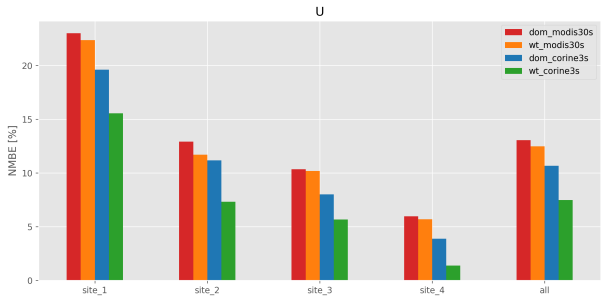

Figure 48. Normalised Mean Biased Error[%] of WRF experiments on long-term mean wind speed at each site and averaged for all sites (rightmost bars)

2.3.8 1-way versus 2-way nesting

As a default all previous runs (except those in the previous section) used 1-way nesting, which means that information from inner domains with finer resolution does not impact the solution in the outer domains with coarser resolution. 2-way nesting means that there is information exchange from inner domain back to outer domain.

A run using 2-way nesting was carried out for the NW domain, covering the whole year 2015, using MYNN PBL scheme, 61 vertical levels and week-long runs with D1 nudging. Results were compared against a run using the same setup with the default 1-way nesting. Difference in yearly average wind speed between 2-way nesting and 1-way nesting is depicted in Figure 49. Results show that the difference for most of the domain is rather small and does not exceed 0.05 m s^{-1}, however there is considerable impact near the edges of the domain. The 2-way nesting yields wind speeds up to 0.3 m s^{-1} lower in the zone that extends up to 100 km from the edge of the domain near the border between Germany and Poland. Interestingly, the influence can also be seen further from the edge of the domain over the Ore mountains (border between Germany and the Czech Republic). Similar influence can be seen near the domain edge near Skagerrak.

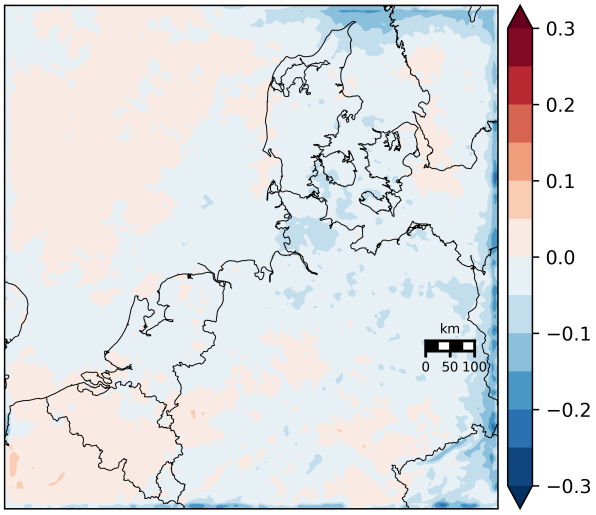

Figure 49. Difference in annual mean wind speed (m s^{-1}) at 100 m during 2015 between results using 2-way nesting and 1-way nesting for the NW domain.

In conclusion, these simulations show that the mean wind climate is rather insensitive to whether the simulations are done in 1-way or 2-way nesting. For simplicity and because several domains will be nested within the same large outer domain, the 1-way approach was chosen for the NEWA production run.

2.3.9 HPC system, compiler and parallelisation

The sensitivity simulations described in this report were performed on several different HPC systems to which the various participants in this task had access. The final NEWA production run will be again performed on a different HPC cluster. Therefore, it was important to establish if this had an effect on the simulated wind climate. To test if running the exact same WRF setup on different HPC systems makes a difference and how large this difference is, an identical simulation was submitted to three different HPC systems:

- Eddy[3] (HPC cluster at University of Oldenburg — a substantial part of the previously described sensitivity tests was performed here)
- Marconi[4] (CINECA, Italy — preparation phase for the NEWA production run)
- MareNostrum 4[5] (BSC, Spain — NEWA production run to be conducted in this facility)

The test run setup covered the first 3 months of 2015 for the NW domain using WRF 3.8.1 and the MYNL61W1 setup described in Chapter 2.1.

Figure 50 reveals that, somewhat surprisingly, the results of a simulation change when submitted to a different HPC cluster. However, the differences are very small compared to differences obtained when comparing different simulation setups. Between "Eddy" and "MareNostrum4", which have a very similar HPC architecture, the differences in the 3-monthly average wind speed at 100 m are below $0.05\,\mathrm{m\,s^{-1}}$ and rather randomly distributed. "Marconi" has a bit different architecture and thus slightly larger differences in the range of $0.1\,\mathrm{m\,s^{-1}}$ are obtained.

Figure 50 shows the differences in wind speed averaged over the length of the calculations (3 months). To answer the question how the runs differ for a specific moment in time, for each grid point the time series from two different HPC systems were compared and for each hour the difference between them was calculated. The maximum value of these differences (at each grid point) is plotted in Figure 51. The differences in the time-series for a specific hour can be very large (up to $20\,\mathrm{m\,s^{-1}}$). Still most of the differences are randomly distributed except for a few band-like structures that could be associated with weather fronts. Note that only the maximum differences are shown, i.e. one specific situation (which can be a different one at each grid point).

While using *ifort* as the standard compiler, we also tested the *pgi* and *gfortran* compilers and found non-negligible effects on the results (not shown). However, we decided to stick to *ifort* as showed a much better performance (in terms of speed).

While the default parallelisation mode in WRF is non-hybrid (using *MPI*), we also tested a hybrid parallelisation with *OpenMP*. This improves the performance of runs on a large number of cores. The effect on results is smaller than effect of WRF version. In the production runs we used the default non-hybrid parallelisation, however.

It can be concluded that the choice of the HPC system or in general technical, IT-related settings as e.g. compilers do affect the simulation results, especially when specific points in time are compared. The long-term statistics are however not systematically changed.

[3] https://uol.de/fk5/wr/hochleistungsrechnen/hpc-facilities/eddy/
[4] http://www.hpc.cineca.it/hardware/marconi
[5] https://www.bsc.es/marenostrum/marenostrum

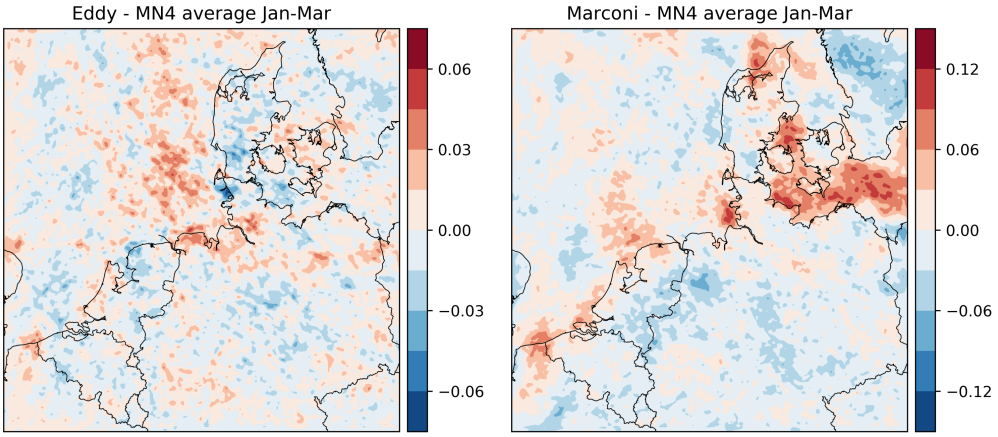

Figure 50. Difference in 3-month averaged wind speeds (January–March 2015, 100 m, $m\,s^{-1}$) of an identical simulation setup performed on different HPC clusters. Left: difference between "Eddy" and "MareNostrum4", right: difference between "Marconi" and "MareNostrum4". Note the different colour labels.

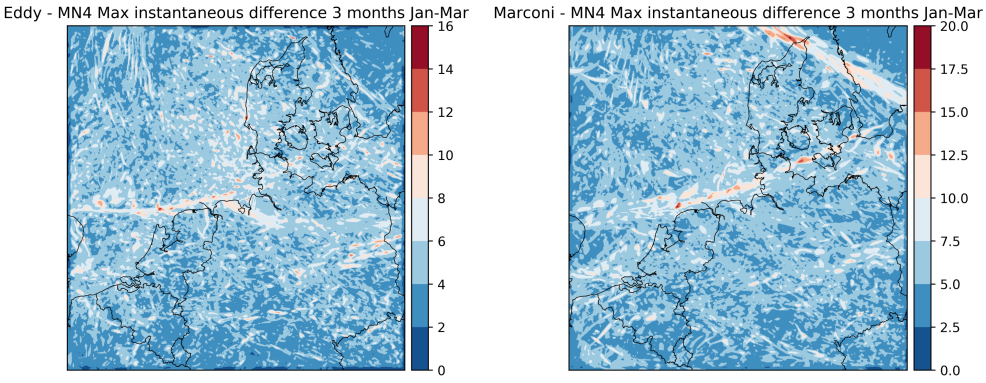

Figure 51. Maximal difference between hourly wind speeds in the period January–March 2015 (100 m, $m\,s^{-1}$) of an identical simulation setup performed on different HPC clusters. Left: difference between "Eddy" and "MareNostrum4", right: difference between "Marconi" and "MareNostrum4" HPC systems, respectively. Note the different colour labels.

2.4 Multi-parameter ensemble simulations

A noteworthy innovative contribution within the NEWA wind atlas is to produce an uncertainty map of model-derived wind-related quantities (e.g. wind speed distributions, extreme winds, atmospheric stability). In an analogous way to what is done in Numerical Weather Prediction and future climate projections, the uncertainty of the wind resource estimate will be estimated based on an ensemble of WRF simulations, where each member has a different setup, i.e. parameterisation schemes, initialisation or boundary conditions, which will add information about uncertainties based on sensitivity to model parameters to the wind atlas.

While the final *NEWA Ensemble* (for the entire NEWA domain) will only contain a reduced number of members to be computationally feasible, a precursor ensemble with a much larger number of members has been assembled and computed for one single domain, the NW domain, which is well-known from the previous studies (Chapters 2.1 and 2.3), covering the full year 2015. The objectives of this *NW-Ensemble* are to find the optimal setup for the mesoscale production runs and to investigate which members (i.e. parameter settings) generate significant spread and should thus be considered as members of the NEWA-Ensemble. In this report we will only focus on the first objective as the second one is covered in detail in Deliverable D4.4.

2.4.1 Ensemble setup

In total 62 members were defined, out of which 47 could successfully be simulated, that is, the simulation could successfully completed. The failing members could not be fixed, even after investing a decent amount of effort, suggesting incompatibility between parameterisation schemes, or incompatibility issues with the compiler option. We grouped the ensemble members into the following categories:

- Land surface, surface layer and PBL multi-physics ensemble
- Sensitivity experiments, including reanalysis, source of SSTs, etc.
- Other model physics, e.g, radiation schemes.

Some of the setups in the sensitivity experiment category overlap ideologically with the numerical experiments described in Chapter 2.3. However, the ensemble runs described here were carried out on a different HPC system (Mare Nostrum 4 HPC system at BSC) and with a different domain configuration. Many additional WRF setup options (e.g. radiation frequency) had to be tested and agreed upon for the production run.

Land surface/PBL multi-physics ensemble As the title suggests, this group includes mainly changes in the physical parameterisations of the WRF model. It consists of 21 members as listed in Table 11. First and foremost, the PBL scheme is varied between MYNN (Nakanishi and Niino, 2009), MYJ (Sušelj and Sood, 2010), YSU (Hong et al., 2006) and ACM2 (Pleim, 2007). Another variable parameter is the land surface model: Noah (Tewari et al., 2004), Noah-MP (Niu et al., 2011), RUC (Benjamin et al., 2004), PX (Noilhan and Planton, 1989) and SLAB (Dudhia, 1996). The third parameter we varied is the surface layer parameterisation: MYNN (Nakanishi and Niino, 2006), MM5 (Jiménez et al., 2012), M-O (Monin and Obukhov, 1954) and P-X LSM (Pleim, 2007; Noilhan and Planton, 1989). It must be mentioned, that some of the ensemble members (using e.g. MYNN3 or QSNE (Sukoriansky et al., 2006)), which where defined as "viable" combinations in the WRF documentation (Skamarock et al., 2008), simply did not run for reasons unknown. These had to be dropped from the list of ensemble members.

Ensemble member	Land surface model	PBL	Surface layer
MYNN-MYNN (base)	**Noah (2)**	**MYNN* (5)**	**MYNN* (5)**
MYNN-MM5	Noah (2)	MYNN* (5)	MM5 (1)
MYNN-MO	Noah (2)	MYNN* (5)	M-O (2)
MYJ-MO	Noah (2)	MYJ (2)	M-O (2)
YSU-MM5	Noah (2)	YSU (1)	MM5 (1)
RUC	RUC (3)	MYNN* (5)	MYNN* (5)
RUC-VEG	RUC (3)	MYNN* (5)	MYNN* (5)
RUC-MYNN-MO	RUC (3)	MYNN* (5)	M-O (2)
RUC-YSU-MM5	RUC (3)	YSU (1)	MM5 (1)
RUC-ACM2-PX	RUC (3)	ACM2 (7)	P-X (7)
PXLSM-ACM2-PX	PX LSM (7)	ACM2 (7)	P-X (7)
PXLSM-ACM2-MM5	PX LSM (7)	ACM2 (7)	MM5 (1)
SLAB-MYNN-MYNN	SLAB (1)	MYNN* (5)	MYNN* (5)
SLAB-MYJ-MO	SLAB (1)	MYJ (2)	M-O (2)
SLAB-YSU-MM5	SLAB (1)	YSU (1)	MM5 (1)
SLAB-ACM2-PX	SLAB (1)	ACM2 (7)	P-X (7)
NOAHMP	Noah-MP (4)	MYNN* (5)	MYNN* (5)
NOAHMP-MYNN-origMP	Noah-MP (4)	MYNN* (5)	MYNN* (5)
NOAHMP-MYNN-optsfc2	Noah-MP (4)	MYNN* (5)	MYNN* (5)
NOAHMP-MYJ-MO	Noah-MP (4)	MYJ (5)	M-O (2)
NOAHMP-YSU-MM5	Noah-MP (4)	YSU (1)	MM5 (1)

Table 11. Overview of ensemble members of the category "Land surface/PBL multi-physics ensemble". The numbers behind the options denote the settings of the respective WRF namelist parameters (`sf_surface_physics` for the land surface model, `bl_pbl_physics` for the PBL scheme and `sf_sfclay_physics` for the surface layer scheme). The member in bold font (MYNN-MYNN) denotes the base run against which each member is compared.

Sensitivity experiments This group includes changes in the atmospheric forcing data, such as the reanalysis data: ERA5 (ECMWF, 2016), ERA-Interim (Dee et al., 2011), MERRA2 (Gelaro et al., 2017), FNL (NCAR, 2000), the SST data: OSTIA (Donlon et al., 2012), OISST (Reynolds et al., 2002), HRSST (Reynolds et al., 2007; Gemmill et al., 2007) and the way the surface roughness length was defined and used in the simulations (constant z_0, annual cycle and aggregated roughness as in Li et al. (2013)). Furthermore, the WRF version, the nudging strategy, and the frequency of calls of the radiation physics have been changed. Also, the 2-way nesting experiment is included. All 20 ensemble members belonging to this group are listed in Table 12.

Other model physics This group contains changes in the icing parameterisation, convection scheme: Kain-Fritsch (Kain, 2004), Grell-Freitas (Grell and Freitas, 2014), and radiation scheme: RRTMG (Iacono et al., 2008), RRTMG fast version, CAM (Collins et al., 2004). The 6 ensemble members belonging to this group are listed in Table 13.

2.4.2 Summary of results

Each individual member has been compared with the base run. In a first step, just the annual mean wind speeds at 100 m height have been looked at. It has been found that all members of the "Land surface/PBL multi-physics ensemble" category (Table 11) have a significant impact on the results. As an example, Figure 52 (left) shows the differences in annual mean wind speed between base run (MYNN PBL and MYNN surface layer) and YSU PBL scheme with MM5

Ensemble member	Atmospheric forcing	SST source	surface roughness	other/ notes
base	**ERA5**	**OSTIA**	**constant z_0**	**ERA5**
xw_36_yw_26	ERA5	OSTIA	constant z_0	nudging: `xwavenum` = 36, `ywavenum` = 26
large_relax	ERA5	OSTIA	constant z_0	`relax_zone` = 9, `spec_bdy_width` = 10, `spec_exp` = 0.33
2-way-nest	ERA5	OSTIA	constant z_0	
grid-nudging-D3	ERA5	OSTIA	constant z_0	grid nudging D1–D3
grid-nudging-D1	ERA5	OSTIA	constant z_0	grid nudging D1
spec-nudging-D3	ERA5	OSTIA	constant z_0	spectral nudging D1–D3
ERAI	ERA-I	OSTIA	constant z_0	
MERRA2	MERRA2	OSTIA	constant z_0	
FNL	FNL	OSTIA	constant z_0	
Vers-361	ERA5	OSTIA	constant z_0	WRF V3.6.1
MYNN-unmod	ERA5	OSTIA	constant z_0	orig. MYNN
Z0-cycle	ERA5	OSTIA	annual cycle z_0	
Z0-cycle-NCAR	ERA5	OSTIA	annual cycle z_0	standard z_0
z_0-aggr	ERA5	OSTIA	aggregated z_0	
z_0-aggr-COR	ERA5	OSTIA	aggregated z_0	z_0 from CORINE
HRSST	ERA5	HRSST	constant z_0	
OISST	ERA5	OISST	constant z_0	
SST_ERA5	ERA5	ERA5	constant z_0	
radt_3	ERA5	OSTIA	constant z_0	radiation time step = 3m
radt_12	ERA5	OSTIA	constant z_0	radiation time step = 12m

Table 12. Overview of ensemble members of the category "sensitivity experiments". The base run (in bold font) is the same as in Table 11.

ensemble member	specifications
wms05_icing	WSM 5-class microphysics + icing code, `sum_qcqi_wsm` = 0
wms05_icing2	WMS 5-class microphysics + icing code, `sum_qcqi_wsm` = 1
thomps_icing	Thompson microphysics + icing code
grell-freitas	Grell-Freitas convection scheme
rrtmg	RRTMG fast version
cam	CAM radiation scheme

Table 13. Overview of ensemble members of the category "other model physics"

surface layer. At most locations in the domain the wind speed is up to 0.5 m s^{-1} higher compared to the base run. Some orographic effects can be seen. Figure 52 (centre) shows the difference between base (Noah, MYNN, MYNN) and a member with SLAB land surface model, MYJ PBL scheme and MO surface layer. This member shows mostly lower wind speeds over land and higher wind speeds over sea compared to the base run. Furthermore the surface roughness seems to play a role, as the largest differences occur over forested regions.

Furthermore, 12 members of the "sensitivity experiments" category affect the results. These include the members with different reanalysis data, roughness changes, nudging changes, the radiation scheme and the WRF version. As an example, Figure 52 (right) shows the differences

in annual mean wind speed between base run (ERA5) and MERRA2. Parts of the domain show higher, other parts show lower wind speeds than the base run. Again the differences which are mostly below 0.2 m s^{-1} seem to be connected to the land-sea distribution although this is not that clear as for some of the PBL schemes.

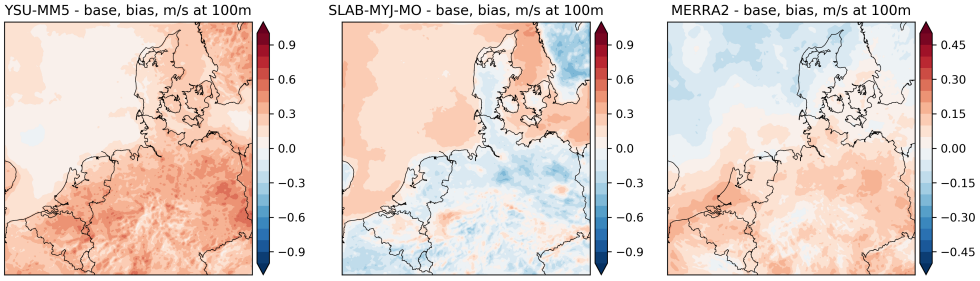

Figure 52. Difference in annual mean wind speed (m s^{-1}) at 100 m for 2015 between the base runs and the members YSU-MM5 (left), SLAB-MYJ-MO (centre) and MERRA2 (left). See text or Tables 11 and 12 for further details. Note the different label bar in the last figure.

The members of the category “other model physics” do not affect the results in a significant or systematic way, with the exception of the member using the CAM radiation scheme.

As in some of the previous studies the simulation results were compared to observations to assess the quality of the ensemble members and to decide which setup to use for the NEWA production run. The observational sites are the same as in the previous chapters (see Table 4 and Figure 25).

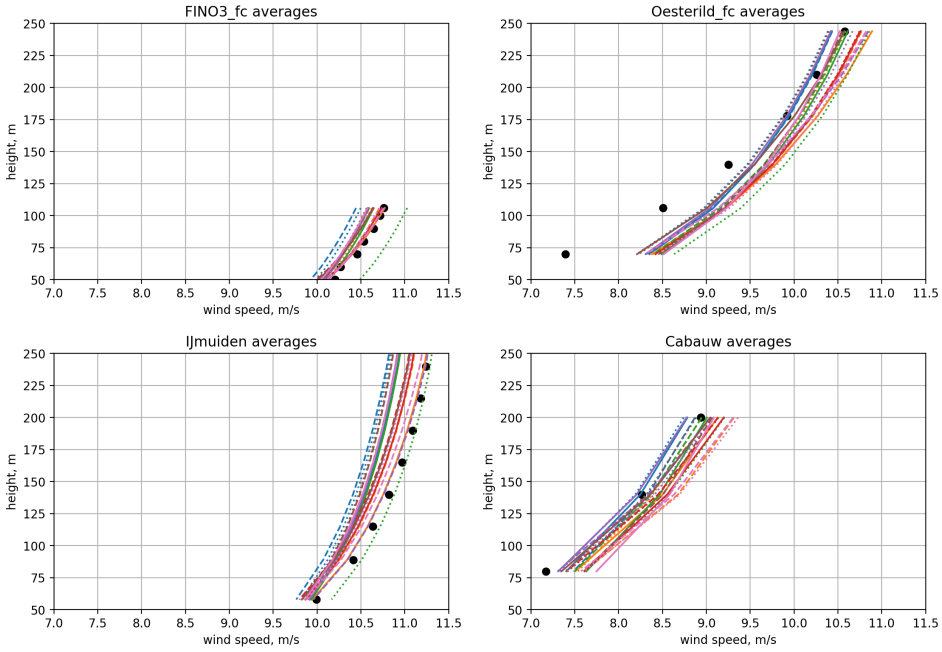

Figure 53. Vertical profiles of annual mean wind speed (m s^{-1}) during 2015 compared to observations at four sites. Multi-physics runs (Table 11). The labels are intentionally left out.

The observed and simulated annual mean wind speed profiles at four sites are presented in Figures 53 (members of the category "Land surface/PBL multi-physics ensemble") and 54 (members of the category "sensitivity experiments"). The ensemble members are mostly clustered in one rather narrow band with only a very few outliers. In general, the simulated annual mean wind speed profiles match those of the observations quite well. At IJmuiden, the WRF simulations slightly underestimate the wind speed. At Østerild the observations are captured well above 175

m but in the lower heights WRF overestimates the mean wind speed by up to $1\,\mathrm{m\,s^{-1}}$, i.e. the vertical wind shear is not represented well. This is due to failure of the WRF model to represent the complicated terrain, which contains forests, coastline and inland fjords, of the real site.

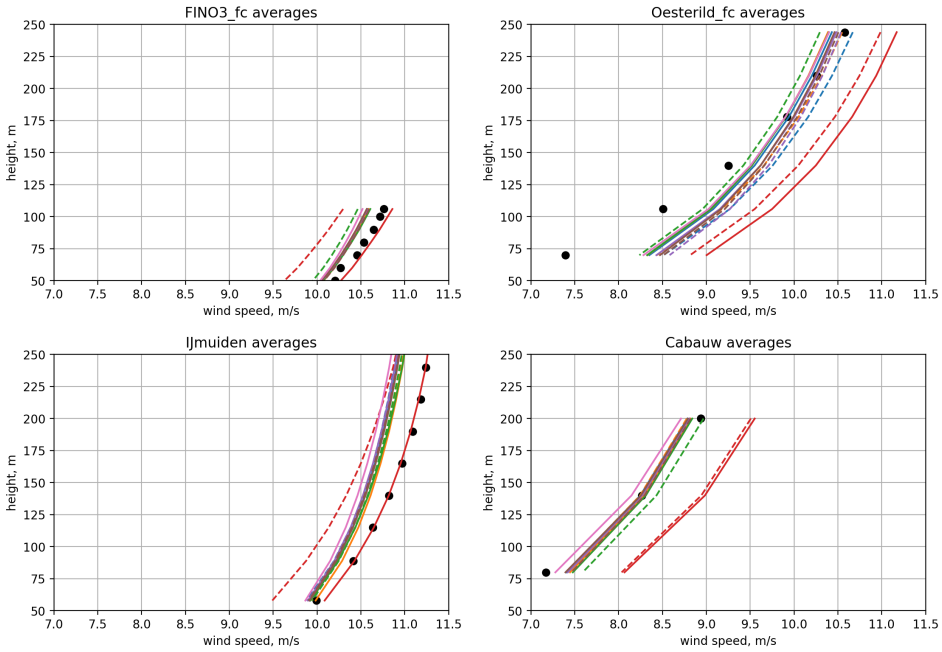

Figure 54. Vertical profiles of annual mean wind speed ($m\,s^{-1}$) during 2015 compared to observations at four sites. Sensitivity runs (Table 12). The labels are intentionally left out.

To get a clear picture of the performance of the individual ensemble members at all sites, the BIAS and RMSE values are shown in a matrix plot in Figure 55 for the "multi-physics" members and in Figure 56 for the "sensitivity" members. One important result is that the differences between the sites are mostly larger than the differences between the ensemble members, as expected since some sites are offshore while others are over land.

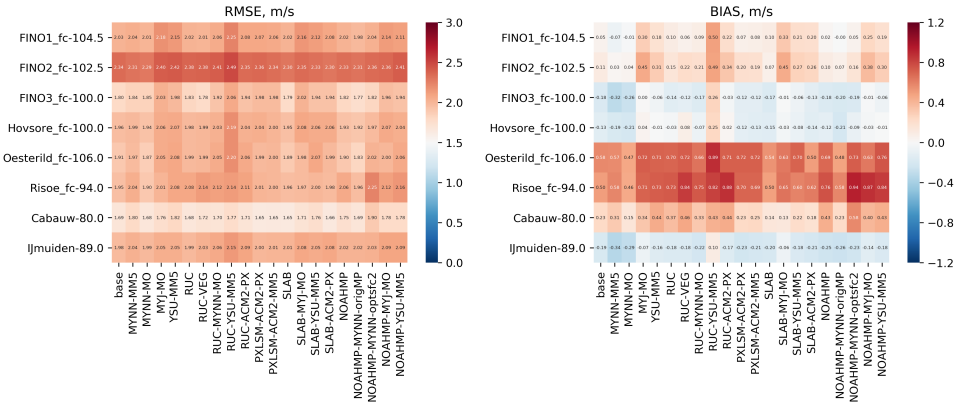

Figure 55. RMSE (left, $m\,s^{-1}$) and BIAS (right, $m\,s^{-1}$) of the wind speed for various ensemble simulations at the eight observation sites. Multi-physics members (Table 11). The left-most column is the base simulation.

We did not only want to compare the ensemble members and observations in terms of BIAS and RMSE, but also evaluate how different the wind speed distributions are, with focus on the largest differences between distributions. The Kolmogorov-Smirnov (K-S) test (Wilks, 2011) describes such a difference, and it is calculated as the maximum difference between two wind

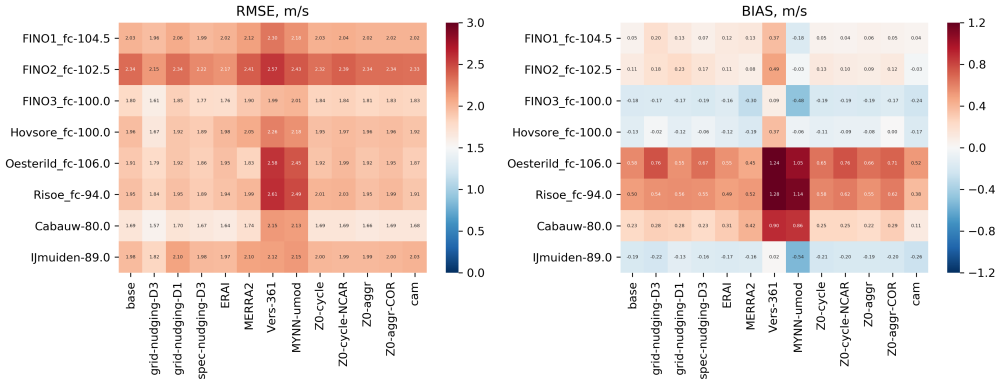

Figure 56. As Figure 55 but for the "sensitivity" members (Table 12).

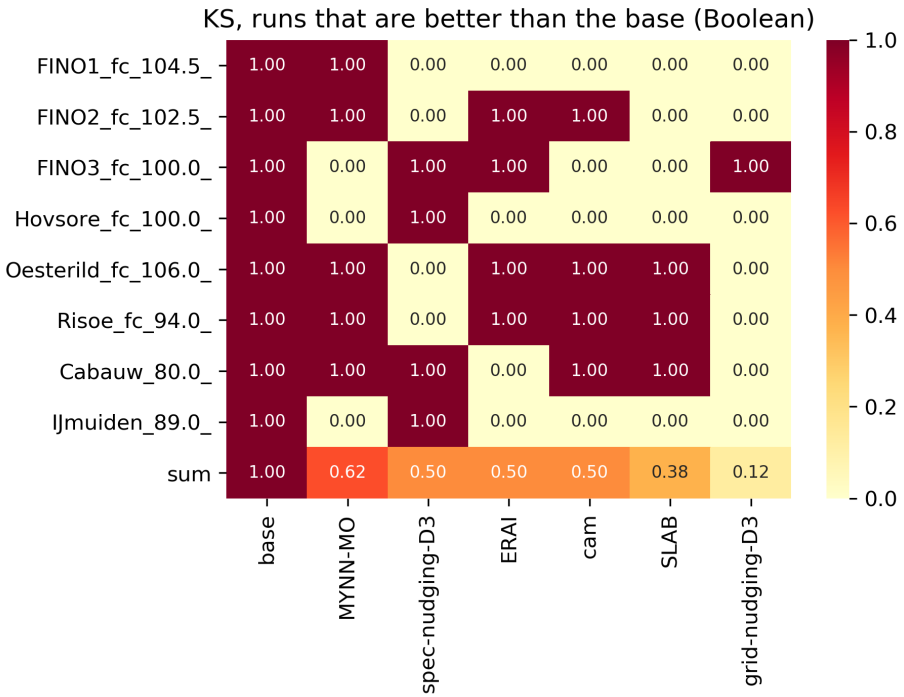

Figure 57. Comparison of the top scored ensemble members against the base run. The metric used is a boolean version of the K-S test (see text for more details).

speed cumulative distribution functions. It is easy to imagine two distributions having completely different shape while at the same time having the same mean. For instance, the model could overestimate the frequency of high and low wind speeds while at the same time underestimating the frequency of moderate wind speeds. In this case the mean could be the same for the both distributions, but the K-S test would show the differences. Therefore, it was decided that the K-S test should be investigated together with other error metrics. The comparison of the K-S test comparing each ensemble member against the base is presented in Figure 57. In this test, if the ensemble is “better” than the base it is given a 1.00, 0.00 otherwise. The last line represents the sum of at all the sites. No single other simulation performs better than the base run at all sites. However, among the “top score” sensitivity simulations, the MYNN-MO simulation has improved statistics at 5 of the 8 verification sites and thus was chosen as the configuration of the NEWA production run.

3 Specifications for final production run

WRF setup Table 14 summarises the WRF setup for the final NEWA production run. The WRF namelist for the production run of the CE domain is attached as an example at the end of this report.

As explained in Chapter 2.3.2 we used a modified version of WRF 3.8.1 with changes in the MYNN PBL. Furthermore, additional code that calculates the presence of ice was added to the WRF code. The icing model was based on the ice growth model from Makkonen (2000). The model was used to simulate the rate of ice growth on a 30 mm diameter cylinder that was fixed in width.

An adaptive time step was used together with the associated parameters as shown in the attached namelist. As we experienced frequent simulation crashes mostly in the winter season, we reduced the maximum time step of the outer domain from 150 s to 120 s for weeks 1-19 and 39-52 of each year which worked reasonably well for most simulations. Still, we experienced crashes for some domains and about 1-3 weekly simulations per year. In these cases we manually reduced the maximum time step to 90 s (D1), 30 s (D2) and 10 s (D3) as well as the horizontal cfl factor (`target_hcfl`) to 0.60.

WRF version	3.8.1 (modified PBL + icing code)
Grid	3 nests: 27 km, 9 km, 3 km; 61 vertical levels, 1-way nesting
Numerical options	480 cores, IO Quilting (1 node used for output)
Land use data	CORINE 100 m, ESA CCI where CORINE not available
Dynamical forcing	ERA5 reanalysis ($0.3^\circ \times 0.3^\circ$ resolution)
SST	OSTIA SST and sea-ice ($1/20^\circ$, approx. 5 km)
Lake temperature	average ground temperature from ERA5, lakes are removed when temperature is present in OSTIA
Land surface model	NOAH-LSM
Simulation length	8 days, including 24 h spin-up
Nudging	Spectral nudging in D1 only, above PBL and level 20
Time step	adaptive (where working)
PBL	MYNN (modified) (5)
Surface layer	MO (Eta similarity) (2)
Microphysics	WRF Single-Moment 5-class scheme (4)
Radiation	RRTMG scheme (4), 12 min calling frequency
Cumulus Parameterisation	Kain-Fritsch scheme (1) on D1 and D2
Icing	WSM5 + icing code + sum of qcloud and qice
Diffusion	Simple diffusion (option 1) 2D deformation (option 4) 6th order positive definite numerical diffusion (option 2) rates of 0.06, 0.08, and 0.1 for D1, D2, and D3 vertical damping.
Advection	Positive definite advection of moisture and scalars.

Table 14. Setup configuration used in the NEWA production run.

Computations To conduct the production run and the ensemble simulation, we applied for computational resources at the tier-0 PRACE research infrastructure (PRACE Partnership for Advanced Computing in Europe, 2019). The project was granted with computational resources to the amount of 56 million core hours on the MareNostrum supercomputer at Barcelona Supercomputing Center (BSC), Spain. Out of these 56 million, 36 million core hours were allocated for the NEWA production runs which were conducted between August 2018 and March 2019.

WRF had already been tested on the MareNostrum system previously (see Chapter 2.3.9). For the production run WRF version 3.8.1 (modified as described above) was installed using the Intel Fortran and C compilers *ifort* and *icc* (version 2017.3.196) together with MPI. Besides the default compiler options we used *O3* optimisation.

Domain layout The final domain layout is presented in Tables 15 and 16 and Figure 58. 10 domains have been defined with the following conditions:

- Domains have to cover the NEWA domain: all EU countries, Turkey, offshore areas 100 km off each coast, complete North and Baltic Seas.
- Domains should not include large regions outside of the NEWA domain.
- Domains must be large enough so that each country is fully covered in one domain (exception: Norway, Sweden and Finland).
- Domains must have sufficient overlap: at least 30 grid points buffer at each domain boundary has to be considered.

The layout of the single domains is presented in Figures 59, 60, 61, 62 and 63. Here, the 30 grid points buffer zone is marked, as well.

parameter	setting
grid resolution	27 km x 27 km
grid size	250 $\times$ 220
map projection	Lambert conformal
reference latitude	54°N
reference longitude	15°E
true lat1	30°N
true lat2	60°N
standard longitude	15°E

Table 15. Projection parameters of the outer WRF model grid.

Domain	Inner grid size	Centre lat/lon	Figure
BA	361 × 361	45.42°N, 24.04°E	Figure 59
CE	541 × 415	51.04°N, 13.47°E	Figure 59
FR	415 × 415	45.84°N, 2.37°E	Figure 60
GB	397 × 541	55.92°N, 6.36°W	Figure 60
GR	325 × 343	38.68°N, 23.06°E	Figure 61
IB	541 × 451	39.89°N, 3.37°W	Figure 61
IT	451 × 487	40.96°N, 12.07°E	Figure 62
SA	559 × 397	67.74°N, 18.13°E	Figure 62
SB	631 × 415	59.22°N, 15.56°E	Figure 63
TR	613 × 397	38.78°N, 35.13°E	Figure 63

Table 16. Grid sizes and centre latitude and longitude for the 10 inner WRF domains used for the NEWA production run as displayed in Figure 58.

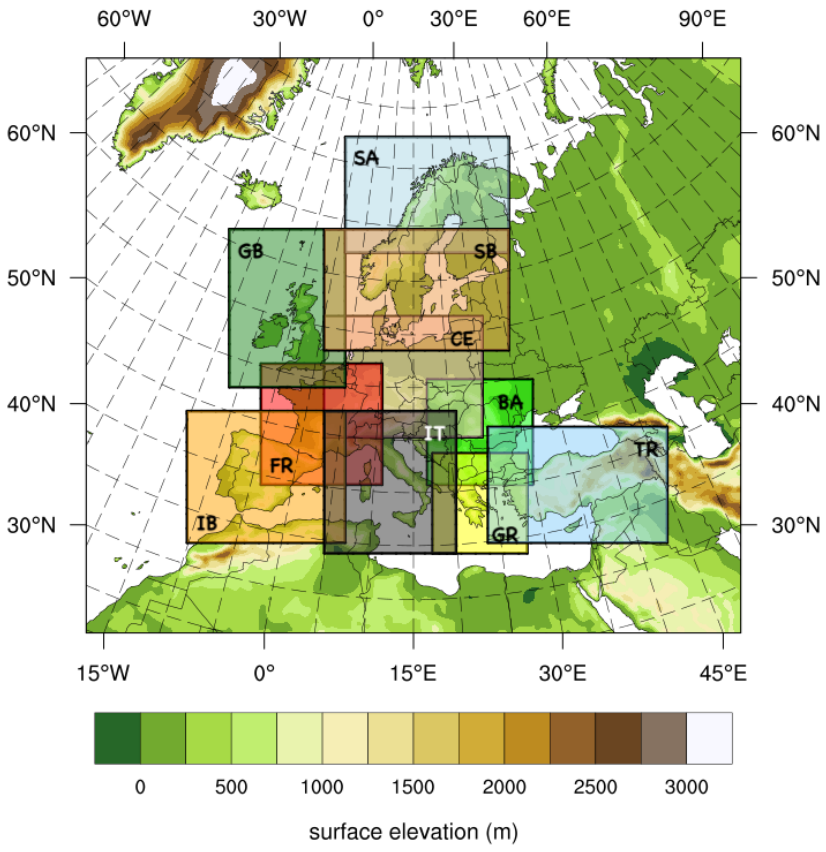

Figure 58. The 10 WRF domains (D3) used in the NEWA production run, excluding 30 edge grid points around each domain. The background map corresponds to D1 which is the same for all simulations. D2 domains are not shown.

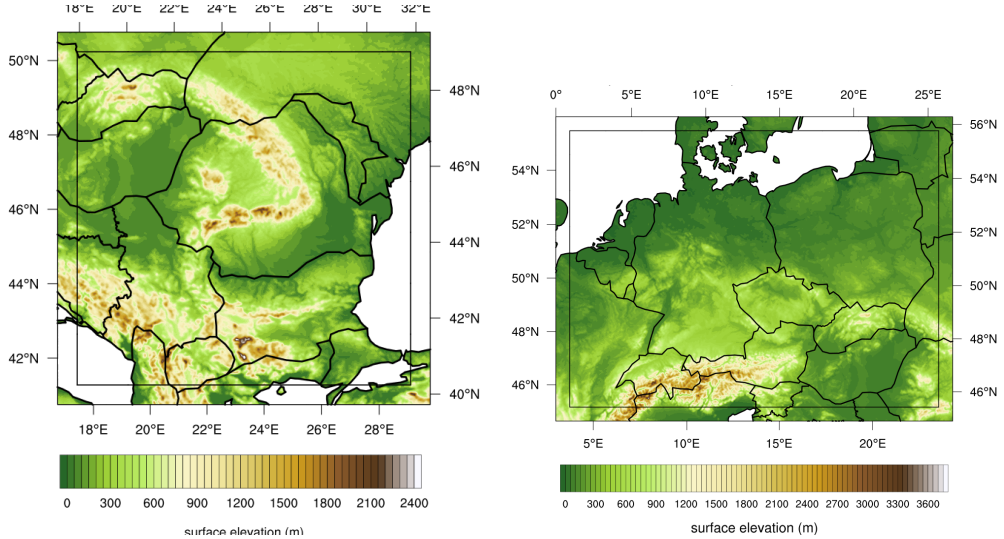

Figure 59. Layout and topography of the BA and CE domains. The fine line represents a 30 grid point edge around each domain.

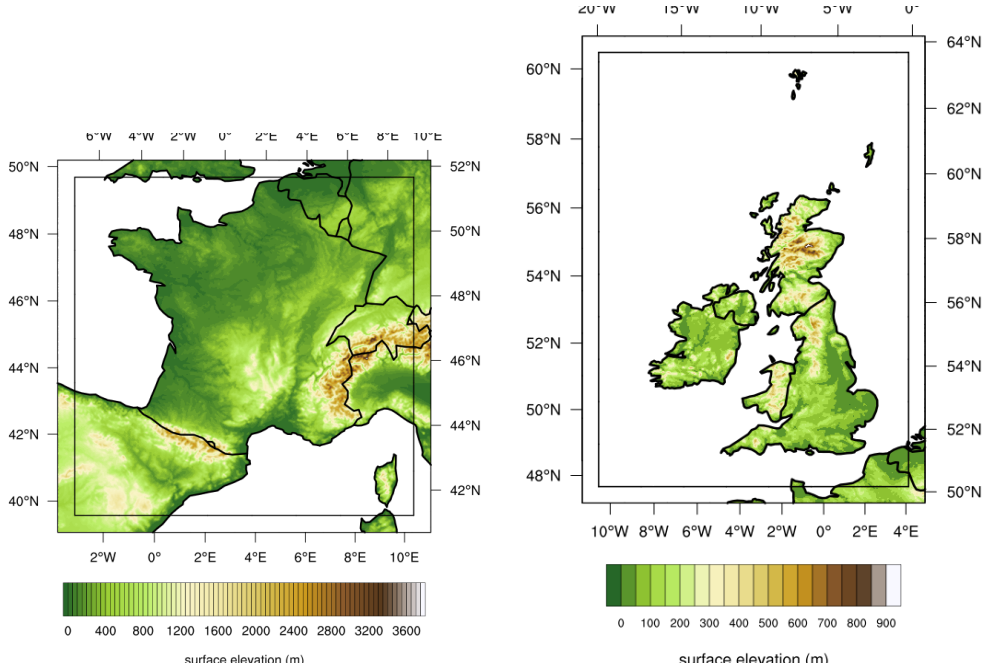

Figure 60. As in Figure 59 but for the FR and GB domains.

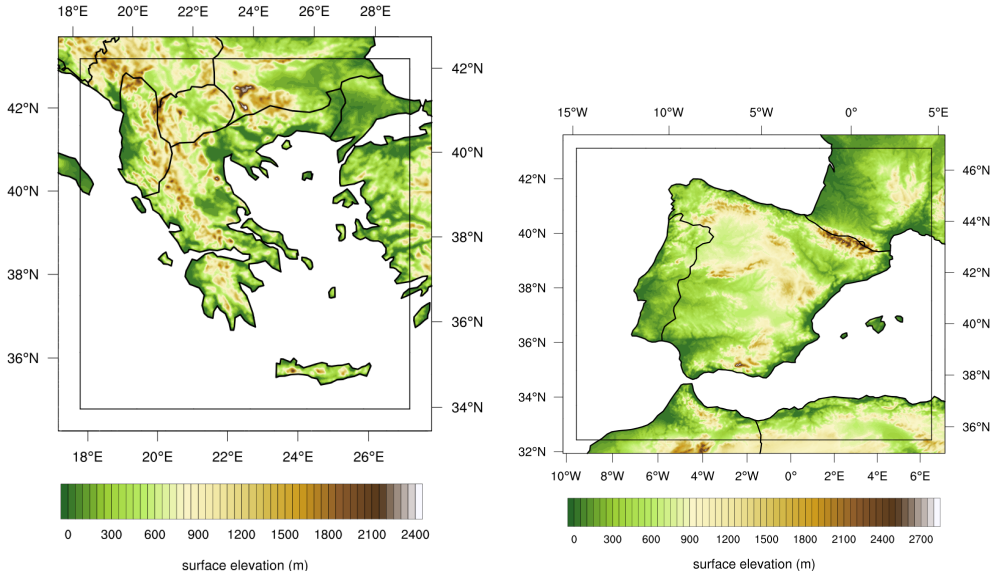

Figure 61. As in Figure 59 but for the GR and IB domains.

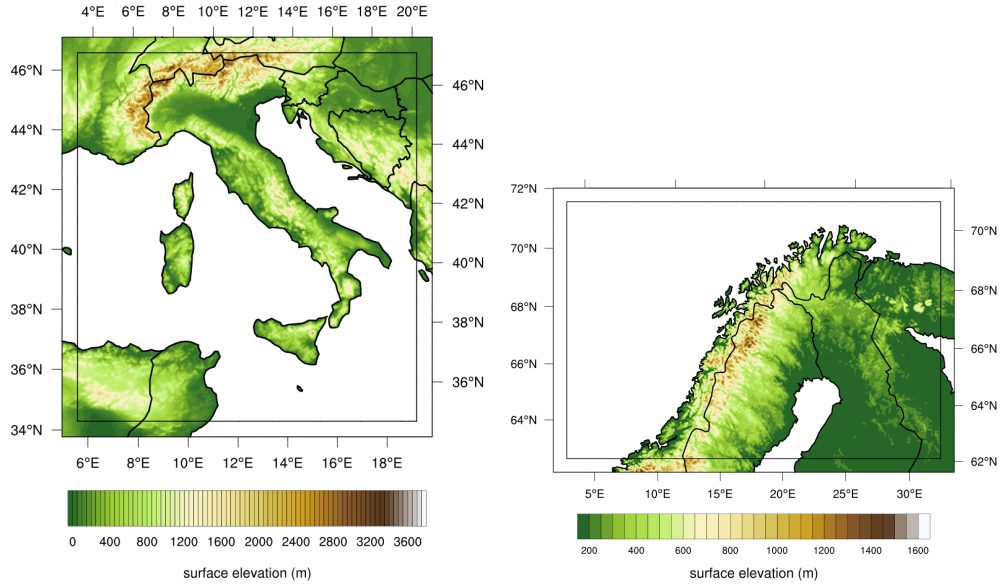

Figure 62. As in Figure 59 but for the IT and SA domains.

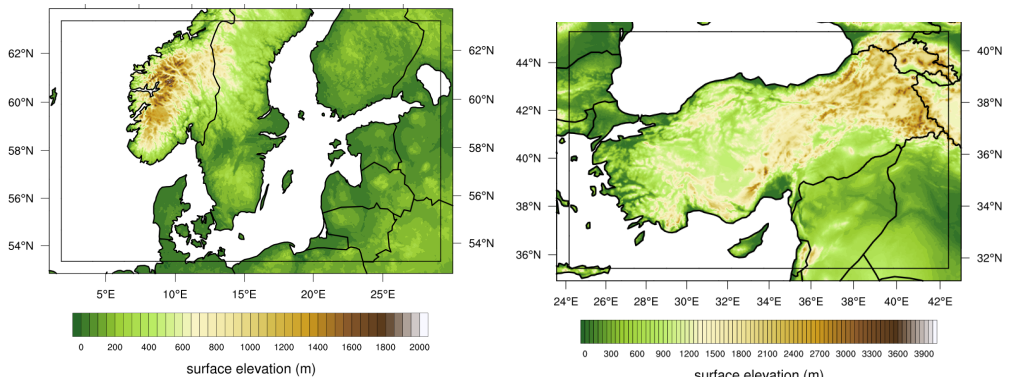

Figure 63. As in Figure 59 but for the SB and TR domains.

Acknowledgements

The NEWA project counts with the support from an ERA-Net Plus consortium composed by the European Commission and 9 funding agencies from 8 member states:

- Public Service of Wallonia, Department of Energy and Sustainable Building (Belgium)
- Department of Economy, Science and Innovation Flemish Government (Belgium)
- Danish Energy Authority (Denmark)
- Federal Ministry for the Economic Affairs and Energy, on the basis of the decision by the German Bundestag (Germany)
- Latvijas Zinatnu Akademija (Latvia)
- Funda cão para a Ciência e a Tecnologia (Portugal)
- Ministerio de Economía y Competitividad (Spain)
- The Swedish Energy Agency (Sweden)
- The Scientific and Technological Research Council of Turkey (Turkey)

The authors would like to acknowledge the help of Caroline Draxl (NREL, USA), Daran Rife (DNV-GL) and Gert-Jan Steeneveld (Wageningen University, The Netherlands) for their help reviewing our selection of the production run setup.

We acknowledge PRACE for awarding us access to MareNostrum at Barcelona Supercomputing Center (BSC), Spain, without which the NEWA simulations would not have been possible. Part of the simulations were performed on the HPC Cluster EDDY at the University of Oldenburg, funded by the German Federal Ministry for Economic Affairs and Energy under grant number 0324005. Simulations have as well been performed at the national HPC center UHEM at Istanbul Technical University, funded by the Scientific and Technological Research Council of Turkey (TUBITAK) under grant number 215M386. This work was partially supported by the computing facilities of the Extremadura Research Centre for Advanced Technologies (CETA-CIEMAT), funded by the European Regional Development Fund (ERDF), CIEMAT and the Government of Spain. In addition, simulations carried out as part of this work also made use of the computing facilities provided by CIEMAT Computer Center.

Furthermore, we would like to thank the Federal Maritime And Hydrographic Agency (BSH) for providing access to the data of the FINO offshore research platforms and Peter Kalverla from Wageningen University for processing and sharing the data from the IJmuiden mast and lidar. We acknowledge the Cabauw Experimental Site for Atmospheric Research (Cesar) for the Cabauw tower observations.

Most of the WRF simulations have been initialised using ERA5 data, downloaded from ECWMF and Copernicus Climate Change Service Climate Data Store (CDS) (Copernicus Climate Change Service (C3S), 2017).

References

Benjamin, S. G., G. A. Grell, J. M. Brown, and T. G. Smirnova, 2004: Mesoscale weather prediction with the RUC hybrid isentropic-terrain-following coordinate model. *Mon. Wea. Rev.*, **132**, 473–494, doi:10.1175/1520-0493(2004)132<0473:MWPWTR>2.0.CO;2.

Borsche, M., A. K. Kaiser-Weiss, and F. Kaspar, 2016: Wind speed variability between 10 and 116 m height from the regional reanalysis COSMO-REA6 compared to wind mast measurements over Northern Germany and the Netherlands. *Adv. Sci. Res.*, **13**, 151, doi: 10.5194/asr-13-151-2016.

Brinckmann, S., S. Krähenmann, and P. Bissolli, 2015: High-resolution daily gridded datasets of air temperature and wind speed for Europe. *Earth Syst. Sci. Data Discuss.*, **8**, 649–702, doi:10.5194/essdd-8-649-2015.

Chen, F., 2007: The NOAH land surface model in WRF: a short tutorial. NCAR, LSM Group Meeting, 17 April 2017, https://www.atmos.illinois.edu/ snesbitt/ATMS597R/notes/noahLSM-tutorial.pdf.

Collins, W. D., P. J. Rasch, B. A. Boville, J. J. Hack, J. R. McCaa, D. L. Williamson, J. T. Kiehl, and B. Briegleb, 2004: Description of the NCAR Community Atmosphere Model (CAM 3.0). Tech. Rep. NCAR/TN-464+STR, Mesoscale & Microscale Meteorology Division, NCAR, USA, 214 pp.

Copernicus Climate Change Service (C3S), 2017: ERA5: Fifth generation of ECMWF atmospheric reanalyses of the global climate. Copernicus Climate Change Service Climate Data Store (CDS).

Copernicus Land Monitoring Service, 2019: CORINE Land Cover. Accessed: 2019-04-15, https://land.copernicus.eu/pan-european/corine-land-cover.

Dee, D. P., E. Kaellen, A. J. Simmons, and L. Haimberger, 2011: Comments on "Reanalyses Suitable for Characterizing Long-Term Trends". *Bull. Amer. Meteor. Soc.*, **92 (1)**, 65–70, doi: 10.1175/2010BAMS3070.1.

Donlon, C. J., M. Martin, J. D. Stark, J. Roberts-Jones, E. Fiedler, and W. Wimmer, 2012: The operational sea surface temperature and sea ice analysis (OSTIA). *Remote Sens. Environ.*, **116**, doi:10.1016/j.rse.2010.10.017.

Draxl, C., A. N. Hahmann, A. Peña, and G. Giebel, 2014: Evaluating winds and vertical wind shear from WRF model forecasts using seven PBL schemes. *Wind Energy*, **17**, 39–55, doi: 10.1002/we.1555.

Dudhia, J., 1996: A multi-layer soil temperature model for MM5. *The Sixth PSU/NCAR Mesoscale Model Users' Workshop*, Boulder, Colorado, USA.

ECMWF, 2016: ERA5 reanalysis is in production. http://www.ecmwf.int/en/newsletter/147/news/era5-reanalysis-production.

Edson, J., and Coauthors, 2013: On the exchange of momentum over the open ocean. *J. Phys. Oceanogr.*, **43**, 1589–1610, doi:10.1175/JPO-D-12-0173.1.

Gelaro, R., W. McCarty, and M. J. S. et al, 2017: The Modern-Era Retrospective Analysis for Research and Applications, Version 2 (MERRA-2). *J. Climate*, **30**, 5419–5454.

Gemmill, W., B. Katz, and X. Li, 2007: Daily real-time global sea surface temperature - high resolution analysis at NOAA/NCEP. Office note nr. 260, 39 pp, NOAA/NWS/NCEP/MMAB.

Grell, G. A., and S. R. Freitas, 2014: A scale and aerosol aware stochastic convective parameterization for weather and air quality modeling. *Atmos. Chem. Phys.*, **14**, 5233–5250, doi: 10.5194/acp-14-5233-2014.

Gryning, S. E., E. Batchvarova, B. Brümmer, H. Jørgensen, and S. Larsen, 2007: On the extension of the wind profile over homogeneous terrain beyond the surface layer. *Bound.-Layer Meteor.*, **124**, 251–268, doi:10.1007/s10546-007-9166-9.

Hahmann, A. N., J. Badger, C. L. Vincent, M. C. Kelly, P. J. H. Volker, and J. Refslund, 2014: Mesoscale modeling for the wind atlas for South Africa (WASA) Project. Tech. rep., http://orbit.dtu.dk/services/downloadRegister/107110172/DTU_Wind_Energy_E_0050.pdf, DTU Wind Energy, 77 pp.

Hahmann, A. N., C. L. Vincent, A. Peña, J. Lange, and C. B. Hasager, 2015: Wind climate estimation using WRF model output: Method and model sensitivities over the sea. *Int. J. Climatol.*, **35**, 3422–3439, doi:10.1002/joc.4217.

Hong, S.-Y., J. Dudhia, and S.-H. Chen, 2004: A revised approach to ice microphysical processes for the bulk parameterization of clouds and precipitation. *Mon. Wea. Rev.*, **132**, 103–120, doi:10.1175/1520-0493(2004)132<0103:ARATIM>2.0.CO;2.

Hong, S.-Y., Y. Noh, and J. Dudhia, 2006: A new vertical diffusion package with an explicit treatment of entrainment processes. *Mon. Wea. Rev.*, **134**, 2318–2341, doi:10.1175/MWR3199.1.

Hu, X.-M., P. M. Klein, and M. Xue, 2013: Evaluation of the updated YSU Planetary Boundary Layer Scheme within WRF for Wind Resource and Air Quality Assessments. *J. Geophys. Res.*, **118**, 10 490–10 505, doi:10.1002/jgrd.50823.

Iacono, M. J., J. S. Delamere, E. J. Mlawer, M. W. Shephard, S. A. Clough, and W. D. Collins, 2008: Radiative forcing by long–lived greenhouse gases: Calculations with the AER radiative transfer models. *J. Geophys. Res.*, **113**, D13 103., doi:10.1029/2008JD009944.

Jerez, S., J. P. Montavez, J. J. Gomez-Navarro, P. A. Jiménez, P. Jimenez-Guerrero, R. Lorente, and J. F. Gonzalez-Rouco, 2012: The role of the land-surface model for climate change projections over the Iberian Peninsula. *J. Geophys. Res.*, **117 (D1)**, doi:10.1029/2011JD016576.

Jiménez, P. A., J. Dudhia, J. F. Gonzalez-Rouco, J. Navarro, J. P. Montavez, and E. Garcia-Bustamante, 2012: A Revised Scheme for the WRF Surface Layer Formulation. *Mon. Wea. Rev.*, **140**, 898–918, doi:10.1175/MWR-D-11-00056.1.

Jiménez, P. A., J. Vilà-Guerau de Arellano, J. F. González-Rouco, J. Navarro, J. P. Montávez, E. García-Bustamante, and J. Dudhia, 2011: The Effect ofHeat Waves and Drought on Surface Wind Circulations in the Northeast of the Iberian Peninsula during the Summer of 2003. *J. Climate*, **24 (20)**, 5416–5422, doi:10.1175/2011JCLI4061.1.

Kain, J. S., 2004: The Kain–Fritsch convective parameterization: An update. *J. Appl. Meteor. Clim.*, **43**, 170–181, doi:10.1175/1520-0450(2004)043<0170:TKCPAU>2.0.CO;2.

Kaiser-Weiss, A., F. Kaspar, V. Heene, M. Borsche, D. Tan, P. Poli, A. Obregon, and H. Gregow, 2015: Comparison of regional and global reanalysis near-surface winds with station observations over Germany. *Adv. Sci. Res.*, **12 (1)**, 187–198, doi:10.5194/asr-12-187-2015.

Kleczek, M. A., G.-J. Steeneveld, and A. A. M. Holtslag, 2014: Evaluation of the Weather Research and Forecasting Mesoscale Model for GABLS3: Impact of Boundary-Layer Schemes, Boundary Conditions and Spin-Up. *Boundary-Layer Meteorol.*, **152 (2)**, 213–243, doi:10.1007/s10546-014-9925-3.

Lawrence, D. M., and Coauthors, 2011: Parameterization improvements and functional and structural advances in version 4 of the Community Land Model. *J. Adv. Model. Earth Sy.*, **3 (1)**, M03 001, doi:10.1029/2011MS00045.

Li, D., E. Bou-Zeid, M. Barlage, F. Chen, and J. A. Smith, 2013: Development and evaluation of a mosaic approach in the WRF-Noah framework. *J. Geophys. Res.*, **118**, 11,918–11,935, doi:10.1002/2013JD020657.

Makkonen, L., 2000: Models for the growth of rime, glaze, icicles and wet snow on structures. *Philos. T. R. Soc. A*, **358**, 2913–2939, doi:10.1098/rsta.2000.0690.

Mann, J., and Coauthors, 2017: Complex terrain experiments in the New European Wind Atlas. *Philos. T. R. Soc. A*, **375 (2091)**, 20160 101, doi:10.1098/rsta.2016.0101.

Mason, P. J., 1988: The formation of areally-averaged roughness lengths. *Q. J. R. Meteorolog. Soc.*, **114 (480)**, 399–420, doi:10.1002/qj.49711448007.

Miguez-Macho, G., G. L. Stenchikov, and A. Robock, 2004: Spectral nudging to eliminate the effects of domain position and geometry in regional climate model simulations. *J. Geophys. Res.*, **109 (D13)**, D13 104, doi:10.1029/2003JD004495.

Monin, A. S., and A. M. Obukhov, 1954: Basic laws of turbulent mixing in the surface layer of the atmosphere. *Contrib. Geophys. Inst. Acad. Sci. USSR*, **151**, 163–187.

Nakanishi, M., and H. Niino, 2006: An improved Mellor-Yamada Level-3 model: Its numerical stability and application to a regional prediction of advection fog. *Bound.-Layer Meteor.*, **119**, 397–407, doi:10.1007/s10546-005-9030-8.

Nakanishi, M., and H. Niino, 2009: Development of an improved turbulence closure model for the atmospheric boundary layer. *J. Meteor. Soc. Japan*, **87**, 895–912, doi:10.2151/jmsj.87.895.

NCAR, 2000: NCEP FNL operational model global tropospheric analyses, continuing from july 1999. Research Data Archive at the National Center for Atmospheric Research, Computational and Information Systems Laboratory, Boulder CO, doi:10.5065/D6M043C6.

Niu, G.-Y., and Coauthors, 2011: The community Noah land surface model with multiparameterization options (Noah-MP): 1. model description and evaluation with local-scale measurements. *J. Geophys. Res.*, **116 (D12)**, D12 109, doi:10.1029/2010JD015140.

Noilhan, J., and S. Planton, 1989: A simple parameterization of land surface processes for meteorological models. *Mon. Wea. Rev.*, **117**, 536–549, doi:10.1175/1520-0493(1989)117<0536:ASPOLS>2.0.CO;2.

Olsen, B. T., A. N. Hahmann, A. M. Sempreviva, J. Badger, and H. E. Jørgensen, 2017: An intercomparison of mesoscale models at simple sites for wind energy applications. *Wind Energy*, **2**, 211–228, doi:10.5194/wes-2-211-2017.

Olson, J., J. Kenyon, J. Brown, W. Angevine, and K. Suselj, 2016: *Updates to the MYNN PBL and surface layer scheme for RAP/HRRR*. NOAA Earth System Research Laboratory, Boulder, CO, USA, URL http://www2.mmm.ucar.edu/wrf/users/workshops/WS2016/oral_presentations/6.6.pdf.

Pleim, J., 2007: A combined local and nonlocal closure model for the atmospheric boundary layer. Part I: Model description and testing. *J. Appl. Meteor. Clim.*, **46**, 1383–1395, doi:10.1175/JAM2539.1.

PRACE Partnership for Advanced Computing in Europe, 2019: Project: NEWA-ProRun: New European Wind Atlas Production Run. http://www.prace-ri.eu/callproject/2017174128/.

Reynolds, R. W., N. A. Rayner, T. M. Smith, D. C. Stokes, and W. Q. Wang, 2002: An improved in situ and satellite SST analysis for climate. *J. Climate*, **15**, 1609–1625, doi:10.1175/1520-0442(2002)015<1609:AIISAS>2.0.CO;2.

Reynolds, R. W., T. M. Smith, C. Liu, D. B. Chelton, K. S. Casey, and M. G. Schlax, 2007: Daily high-resolution-blended analyses for sea surface temperature. *J. Climate*, **20**, 5473–5496, doi:10.1175/2007JCLI1824.1.

Sanz Rodrigo, J., and Coauthors, 2017: Mesoscale to microscale wind farm flow modeling and evaluation. *WIREs Energy Environ.*, **6 (2)**, doi:10.1002/wene.214.

Seneviratne, S. I., T. Corti, E. L. Davin, M. Hirschi, E. B. Jaeger, I. Lehner, B. Orlowsky, and A. J. Teuling, 2010: Investigating soil moisture–climate interactions in a changing climate: A review. *Earth-Sci. Rev.*, **99 (3-4)**, 125–161, doi:10.1016/j.earscirev.2010.02.004.

Skamarock, W. C., and Coauthors, 2008: A Description of the Advanced Research WRF Version 3. Tech. Rep. NCAR/TN-475+STR, National Center for Atmospheric Research.

Smirnova, T. G., J. M. Brown, S. G. Benjamin, and J. S. Kenyon, 2016: Modifications to the Rapid Update Cycle Land Surface Model (RUC LSM) available in the Weather Research and Forecasting (WRF) model. *Mon. Wea. Rev.*, **144 (5)**, 1851–1865, doi:10.1175/MWR-D-15-0198.1.

Sukoriansky, S., B. Galperin, and V. Perov, 2006: A quasi-normal scale elimination model of turbulence and its application to stably stratified flows. *Nonlin. Processes Geophys.*, **13**, 9–22, doi:10.5194/npg-13-9-2006.

Sušelj, K., and A. Sood, 2010: Improving the Mellor-Yamada-Janjić parametrisation for wind conditions in the marine planetary boundary layer. *Bound.-Layer Meteor.*, **136**, 301–324, doi:10.1007/s10546-010-9502-3.

Tewari, M., and Coauthors, 2004: Implementation and verification of the unified Noah land surface model in the WRF model. *20th conference on weather analysis and forecasting/16th conference on numerical weather prediction, Seattle, 12-16 January 2004*, AMS.

Vincent, C. L., and A. N. Hahmann, 2015: The impact of grid and spectral nudging on the variance of the near-surface wind speed. *J. Appl. Meteor. Clim.*, **54**, 1021–1038, doi:10.1175/JAMC-D-14-0047.1.

Wang, W., J. Dudhia, and M. Chen, 2019: *Application of WRF - How to get better performance*. National Center for Atmospheric Research, Boulder, CO, USA, URL http://www2.mmm.ucar.edu/wrf/users/tutorial/201901/chen_best_practices.pdf.

Warner, T., R. Peterson, and R. Treadon, 1997: A tutorial on lateral boundary conditions as a basic and potentially serious limitation to regional numerical weather prediction. *Bull. Amer. Meteorol. Soc.*, **78 (11)**, 2599–2617, doi:10.1175/1520-0477(1997)078<2599:ATOLBC>2.0.CO;2.

Wilks, D., 2011: *Statistical Methods in the Atmospheric Sciences*, International Geophysics Series, Vol. 100. 3rd ed., Academic Press, 704 pp., iSBN: 9780123850232.

Yang, Z.-L., and Coauthors, 2011: The community Noah land surface model with multiparameterization options (Noah-MP): 2. Evaluation over global river basins. *J. Geophys. Res.*, **116 (D12)**, doi:10.1029/2010JD015140.

Zhang, B., R. S. Lindzen, V. Tallapragada, F. Weng, Q. Liu, J. A. Sippel, Z. Ma, and M. A. Bender, 2016: Increasing vertical resolution in us models to improve track forecasts of Hurricane Joaquin with HWRF as an example. *P. Natl. Acad. Sci. USA*, **113 (42)**, 11 765–11 769, doi:10.1073/pnas.1613800113.

WRF namelist, CE domain

```
&time_control
 interval_seconds                    = 21600,
 input_from_file                     = .T., .T., .T.,
 history_interval                    = 60, 60, 30,
 frames_per_outfile                  = 24, 24, 48,
 restart                             = .false.,
 restart_interval                    = 100000,
 io_form_history                     = 2
 io_form_restart                     = 2
 io_form_input                       = 2
 io_form_boundary                    = 2
 auxinput4_inname                    = "wrflowinp_d<domain>",
 auxinput4_interval                  = 360,360,360,
 io_form_auxinput4                   = 2,
 iofields_filename                   = "WAFields.txt","WAFields.txt","WAFields.txt",
 ignore_iofields_warning             = .true.,
 debug_level                         = 0,
/

&domains
 use_adaptive_time_step              = .true.,
 step_to_output_time                 = .true.,
 target_cfl                          = 0.60, 0.60, 0.60,
 target_hcfl                         = 0.84, 0.84, 0.84,
 max_step_increase_pct               =    5,  51,  51,
 starting_time_step                  =   90,  40,  13,
 max_time_step                       =  150,  45,  15,
 min_time_step                       =   30,  10,   3,
 adaptation_domain                   =   1,
 parent_id                           =   1,    1,   2,
 parent_grid_ratio                   =   1,    3,   3,
 i_parent_start                      =   1,   79,  39,
 j_parent_start                      =   1,   63,  39,
 e_we                                =  250, 259, 541,
 e_sn                                =  220, 217, 415,
 s_sn                                =    1,   1,   1,
 s_we                                =    1,   1,   1,
 e_vert                              =   61,  61,  61,
 grid_id                             =    1,   2,   3,
 parent_time_step_ratio              =    1,   3,   3,
 num_metgrid_levels                  = 33,
 num_metgrid_soil_levels             = 4,
 dx                                  = 27000.,9000.,3000.0,
 dy                                  = 27000.,9000.,3000.0,
 p_top_requested                     = 5000,
 eta_levels = 1.000000, 0.998600, 0.996000, 0.994000, 0.992000,
              0.990000, 0.987592, 0.984486, 0.980977, 0.977016,
              0.972544, 0.967500, 0.961813, 0.955403, 0.948185,
              0.940062, 0.930929, 0.920670, 0.909158, 0.896257,
              0.881820, 0.859633, 0.830162, 0.794019, 0.751945,
```

```
              0.704330, 0.659043, 0.615990, 0.575078, 0.536219,
              0.499329, 0.464324, 0.431126, 0.399657, 0.369845,
              0.341616, 0.314904, 0.289641, 0.265763, 0.243210,
              0.221922, 0.201841, 0.182641, 0.164410, 0.148206,
              0.132526, 0.117709, 0.104002, 0.091398, 0.079808,
              0.069150, 0.059351, 0.050340, 0.042054, 0.034434,
              0.027428, 0.020986, 0.015062, 0.009615, 0.004606,
              0.000000,
 smooth_option = 2,
 feedback = 0,
/

&physics
 mp_physics                          =  4,  4,  4,
 ra_lw_physics                       =  4,  4,  4,
 ra_sw_physics                       =  4,  4,  4,
 radt                                = 12, 12, 12,
 swint_opt                           =  1,
 sf_surface_physics                  =  2,  2,  2,
 sf_sfclay_physics                   =  2,  2,  2,
 bl_pbl_physics                      =  5,  5,  5,
 bl_mynn_mixlength                   =  0,
 bldt                                =  0,  0,  0,
 cu_physics                          =  1,  1,  0,
 cudt                                =  5,  5,  5,
 fractional_seaice                   = 0,
 tice2tsk_if2cold                    = .true.,
 seaice_threshold                    = 0.,
 isfflx                              = 1,
 icloud                              = 1,
 surface_input_source                = 1,
 num_land_cat                        = 28,
 num_soil_layers                     = 4,
 sst_update                          = 1,
 ensdim                              = 144,
 prec_acc_dt                         = 60, 60, 30,
/
&ice_blade
 iceblade_opt = 1,1,1,
 sum_qcqi_wsm = 1,1,1,
/
&fdda
 grid_fdda                           = 2,     0,    0,
 gfdda_inname                        = "wrffdda_d<domain>",
 gfdda_end_h                         = 300,   0,    0,
 gfdda_interval_m                    = 360,   0,    0,
 fgdt                                = 0,     0,    0,
 if_no_pbl_nudging_uv                = 0,     0,    0,
 if_no_pbl_nudging_t                 = 1,     0,    0,
 if_no_pbl_nudging_q                 = 1,     0,    0,
 if_zfac_uv                          = 1,     0,    0,   0,
  k_zfac_uv                          = 20,    0,    0,   0,
 if_zfac_t                           = 1,     0,    0,   0,
  k_zfac_t                           = 20,    0,    0,   0,
```

```
 if_zfac_q                           = 1,     0,    0,   0,
  k_zfac_q                           = 20,    0,    0,   0,
 guv                                 = 0.0003, 0.000075, 0.000075,
 gt                                  = 0.0003, 0.000075, 0.000075,
 gq                                  = 0.0003, 0.000075, 0.000075,
 xwavenum                            = 14,
 ywavenum                            = 10,
 if_ramping                          = 0,
 dtramp_min                          = 60.0,
 io_form_gfdda                       = 2,
/

&dynamics
 w_damping                           = 1,
 diff_opt                            = 1,
 km_opt                              = 4,
 diff_6th_opt                        = 2,    2,    2,
 diff_6th_factor                     = 0.06, 0.08, 0.1,
 base_temp                           = 290.
 damp_opt                            = 0,
 zdamp                               = 5000., 5000., 5000.,
 dampcoef                            = 0.15,  0.15,  0.15,
 khdif                               = 0,     0,    0,
 kvdif                               = 0,     0,    0,
 non_hydrostatic                     = .true.,.true.,.true.,
 moist_adv_opt                       = 1,     1,    1,
 scalar_adv_opt                      = 1,     1,    1,
/
&bdy_control
 spec_bdy_width                      = 5,
 spec_zone                           = 1,
 relax_zone                          = 4,
 specified                           = .true., .false.,.false.,
 nested                              = .false., .true., .true.,
/
&grib2
/
&namelist_quilt
  nio_tasks_per_group = 8,
  nio_groups = 3,
/
```


eUDP
Energiteknologisk udvikling og demonstration
Energimyndigheten
Wallonie
SPW
Service public
de Wallonie
Latvijas Zinātņu akadēmija
Latvian Academy of Sciences
Supported by:
Federal Ministry
for Economic Affairs
and Energy
on the basis of a decision
by the German Bundestag
EWI
GOBIERNO
DE ESPAÑA
MINISTERIO
DE ECONOMÍA
Y COMPETITIVIDAD
FCT
Fundação para a Ciência e a Tecnologia
TÜBİTAK